藥學博士 學位論文

Epithelial-Mesenchymal Transition-mediated regulation of gefitinib resistance and invasion through three dimensional (3D) collagen gels

상피-중배엽 세포전이에 의한 항암제 내성 유발 기전 및 3 차원적 전이 제어에 관한 연구

2014 年 2 月

서울大學校 大學院

藥學科 醫藥生命科學專攻

李 美 淑

Epithelial Mesenchymal Transition-mediated regulation of gefitinib resistance and invasion through three dimensional (3D) collagen gels

상피-중배엽 세포전이에 의한 항암제 내성 유발 기전 및 3 차원적 전이 제어에 관한 연구

指導敎授 李 正 源

이 論文을 藥學博士 學位論文으로 提出함

2014 年 2 月

서울大學校 大學院

藥學科 醫藥生命科學專攻

李 美 淑

李 美 淑 의 藥學博士 學位論文을 認准함

2013 年 12 月

委 員 長 _____ 印

副委員長 _____ 印

委 員 _____ 印

委 員 _____ 印

委 員 _____ 印

Epithelial-Mesenchymal Transition-mediated regulation of gefitinib resistance and invasion through three dimensional (3D) collagen gels

by

Mi-Sook Lee

A thesis submitted in partial fulfillment of the requirements

for the degree of

DOCTOR OF PHILOSOPHY

(Pharmacy: Pharmaceutical bioscience major)

under the supervision of Professor Jung Weon Lee

at the College of Pharmacy,

Seoul National University

February 2014

ABSTRACT

Epithelial-Mesenchymal Transition-mediated regulation of gefitinib resistance and invasion through three dimensional (3D) collagen gels

MI-SOOK LEE

Under the supervision of Professor Jung Weon Lee

at the College of Pharmacy, Seoul National University

Normal epithelial cells are attached with one another or to the extracellular environment by cell-cell or cell-extracellular Matrix (ECM) interactions, respectively. By accumulated genetic alterations or other factors, the epithelial cells can become tumorigenic, with forming heterogeneous tumor masses. Among the tumor cell mass, certain metastatic cells lost their cell polarity and cell-cell adhesions, being converted to mesenchymal-like cells. This epithelial-mesenchymal transition (EMT) is critically involved in the cancer metastasis. This EMT process also causes resistance of cancer cells to anti-cancer reagents, leading to an attenuation of drug efficiency and enhances migration and invasion for metastatic potential of cancer cells. In this study, I investigated how EMT causes gefitinib resistance of NSCLC by virtues of TM4SF5 (transmembrane 4

L6 family member 5)-mediated EMT induction in NSCLC cells, and how EMT-rendered mesenchymal properties of cancer cells could regulate invasion of TM4SF5-positive and E-cadherin negative to be mesenchymal cells-like, through 3D collagen I gel systems. One of the most important pathways in NSCLC is the epidermal growth factor receptor (EGFR) pathway during tumor progression. In many cases, NSCLC patients can be initially treated with the EGFR-TKI (Tyrosine Kinase Inhibitor), gefitinib. However, continued gefitinib therapy does not benefit the survival of patients due to acquired resistance through additional EGFR mutations, c-MET amplification, or EMT. It is of further interest to determine whether mesenchymal-like, but not epithelial-like, cancer cells can become resistant to gefitinib by bypassing EGFR signaling and acquiring alternative routes of proliferative and survival signaling. Here I examined whether gefitinib resistance of cancer cells can be caused by TM4SF5, which has been shown to induce EMT via cytosolic $p27^{Kip1}$ stabilization. Gefitinib resistant cells exhibited higher and/or sustained TM4SF5 expression, cytosolic $p27^{Kip1}$ stabilization, and mesenchymal phenotypes, compared with gefitinib-sensitive cells. Conversion of gefitinib-sensitive to -resistant cells by introduction of the T790M EGFR mutation caused enhanced and sustained expression of TM4SF5, phosphorylation of $p27^{Kip1}$ Ser10 (responsible for cytosolic location), loss of E-cadherin from cell-cell contacts, and gefitinib-resistant EGFR and survival signaling activities. Additionally, TM4SF5

overexpression lessened the sensitivity of NSCLC cells to gefitinib. Suppression of TM4SF5 or $p27^{Kip1}$ in gefitinib-resistant cells via the T790M EGFR mutation or TM4SF5 expression rendered them gefitinib-sensitive, displaying more epithelial-like and less mesenchymal-like characteristics. These results indicate that TM4SF5-mediated EMT may have an important function in the gefitinib resistance of cancer cells. I have then investigated whether TM4SF5 induced EMT for enhanced cell migration and invasion to investigate how mesenchymal cell properties following EMT process may regulates the invasive properties such as invadopodia formation and ECM degradation in 3D collagen I-surrounded condition. The two dimensional (2D) cell culture systems can stratify neither the environments around *in vivo* cancer cells nor evaluation of efficacy of anti-cancer drug candidates with regards to cancer cell invasion and metastasis. For this reasons, I have used three dimensional (3D) cell culture systems using type 1 collagen matrices to study invasive behaviors and mechanisms of tumor cells. In this 3D cell culture system, revealing the TM4SF5-positive cell behaviors involved a technical problem of cell precipitation toward the bottom of the collagen I gels, leading to no-real 3D environment. Therefore, alternatively using highly-invasive and TM4SF5-positive MDA-MB-231 breast cancer cells, their invasive properties in 3D collagen I gels with normal serum-containing media were monitored for the underlying mechanisms. Although an *in vitro* 3D environment cannot completely mimic the *in vivo* tumor site, embedding tumor

cells in a 3D extracellular matrix (ECM) allows for our study of cancer cell behaviors and the screening of anti-metastatic reagents with a more *in vivo*-like context. I explored the behaviors of MDA-MB-231 breast cancer cells embedded in 3D collagen I. Diverse tumor environmental conditions (including cell density, extracellular acidity, or hypoxia as mimics for a continuous tumor growth) reduced JNKs, enhanced TGFβ1/Smad signaling activity, induced Snail1, and reduced cortactin expression. The reduced JNKs activity blocked efficient formation of invadopodia labeled with actin, cortactin, or MT1-MMP. JNKs inactivation activated Smad2 and Smad4, which were required for snail1expression. Snail1 then repressed cortactin expression, causing reduced invadopodia formation and prominent localization of MT1-MMP at perinuclear regions. MDA-MB-231 cells thus exhibited less efficient invasion in 3D collagen I upon JNKs inhibition. These observations support a signaling network among JNKs, Smads, Snail1, and cortactin to regulate the invasion of MDA-MB-231 cells embedded in 3D collagen I, which may be targeted during screening of anti-invasion reagents. Altogether, this study reveals that mesenchymal properties acquired by EMT process, which can be induced by membrane proteins such as TM4SF5 can cause drug resistance and enhanced metastatic potentials of cancer cells, suggesting that EMT process can be targeted for anti-metastatic reagents.

Keywords

NSCLC (Non-small cell lung carcinoma), EMT (Epithelial–mesenchymal transition), Gefitinib, Drug resistance, EGFR (Epidermal growth factor Receptor), TM4SF5 (transmembrane 4 L six family member 5), $p27^{Kip1}$, 3D culture, Collagen type 1, Breast cancer, Cortactin, Invadopodia, Snail1, MT1-MMP

Student Number : 2010-30467

TABLE OF CONTENTS

LIST OF FIGURES

Ⅰ. Background

Ⅱ. Chapter 1

Ⅲ. Chapter 2

LIST OF ABBREVIATIONS

NSCLC, Non-small-cell lung cancer

EGFR, Epithelial growth factor receptor

TM4SF5, Transmembrane 4 L six family member 5

EMT, Epithelial–mesenchymal transition

TKIs, Tyrosine kinase inhibitors

c-MET, MET or MNNG HOS Transforming gene

FN, Fibronectin

DAPI, 4',6-Diamidino-2-Phenylindole, Dihydrochloride

α-SMA, α-smooth muscle actin

ERK, Extracellular signal-regulated kinases

TERM, Tetraspanin-enriched microdomain

Ad-siRNA, Adenoviral small interfering ribonucleic acid

DMSO, Dimethyl sulfoxide

ECM, Extracellular matrix

JNK1, C-Jun N-terminal Kinase 1

2D, Two dimensional

3D, Three dimensional

SP, SP600125

TGF-β1, Transforming growth factor-β1

MT1-MMP, Membrane type I matrix metalloproteinase

PCNA, Proliferating cell nuclear antigen

GFP, Green fluorescent protein

ChIP, Chromatin immunoprecipitation

RT-PCR, Real time polymerase chain reaction

PCR, Polymerase chain reaction

WT, Wild type

PDMS, Polydimethylsiloxane prepolymer

FITC, Fluorescein isothiocyanate

GAPDH, Glyceraldehyde 3-phosphate dehydrogenase

EDTA, Ethylenediaminetetraacetic acid

SDS, Sodium dodecyl sulfate

TE buffer, Tirs ethylenediaminetetraacetic acid buffer

shRNA, Short hairpin ribonucleic acid

siRNA, Small interfering ribonucleic acid

ActD, Actinomycin D

CHX, Cycloheximide

DN-JNK1, Dominant-negative c-Jun N-terminal Kinase 1

IDC, Invasive ductal carcinoma

DCIS, Ductal carcinoma in situ

Ⅰ. Background

1. Cell-Cell adhesion and Cell-Matrix interactions

Epithelial monolayer on the basement membranes is maintained by adhesions between integrins on cell surface and extracellular matrix proteins, and by cell-cell adhesions between adjacent cells [1]. Cell-cell adhesion is achieved through intercellular junctions composed of the tight junction, adherens junctions, desmosome, and cell-matrix junctions (focal adhesion and hemidesmosome) between two neighboring cells [2]. Specialized cell junctions occur at adhesion molecules complexes of cell-cell and cell-matrix contacts in all tissues (Fig. Ⅰ-1). Specially, adherens junctions and tight junctions play a central role in regulating the activity of the entire junctional complex [3]. The tight junctions that lie apical to adherens junctions regulate the paracellular pathway for the movement of ions and solutes between epithelial cells and seal neighboring cells together so that they function as barriers to the diffusion of some membrane proteins and lipids between apical and basolateral domains of the plasma membrane [4]. Tight junctions are mainly composed of occludin and claudin, and the cytoplasmic scaffolding proteins ZO-1,-2, and -3 [5]. Adherens junctions mechanically attach cells and their cytoskeletons to their neighbors or to the extracellular matrix. Adherens junctions composed of the transmembrane protein E-cadherin and intracellular components, such as p120-catenin, β-catenin, and α-catenin [4]. The desmosome is a specialized adhesive junction that interacts with the cytoskeleton and participates in crosstalk

with gap and adherens junctions. Desmosomes appear as thickened patches in the cell membrane region between two cells. Desmosomes contain specialized proteins such as desmosomal cadherins called desmocollins and desmogleins and are linked to intermediate filaments (IFs) through desmoplakin [2] .

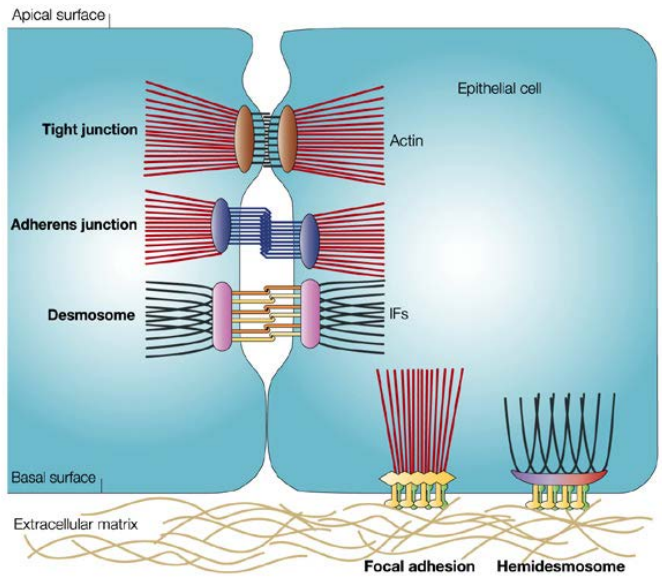

Fig. Ⅰ-1. Five different types of junctions [2].

Cell–matrix adhesions are regulated by hemidesmosomes or focal adhesions that are linked to actin filaments by integrins and adaptor proteins such as talin, filamin, and vinculin [2]. The cell-matrix interactions play a significant role in *in vitro* models. One example of such significance is the evidence showing alterations in the spectrum of molecules involved in cell-ECM interactions in transformed malignant cells [6]. Transformed cells are generally characterized by decreased

expression of ECM proteins, ECM receptors, and cytoplasmic components of adhesion plaques [6]. The downregulation of these molecules is important for transformation in a variety of cell types because restoration of their levels reverts features of the tumorigenic phenotype such as abnormal cell morphology, anchorage-independent growth, and the ability to form tumors in transplantation models [6]. These cell-cell adhesion and cell-ECM interactions determine the polarity of cells and participate in the maintenance of tissues. The disrupted cell-cell or cell-ECM adhesion significantly contributes to uncontrolled cell proliferation and progressive distortion of normal tissue architecture.

2. Cell adhesion and EMT in cancer

Like normal epithelial cells, benign tumor cells *in situ* maintain cell polarity which is supported by cell-cell adhesions and cell-ECM interactions. However, during cancer progression, some carcinoma cells lose the cell polarity and invade through their basement membrane and then into connective tissue. This phenomenon is referred to as epithelial-mesenchymal transition (EMT) and thought to be a crucial event of cancer progression [7-9]. The EMT in cancer is a process by which epithelial cells lose their cell polarity and cell-cell adhesion, and gain migratory and invasive properties to become mesenchymal cells [10]. During EMT process, upstream signals through growth factors of the tumor stroma lead to the activation of transcriptional repressors, including ZEB1, Twist, and Snail1 and 2, which

directly and indirectly inhibit E-cadherin transcription [11, 12]. E-cadherin which is a calcium-dependent cell adhesion molecule is expressed exclusively in epithelial cells and its expression is commonly suppressed in tumors of epithelial origins. The cytoplasmic domain of E-cadherin interacts with β-catenins to establish an intracellular linkage with the actin filaments [13, 14]. This results in the disturbance of apico-basal polarity and cell anchoring to the basement membrane, which, in turn, allows the cells to acquire a mobile mesenchymal phenotype [15]. Loss of cell adhesion and polarity by EMT allows tumor cells to detach from primary tissue and to escape from the primary mass. This event is accompanied with morphological changes of cells and transformed cells gain a more motile and invasive phenotype. As consequence, non-invasive cells could convert to the malignant tumor cells and break down the ECM and eventually invade and metastasize to distal organs [11, 15]. Thus, EMT-dependent invasion and metastasis programs are strongly responsive to microenvironmental changes and adaptive in their signaling program and associated invasion dynamics.

3. Tumor microenvironment

Solid tumors contain heterogeneous cell types that comprise cancer cells and stromal cells (i.e., fibroblasts and inflammatory cells), and multiple different components that are embedded in an extracellular matrix [16]. The tumor microenvironment is the cellular environment in which the tumor exists, including

surrounding blood vessels, immune cells, fibroblasts, other cells, signaling molecules, and the extracellular matrix such as collagen [17, 18]. The tumor and its microenvironment affect the fate of one another. Tumor mass can control the microenvironment by releasing extracellular signals, such as in tumor angiogenesis while the microenvironment helps drive the process of tumor progression such as in hypoxia and acidity [19]. The tumor microenvironment is now recognized as an important factor of tumor progression and responses to cancer treatment. Recent reports demonstrate significant gene expression and epigenetic alterations in cells composing the microenvironment during disease progression, which can be explored as biomarkers and targets for therapy. As a result, there is increasing interest in developing novel therapies targeting the tumor microenvironment, particularly as it relates to invasive and metastatic progression [20].

4. Three dimensional cell culture in cancer

Tissues and organs *in vivo* are made three dimensional (3D) constructs of organized assembly of different cell types that contribute to the architecture for functional differentiation. However, cells grown *in vitro* on flat 2D tissue culture substrates can differ considerably in their morphology, cell-cell and cell-ECM interactions, and differentiation form those growing in more physiological 3D environments [21]. 3D *in vitro* cell culture models have an invaluable role in understanding the behavior of tumor cells in a well-defined microenvironment [21, 22]. 3D cell

culture aims at recapitulating normal and pathological tissue architectures, hence providing physiologically relevant models to study normal development and disease [23]. In 3D culture systems, cells attach and proliferate to one another and form natural cell-cell and cell-ECM interactions. Additionally, both the composition and stiffness of the ECM have major effects on cell signaling and behavior [24-26]. The cell-ECM adhesions synthesize and secrete the natural products to which cells are attached in 3D. It is flexible and pliable like *in vivo* tissues. It is made of complex proteins in their native configuration and so provides important biological instructions to the cells [21]. The advantages of 3D cell culture manifest when mimicking pathological conditions such as cancer and specific tissues. In a 3D matrix environment, embedding single tumor cells form clustered, and rounded morphology, respectively, and result in individual cell migration and invasion, collective cell invasion or mixtures of invasive and necrotic cells as they do *in vivo* like environment [21, 27]. Additionally, 3D cell cultures and tissue models should promote advances in tissue engineering and could also facilitate the development and screening of new therapeutics [21, 28]. For example, cancer cells grown in 2D can easily be killed by low doses of chemotherapeutic drugs or low doses of radiation. If those same cells are treated in 3D matrix environment, they are resistant to the same doses of chemotherapeutic drugs or radiation, just like cancer as their found *in vivo* [29, 30]. For this reason, 3D cell culture could be more valid methods for testing and discovering new drugs

to treat cancer. Besides, providing 3D model systems for testing ideas and potential therapeutic interventions, they may also permit high-throughput drug screening on human tissues *in vitro* [21, 29, 30].

5. Objective

Epithelial-Mesenchymal Transition occurs via alteration in cell-cell contacts and cellular polarity, and is critical for cancer metastasis. EMT is supportive for different biological phenotypes, such as abnormal proliferation, enhanced migration, drug resistance, and self-renewal capacities. In this study, I have studied on EMT-mediated drug resistance as well as invasion of mesenchymal-like cells through 3D collagen gels. In the chapter 1, I focused on the roles of TM4SF5 (transmembrane 4 L6 family member 5) -mediated EMT in the gefitinib resistance of non-small cell lung cancer cells (NSCLC). I have hypothesized that TM4SF5 expression mediates EMT and leads to acquirement of gefitinib resistance in NSCLC. Further in the chapter 2, I have investigated how mesenchymal cell properties following EMT process may regulates the invasive properties such as invadopodia formation and ECM degradation in 3D collagen I-surrounded condition. However, unexpectedly 3D culture system using TM4SF5 stably overexpressing cells shows the technical problem of cell precipitation toward the bottom of the collagen I gels, which could not mimic real 3D environment. Therefore, alternatively using highly-invasive MDA-MB-231 breast cancer cells

which express high level of TM4SF5 in 3D collagen I gels were monitored for the underlying signaling mechanisms of invasive properties and for an establishment of an assay system to screen anti-metastatic reagents.

Ⅱ. Chapter 1

Gefitinib resistance of cancer cells correlated with TM4SF5-mediated epithelial–mesenchymal transition

1. Introduction

Based on pathological classification, lung cancer has been categorized into two, non-small cell lung cancer (NSCLC; 80% incidence) and small cell lung cancer (SCLC; 20% incidence [31]. One of the most important pathways in non-small cell lung cancer (NSCLC) is the epidermal growth factor receptor (EGFR) pathway. This pathway affects several crucial processes in tumor development and progression, including tumor cell proliferation, apoptosis regulation, angiogenesis, and metastatic invasion [32]. EGFR is a member of the receptor tyrosine kinase (TK) family that includes ERBB2, ERBB3, and ERBB4 [33]. The activation of receptor TKs leads to the autophosphorylation of the intracellular domain of EGFR, resulting in the activation of the Ras/mitogen-activated protein kinase (MAPK) pathway, phosphatidylinositol 3-kinases (PI3K)/Akt pathway, as well as signal transducers and activators of transcription signaling pathways [32]. For unknown reasons, EGFR kinase domain mutations seem to be restricted to a subset of NSCLC, although very rare mutations have also been reported in SCLC, cholangiocarcinoma, ovarian, colorectal, head and neck, oesophageal and pancreatic cancers [32]. Most NSCLC patients with activating EGFR mutations such as exon 19 deletion and the exon 21 L858R substitution were significantly sensitive to EGFR-TKIs [34]. Early NSCLC clinical trials can be initially treated with tyrosine kinase inhibitors (TKIs), such as epidermal growth factor receptor

(EGFR) inhibitor gefitinib [35, 36]. Treatment with continued EGFR-targeted therapy results in tumor responses, which are blunted by the selection or evolution of clones with resistant EGFR (T790M or S492R) or activation, upregulation or amplification of a bypass pathway such as *MET, HER2* or *KRAS*, or histologic transformation, EMT [37] (Fig.1).

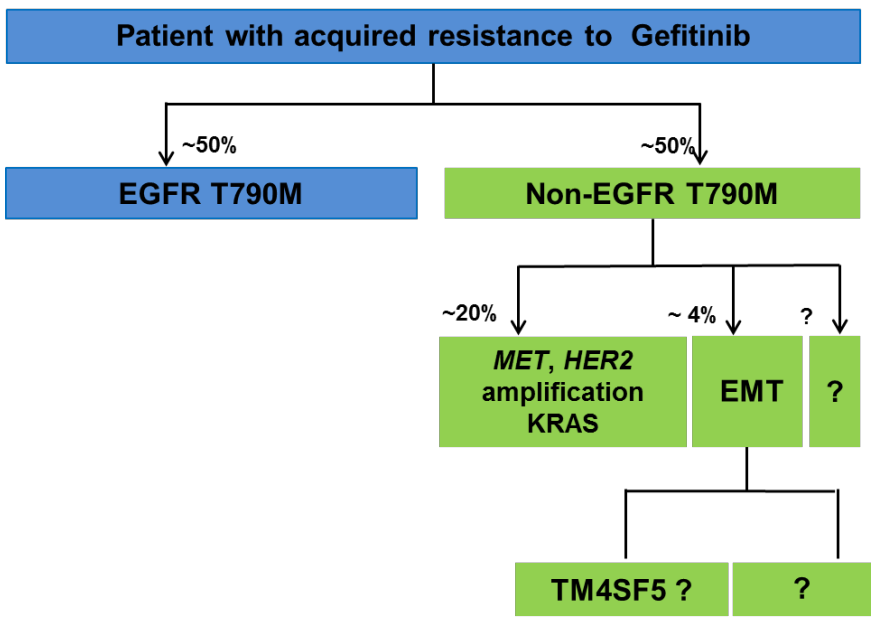

Fig. Ⅱ-1. Mechanism of acquired resistance to gefitinib in non-small cell lung cancer (NSCLC)

The T790M mutation occurs in approximately 50% of lung cancer patients with mutant EGFR, causes steric hindrance to TKI binding and enhances EGFR affinity for ATP with competitively decreased binding to gefitinib, an ATP-competitive kinase inhibitor [38, 39]. Except for T790M mutation, resistance to EGFR-targeted

therapies may occur through numerous pathways are clinically validated to trigger resistance to EGFR-TKIs and monoclonal antibodies, including amplification of KRAS, MET or HER2 (Fig. Ⅱ-1). The EMT was reported as an EGFR resistance mechanism in lung adenocarcinoma cell lines [40] and in patients treated with EGFR TKIs independent of a T790M mutation [41]. Among NSCLC, representatively gefitinib-sensitive (with an IC_{50} less than 0.025 μM) HCC827 cells have a deletion mutation in EGFR (from E746 to A750 in exon 19), whereas gefitinib-resistant (with an IC_{50} higher than 10 μM) NCI-H1975 cells have mutations in EGFR of T790M (within exon 20) and L858R (within exon 21) [42, 43]. However, acquired resistance to gefitinib in NSCLC can also be attributed to amplification of c-MET, a gene that encodes a receptor tyrosine kinase for hepatocyte growth factor [44]. A subpopulation from gefitinib-sensitive HCC827 cells (derived from the selection of resistant cells by culturing the cells to increasing gefitinib concentrations) demonstrates TKI resistance that maintains ErbB3/PI3K/Akt pathway activation and c-MET amplification, and inhibition of c-MET restored the sensitivity to gefitinib [45]. A gefitinib-resistant subpopulation of gefitinib-sensitive A549 cells shows activated PI3K activity and IGF1R pathway and inhibition of IGFIR restored the sensitivity to gefitinib [46]. Thus, bypassing EGFR signaling for cell growth and proliferation appears to be another mechanism for gefitinib resistance. Additionally, acquired TKI resistance of NSCLC appears

to correlate with epithelial–mesenchymal transition (EMT) that affects cell–cell contacts [40]. TGFβ1-mediated EMT causes resistance to gefitinib in addition to loss of E-cadherin and cytokeratin expression [47]. Thus, mesenchymal-like, but not epithelial-like, NSCLC cells may likely be resistant to TKI inhibition such that mesenchymal-like cells bypass EGFR signaling and acquire alternative routes of proliferative and survival signaling. For this reasons, membrane receptors may be cooperative to specify the alternative signaling pathway(s) or organized to allow synergistic or antagonistic relationships between them during communications of cancer cells with diverse extracellular cues. EMT enhances cell proliferation, migration, and invasion [48]. In addition to the TGFβ receptor and c-MET pathways, tetraspan TM4SF5 also induces EMT with persistent proliferation even under confluent conditions [49], and accelerates S-phase entry [50]. TM4SF5 expression decreases expressions of E-cadherin and ZO-1, and increases expression of smooth muscle actin (α-SMA) leading to a loss of cell–cell contacts, depending on cytosolic $p27^{Kip1}$-mediated RhoA inactivation and morphological changes; the TM4SF5-mediated EMT is blocked by a suppression of TM4SF5 or $p27^{Kip1}$ [49]. Even hepatocyte growth factor (HGF)-mediated EMT of endogenously TM4SF5-expressing hepatocytes was also blocked by TM4SF5 suppression [49]. The tetraspan TM4SF5 homologous to the lung cancer antigen L6 forms the

transmembrane 4 L six family with L6, IL-TIMP, and L6D [51]. This family shares four-membrane spanning membrane topology with genuine TM4SF (transmembrane 4 superfamily) or tetraspanins [52]. TM4SFs are known to regulate the integrity of a membrane receptor network, known as a ′tetraspanin-web′ or ′tetraspanin-enriched microdomain (TERM)′ where they collaboratively perform their biological function [53]. TM4SF5 collaborates with integrins or growth factor receptors for cellular function [54, 55]. Thus, we rationalized that gefitinib-resistant cells may adapt an alternative signaling pathway to bypass EGFR-dependent proliferation and survival signaling pathways via integrative roles by other membrane receptors such as tetraspanins. In this study, we explored whether TM4SF5 was involved in gefitinib resistance of cancer cells, because TM4SF5 has been shown to induce EMT and collaborate with other receptors on the cell membrane surface [54, 55]. We examined the expression and activity levels of signaling molecules in gefitinib-sensitive HCC827 and -resistant NCI-H1975 [42, 43] cells to determine whether TM4SF5-mediated signaling and cellular function correlate with resistance to gefitinib. We found that TM4SF5-mediated effects, including cytosolic $p27^{Kip1}$ stabilization and EMT, appeared to be involved in gefitinib resistance of NSCLC cells

2. Materials and Methods

1. Cells

HCC827 (with EGFR mutation of deletion from E746 to A750), NCI-H1975 (with EGFR mutation of L858R and T790M), NCI-H358 (with K-Ras mutation of G12C) lung carcinoma and MKN45 (with c-MET amplification) gastric adenocarcinoma cells (ATCC, Manassas, Virginia) were maintained in RPMI-1640 with 10% FBS, 10 U/ml penicillin, and 10 μg/ml streptomycin at 37 °C and 5% CO2. HCC827 cells stably-expressing mock or T790M EGFR or FLAG-TM4SF5 were established via transfection and G418 (500 μg/ml, A.G. Scientifics) selection and maintained in RPMI-1640 containing 10% FBS and 250 μg/ml G418.

2. Standard Western blots

Cells were transiently transfected with shRNA against control sequence or TM4SF5 for 24 h, or infected with adenovirus encoding for siRNA against control or $p27^{Kip1}$ sequence [49] overnight, before treatment with DMSO or gefitinib (LC Laboratories) for 24 h at different concentrations. Cells were then harvested for whole cell lysates with RIPA buffer (50 mM HEPES, pH 7.5, 0.1% SDS, 1% NP-40, 0.5% sodium deoxycholate, 150 mM NaCl, 50 mM NaF, 1 mM Na_2VO_4, 1 mM nitrophenylphosphate, and protease inhibitors). The lysates were normalized and processed for standard Western blots using antibody against E-cadherin (#610182,

BD Bioscience; sc-8426, Santa Cruz Biotech.), active EGFR (#610025), $p27^{Kip1}$ (#610241, BD Transduct. Lab.), $pS10p27^{Kip1}$ (#AP3191a, ABGENT), β-catenin (sc-7963, Santa Cruz Biotech.), pY1173EGFR (#4407), phospho-Y992EGFR (#2235), phospho-Y845EGFR (#2231), phospho-Y1045EGFR (#2237), phospho-Y1068EGFR (#2234), Erk1/2 (#9102, Cell Signaling), phospho-Erk1/2 (#9101s,Cell Signaling), FLAG (#2368), phospho-S473Akt (#9272, Cell Signaling), Akt (sc-7985R, Santa Cruz Biotech.), α-smooth muscle actin (SMA, #A2547, Sigma), vimentin (#V5255, Sigma), α-tubulin (#T5168, Sigma), EGFR (sc-03, Santa Cruz Biotech.), or TM4SF5 [49].

3. Cell imaging

Cells in normal culture media were imaged using a camera quipped CX41 microscopy (Olympus).

4. MTT assay

Cells (3-5 × 10^3 cells/well) were seeded in 96 well plates and 24 h later DMSO or gefitinib was treated at different concentrations (0 to 10 μM) for additional 72 h. After the reaction, cells were incubated with 20 μl MTT 3-(4,5-dimethylthiazol-2-yl)-2,5-diphenyltetrazolium bromide (Sigma) solution for 4 h at 37℃ and added150 μl

MTT solvent. Cover with tinfoil and agitate cells on orbital shaker for 5 min and read absorbance at 540nm.

5. Co-Immunoprecipitation

Whole cell lysates from stably FLAG-mock or FLAG-TM4SF5 expressing HCC827 cells under a subconfluent normal culture condition were incubated with anti-FLAG M2 sepharose beads (Sigma, 1 mg protein/40 μl of 50% slurry/condition) overnight at 4℃, washed twice with lysis buffer, and then twice with cold PBS. Immunoprecipitates were boiled within 2× SDS-PAGE sample buffer, and immunoblotted with anti-FLAG M2 (#2368, Sigma) or -EGFR (sc-03, Santa Cruz Biotech.) antibody.

6. Indirect immunofluorescence

Cells were seeded on precoated cover slips coated with fibronectin (10 mg/mL; BD Biosciences). The cells were incubated with normal conditions (10% FBS in RPMI 1670) for overnight and then treated with DMSO or 0.01 μM gefitinib for additional 18 h and fixed in 4% paraformaldehyde in PBS for 5 minutes. After being thoroughly washed with PBS, the cells were blocked with 3% BSA in PBS, and stained with anti-E-cadherin (#610182, BD Biosource) and vimentin(#V5255, Sigma) or anti-$p27^{Kip1}$ (#610241, BD Transduction, Lab) antibodies. DNA in

nucleus was stained by DAPI (Molecular Probes). Epifluorescence Microscope images were acquired on a microscope (BX51TR, Olympus) using 406/0.75 or 1006/1.3 (oil) NA U plan semi Apochromat objective lens (Olympus). The filters for GFP or Red fluorescent protein (RFP) were XF105-2 or XF115-2, respectively. A JVC KY-F75U CCD digital camera with IEEE 1394 interface was used. The TOMORO image analyzer software (Techsan Community Co., Korea) was used for image analysis.

7. DNA sequencing

DNA was extracted from cell pellets using the QIAamp DNA Mini kit (Qiagen, Hilden, Germany). DNA sequencing was performed as previously described [56].

3. Results

1. Gefitinib-resistant NCI-H1975 cells efficiently grow in a scattered pattern despite decreased EGFR signaling activity

While trying to understand the mechanisms underlying gefitinib resistance of NSCLC cells, we hypothesized that resistance might be caused by alternative signaling pathways emanating from membrane receptors that closely collaborate with EGFR. To test this hypothesis, we first compared the characteristics of gefitinib-sensitive HCC827 and -resistant NCI-H1975 cells [42]. To first confirm their susceptibility to gefitinib, we performed MTT assay using the cell lines treated with vehicle or gefitinib at various concentrations (0 to 10 μM). As we expected, HCC827 cells were sensitive to gefitinib with an IC_{50} of approximately 0.02 μM, whereas NCI-H1975 cells were resistant with an $IC_{50} \geq 10$ μM (Fig. Ⅱ-2A). Immunoblotting for EGFR and survival signaling molecules from subconfluent cells cultured under normal culture conditions showed that HCC827 cells exhibited higher phosphorylation and activity of EGFR than NCI-H1975 cells, whereas phosphorylation of Akt and Erk1/2 was slightly higher in the NCI-H1975 cells (Fig. Ⅱ-2B, middle). NCI-H1975 cells were more efficiently proliferative under normal culture conditions, compared with HCC827 cells (Fig. Ⅱ-2C). This pro-proliferative phenotype of NCI-H1975 cells indicates that alternative

EGFR-bypassing signaling pathway(s) may still be prominent. Additionally, NCI-H1975 cells grew in a scattered pattern whereas HCC827 cells grew in colonies (Fig. Ⅱ-2D). We also checked the expression level of TM4SF5 because of its pro-proliferative function [49] and role in EMT [57]. NCI-H1975 cells with a higher TM4SF5 expression showed a less E-cadherin (an epithelial marker) expression but more α-SMA and vimentin (mesenchymal markers) expressions, compared with HCC827 cells expressing a lower TM4SF5 level (Fig. Ⅱ-2B, bottom); thus, highly expressed TM4SF5 might presumably cause a scattered-growth pattern (Fig. Ⅱ-2D). Being consistent, HCC827 cells growing in a cobblestone pattern well-established cell–cell adhesions with E-cadherin at the cell–cell contact sites but showed a less vimentin expression, whereas NCI-H1975 cells growing in a scattered pattern showed less significant cell–cell adhesions with a lower E-cadherin expression and a more vimentin expression (Fig. Ⅱ-2E). Interestingly, both HCC827 and NCI-H1975 cell lines were not homogeneous with regards to E-cadherin and vimentin expressions; cell–cell contacts between HCC827 cells thus showed more E-cadherin in certain contacts but less in other contacts (Fig. Ⅱ-2E up and left), and NCI-H1975 cells showed more vimentin in certain cells but less in other cells (Fig. Ⅱ-2E, bottom and right). Taken together, these results suggest that NCI-H1975 cells have certain growth and survival

signaling activities presumably via TM4SF5 that are sufficient to alternatively bypass the EGFR signaling pathway, where a higher relative level of TM4SF5 to EGFR expression in NCI-H1975 cells was correlative with a less dependence on EGF signaling, compared with HCC827 cells, although cells might have heterogeneous EGFR and TM4SF5 expression levels.

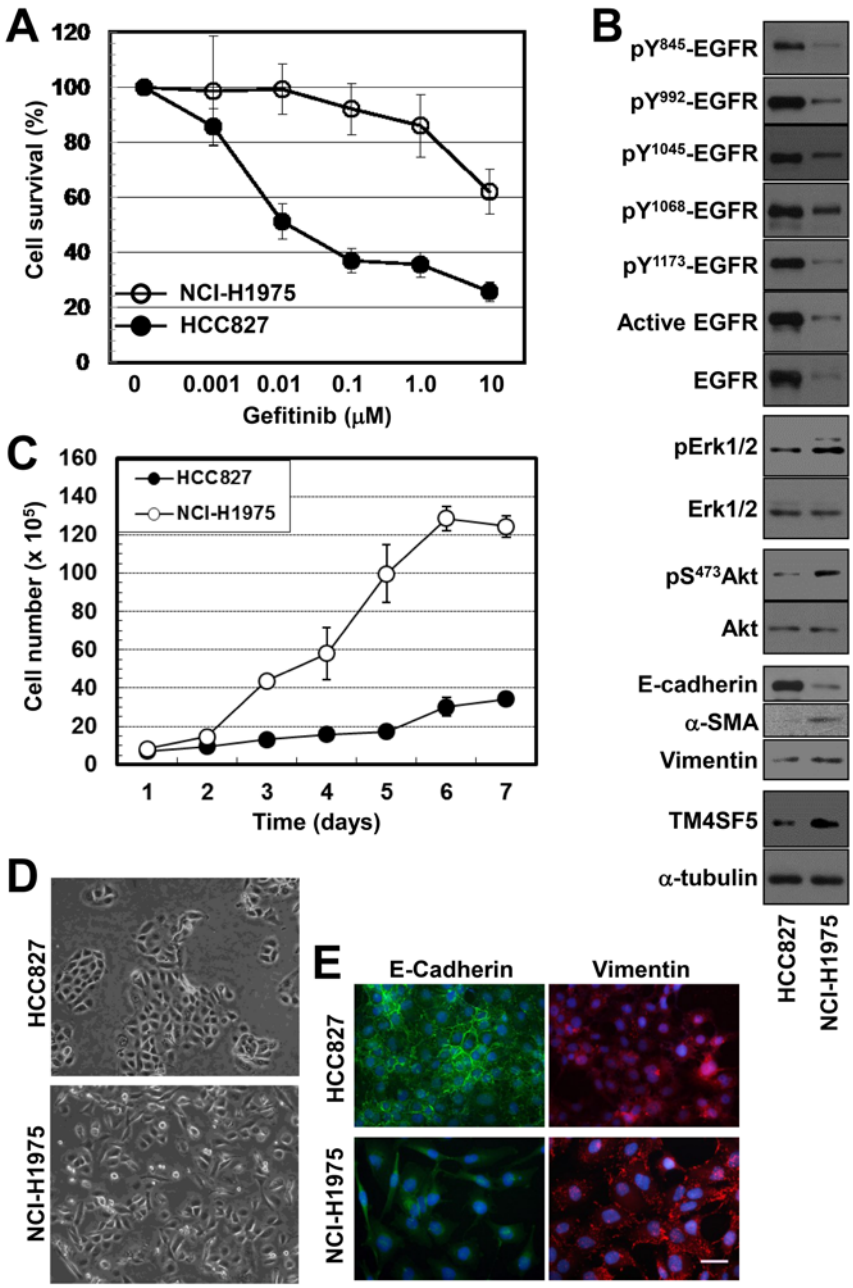
A
Cell survival (%)
120
100
80
60
40
20
0
NCI-H1975
HCC827
0
0.001
0.01
0.1
1.0
10
Gefitinib (μM)
B
pY845-EGFR
pY992-EGFR
pY1045-EGFR
pY1068-EGFR
pY1173-EGFR
Active EGFR
EGFR
pErk1/2
Erk1/2
pS473Akt
Akt
E-cadherin
α-SMA
Vimentin
TM4SF5
α-tubulin
HCC827
NCI-H1975
C
Cell number (x 10^5)
160
140
120
100
80
60
40
20
0
HCC827
NCI-H1975
1
2
3
4
5
6
7
Time (days)
D
HCC827
NCI-H1975
E
E-Cadherin
Vimentin
HCC827
NCI-H1975

Fig. Ⅱ-2. Gefitinib-resistant NCI-H1975 cells efficiently grow in a scattered pattern despite decreased EGFR signaling activity. (A) Gefitinib-sensitive HCC827 and -resistant NCI-H1975 cells were analyzed for survival in the presence of treatment with gefitinib at different concentrations (0 to 10 μM) via MTT assay. Each value was averaged from hexaplicate in one experiment of 3 independent MTT assay (i.e., hexaplicate×3 times). (B) The subconfluent cells were harvested and processed for standard Western blots for the indicated molecules. (C) Proliferations of the cells in the normal culture media were examined by determination of cell numbers at different times after cell seeding at the same number. (D) Phase-contrast images were saved at a subconfluent condition within the normal culture media. (E) Cells were seeded onto normal culture media-precoated cover glasses for 24 h and then immunostained for E-cadherin or vimentin, as explained in the Materials and Methods. Scale bar; 20 μm. The data shown are representative from 3 independent experiments.

2. Survival of gefitinib resistant cells in the presence of gefitinib correlated with sustained TM4SF5 expression

Further, the cells resistant to gefitinib due to an active mutation (G12C) in K-Ras (NCI-H358 cells) or amplification of c-MET (MKN45 cells) showed values of IC_{50} against gefitinib higher than 10 μM (data not shown) and also showed higher and sustained expressions of TM4SF5 in the presence of gefitinib treatment, compared to gefitinib-sensitive HCC827 cells (Fig. Ⅱ-3A and B). Interestingly, EGFR inhibition in gefitinib-sensitive HCC827 cells caused a reduced TM4SF5 expression (Fig. Ⅲ-A and B), which may be explained by the observations that TM4SF5 induction involves a cross-talk between TGFβ1 and EGFR signaling pathways and inhibition of EGFR activity abolishes the TM4SF5 expression [58]. This correlation between gefitinib resistance and sustained TM4SF5 expression may indicate a close functional relationship between EGFR and TM4SF5. Such an indication may also be supported by a concept that TM4SF5 as a tetraspanin or TM4SFs can function in regulation of membrane receptor integrity on cell surface [59]. Thus, we next examined whether a physical linkage between EGFR and TM4SF5 exists. From HCC827 cells stably-transfected with FLAG-mock or FLAG-TM4SF5 plasmid, EGFR was co-immunoprecipitated with FLAG-TM4SF5 and vice versa (Fig. Ⅱ-3B). These observations indicate that TM4SF5 may play

roles in the signaling for sufficient growth of the gefitinib-resistant cells, alternatively bypassing the EGFR signaling pathway.

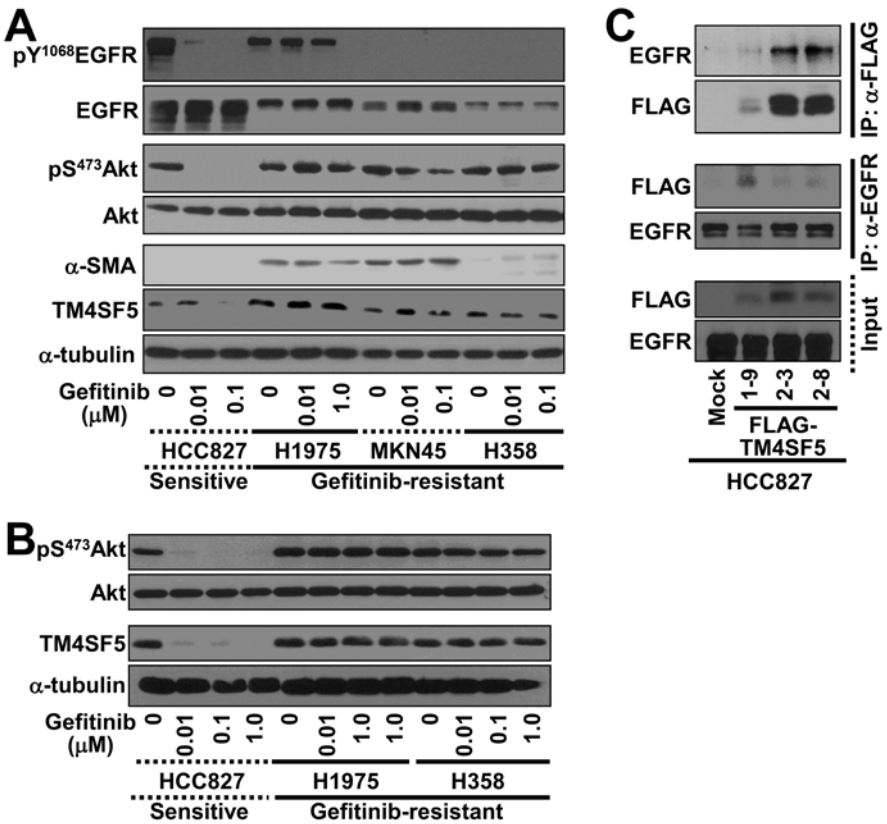
A
pY1068EGFR
EGFR
pS473Akt
Akt
α-SMA
TM4SF5
α-tubulin
Gefitinib (μM)
0 0.01 0.1 0 0.01 1.0 0 0.01 0.1 0 0.01 0.1
HCC827
H1975
MKN45
H358
Sensitive
Gefitinib-resistant
B
pS473Akt
Akt
TM4SF5
α-tubulin
Gefitinib (μM)
0 0.01 0.1 1.0 0 0.01 1.0 1.0 0 0.01 0.1 1.0
HCC827
H1975
H358
Sensitive
Gefitinib-resistant
C
EGFR
FLAG
IP: α-FLAG
FLAG
EGFR
IP: α-EGFR
FLAG
EGFR
Input
Mock
1-9
2-3
2-8
FLAG-TM4SF5
HCC827

Fig. Ⅱ-3. Survival of gefitinib resistant cells in the presence of gefitinib correlated with sustained TM4SF5 expression. (A and B) Sub-confluent gefitinib-sensitive HCC827 and –resistant NCI-H1975, MKN45, and H358 cells were grown with or without gefitinib at different concentrations for 24 h before preparation of whole cell lysates. (C) Whole cell lysates from sub-confluent FLAG-mock and FLAG-TM4SF5-stably expressing cells were immunoprecipitated with anti-FLAG M2 or -EGFR antibody-conjugated with sepharose before immunoblottings against EGFR or FLAG. The data shown represent 3 different experiments.

3. Sustained EGFR, Erk, and Akt signaling activities in gefitinib-resistant cells after gefitinib treatment correlated with TM4SF5-mediated effects, including cytosolic $p27^{Kip1}$ stabilization

When cells were treated with gefitinib at different concentrations from 0 to 1.0 μM, phosphorylation of EGFR, Akt, and Erk1/2 in gefitinib-resistant NCI-H1975 cells was sustained. However their basally-robust phosphorylation in gefitinib-sensitive HCC827 cells was dramatically reduced (Fig. Ⅱ-4A), as we have shown previously[60]. We thus tried to test whether such a differential response to gefitinib between HCC827 and NCI-H1975 cells might also correlated with higher and sustained TM4SF5 expression. Sustained TM4SF5-expression correlated with a different pattern of signaling activities between both cell lines treated with gefitinib: TM4SF5 levels in NCI-H1975 cells were highly sustained even with gefitinib treatment whereas TM4SF5 levels in HCC827 cells were reduced (Fig. Ⅱ-4A, bottom). An enhanced and sustained TM4SF5 expression results in stabilization of $p27^{Kip1}$ in the cytosol during TM4SF5-mediated EMT, multilayer growth [49], and acceleration of G1- to S-phase entry [50]. Therefore, cytosolic $p27^{Kip1}$ appears to play pro-tumorigenic roles in cell proliferation and migration. We thus examined the localization and expression of $p27^{Kip1}$ in HCC827 and NCI-H1975 cells in the absence or presence of gefitinib. Without gefitinib treatment, HCC827 cells showed $p27^{Kip1}$ expression mostly in the nucleus whereas NCI-

H1975 cells clearly demonstrated cytosolic $p27^{Kip1}$ (Fig. Ⅱ-4B, top). With gefitinib treatment, HCC827 cells exhibited more enhanced $p27^{Kip1}$ in the nucleus, suggestive of the gefitinib-mediated cell growth arrest and death. However, NCI-H1975 cells still showed cytosolic $p27^{Kip1}$ stabilization (Fig. Ⅱ-4B, bottom), indicating that TM4SF5 in NCI-H1975 cells might play tumorigenic roles even in the presence of gefitinib (Fig. Ⅱ-4B, bottom).

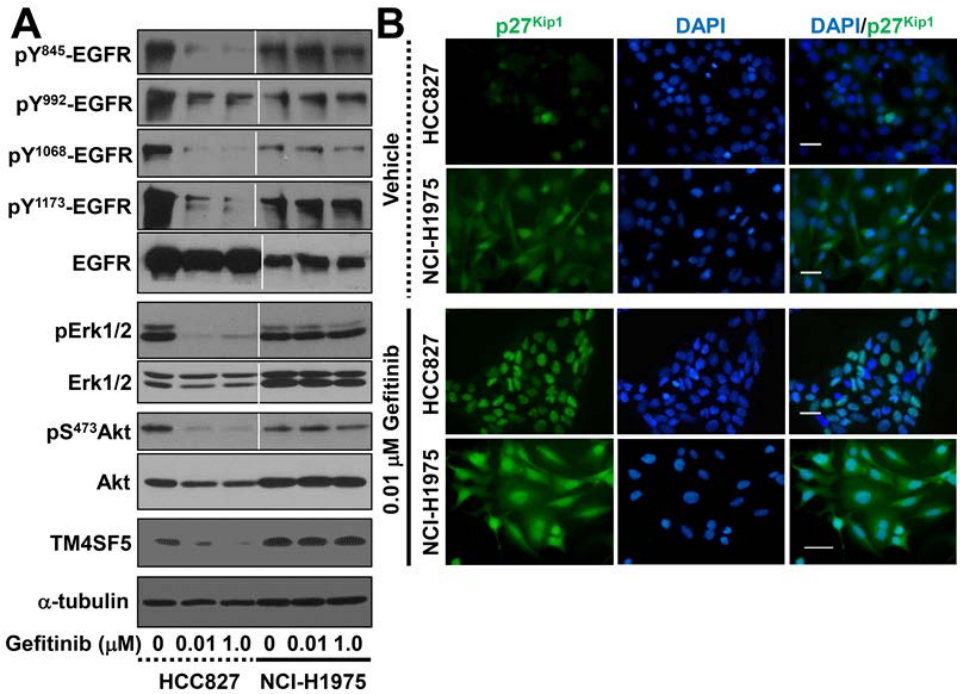
A
pY845-EGFR
pY992-EGFR
pY1068-EGFR
pY1173-EGFR
EGFR
pErk1/2
Erk1/2
pS473Akt
Akt
TM4SF5
α-tubulin
Gefitinib (μM) 0 0.01 1.0 0 0.01 1.0
HCC827 NCI-H1975
B
p27Kip1
DAPI
DAPI/p27Kip1
Vehicle
0.01 μM Gefitinib
HCC827
NCI-H1975
HCC827
NCI-H1975

Fig. Ⅱ-4. Sustained EGFR, Erk, and Akt signaling activities in gefitinib-resistant cells on gefitinib treatment correlated with TM4SF5-mediated effects including cytosolic p27^{Kip1} stabilization. Cells were treated with gefitinib at different concentrations (0 to 1.0 μM) for 24 h before preparation of whole cell lysates for immunoblottings for the indicated molecules (A), or reseeded on cover glasses precoated with fibronectin (10 μg/ml) for 2 h with DMSO or 0.01 μM gefitinib treatment before staining or indirect immunofluorescence using DAPI (blue) or anti-p27^{Kip1} antibody (green), respectively (B). Scale bars depict 20 μm. Representative data were from 3 isolated experiments

4. T790M EGFR mutation-mediated gefitinib resistance correlated with sustained TM4SF5 expression and EMT process

The T790M EGFR mutation renders gefitinib resistance in NSCLC cells [34]. Therefore, we investigated whether T790M EGFR introduction into HCC827 cells (already with EGFR mutation of deletion from E746 to A750) caused cells to concomitantly become gefitinib-resistant and display TM4SF5-mediated phenotypes. When the MTT assay was performed with HCC827 stable transfectants (mock and T790M EGFR clones 1–5 and 2–1) and NCI-H1975 cells in the presence of gefitinib treatment at different concentrations for 72 h, HCC827-T790M clones and NCI-H1975 cells clearly showed resistance to gefitinib, although HCC827 mock cells were sensitive (Fig. Ⅱ-5A). HCC827-T790M clones enhanced and sustained the phosphorylation of EGFR and Akt after gefitinib treatment (Fig. Ⅱ-5B). Unlike HCC827 mock cells growing in a pattern of cobble stones, HCC827-T790M cells grew in a scattered pattern (Fig. Ⅱ-5C). HCC827-T790M cells also increased α-SMA (a mesenchymal marker) and decreased E-cadherin (an epithelial marker) expression, indicating an EMT by T790M EGFR introduction, which were accompanied with enhanced and sustained TM4SF5 expression in the presence of gefitinib treatment (Fig. Ⅱ-5D). T790M EGFR transfection-mediated growth pattern in a scattering pattern was correlated

with the loss of E-cadherin from cell–cell contacts and more $p27^{Kip1}$ in the cytosol compared with mock-transfectants (Fig. Ⅱ-5E). These observations using HCC827-T790M clones may suggest that TM4SF5 is involved in gefitinib resistance that is associated with the T790M EGFR mutation.

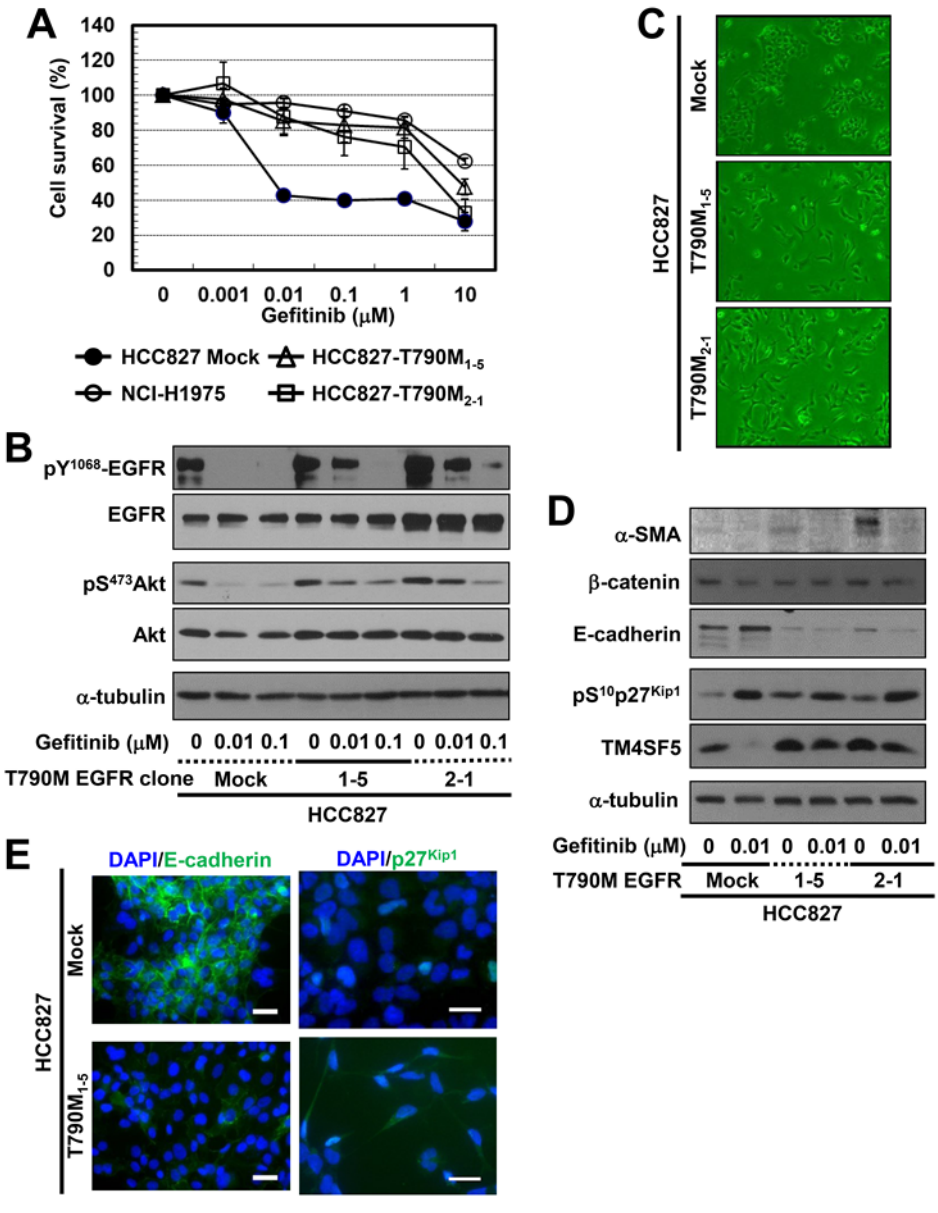
A
Cell survival (%)
140
120
100
80
60
40
20
0
0 0.001 0.01 0.1 1 10
Gefitinib (μM)
HCC827 Mock
HCC827-T790M1-5
NCI-H1975
HCC827-T790M2-1
B
pY1068-EGFR
EGFR
pS473Akt
Akt
α-tubulin
Gefitinib (μM) 0 0.01 0.1 0 0.01 0.1 0 0.01 0.1
T790M EGFR clone Mock 1-5 2-1
HCC827
C
HCC827
Mock
T790M1-5
T790M2-1
D
α-SMA
β-catenin
E-cadherin
pS10p27Kip1
TM4SF5
α-tubulin
Gefitinib (μM) 0 0.01 0 0.01 0 0.01
T790M EGFR Mock 1-5 2-1
HCC827
E
DAPI/E-cadherin
DAPI/p27Kip1
HCC827
Mock
T790M1-5

Fig. Ⅱ-5. T790M EGFR mutation-mediated gefitinib resistance correlated with sustained TM4SF5 expression and EMT process. (A) HCC827 cells stably-transfected with mock or T790M EGFR plasmids or NCI-H1975 cells were processed to MTT assay with DMSO or gefitinib treatment at different concentrations (0.001 to 10 μM). Each value was averaged from hexaplicate in one experiment of 3 independent MTT assay (i.e., hexaplicate x 3 times). (B and D) The cells were treated with DMSO or gefitinib at different concentrations for 24 h before whole cell lysates preparation for standard Western blots for the indicated molecules. (C) Subconfluent cells were imaged using a phase-contrast microscope. (E) HCC827 cells stably transfected with mock or T790M EGFR (clones 1–5) were reseeded on cover glasses precoated with fibronectin (10 μg/ml) for 2 h before indirect immunofluorescence to co-stain nuclear DNA (blue with DAPI) and E-cadherin (green, left) or $p27^{Kip1}$ (green, right). Scale bars: 20 μm. Data shown represent 3 different experiments.

5. TM4SF5 overexpression rendered gefitinib-sensitive cells to be gefitinib-resistant cells with EMT phenotypes

To test whether enhanced and sustained TM4SF5 expression causes gefitinib-resistance, we overexpressed TM4SF5 in HCC827 cells and examined whether the stable HCC827-TM4SF5 transfectants might become resistant against gefitinib, using the MTT assay. When cells were treated with gefitinib at different (0 to 10 μM) concentrations, TM4SF5-overexpressing HCC827 clones showed less sensitivity to gefitinib than did HCC827 mock cells, although they were less resistant than HCC827-T790M_{2-1} cells (Fig. Ⅱ-6A). At 0.01 μM gefitinib treatment, all TM4SF5-positive clones were significantly ($p \leq 0.05$) gefitinib-resistant differently from gefitinib-sensitive HCC827 cells, whereas at a higher 0.1 μM, HCC827-TM4SF5_{2-8} clone was insignificantly gefitinib-resistant, similar to HCC827 cells (Fig. 5A). This observation indicates that the TM4SF5 expression may not be all requirements for the gefitinib resistance. Additionally, the HCC827-TM4SF5 clones not only enhanced and sustained phosphorylation of EGFR and Akt but also enhanced TM4SF5 expression and $p27^{Kip1}$ Ser10 phosphorylation, which is known to cause its cytosolic localization [49], although their levels were slightly differential between clones (Fig. Ⅱ-6B). Indeed, compared with HCC827 cells, HCC827-TM4SF5 cells clearly showed cytosolic

localization of $p27^{Kip1}$ under basal and gefitinib-treated conditions (Fig. Ⅱ-6C). HCC827-TM4SF5 cells also grew in a scattered pattern (Fig. Ⅱ-6D), and showed increased mesenchymal marker expression (i.e., vimentin and α-SMA) and decreased an epithelial marker expression such as E-cadherin (Fig. Ⅱ-6E), again indicating that gefitinib-resistant HCC827-TM4SF5 cells underwent EMT.

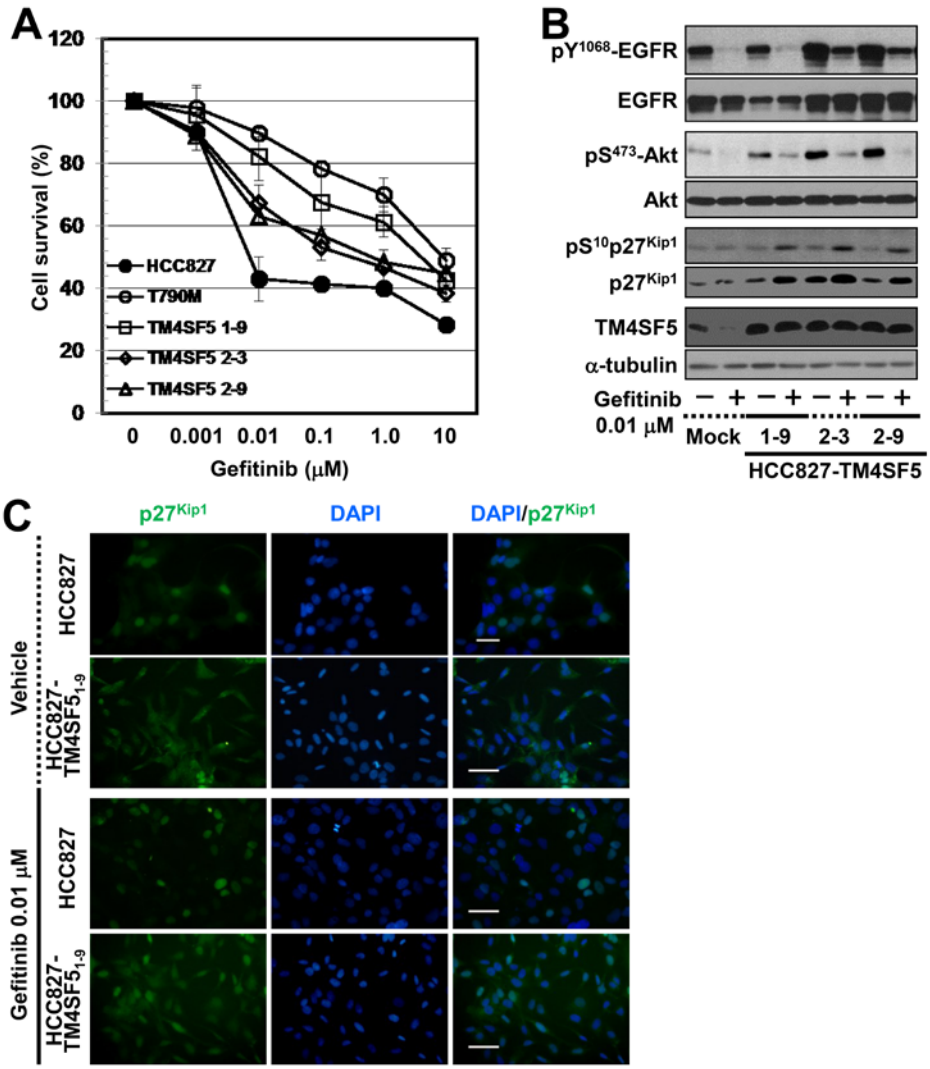
A
120
100
80
60
40
20
0
Cell survival (%)
HCC827
T790M
TM4SF5 1-9
TM4SF5 2-3
TM4SF5 2-9
0
0.001
0.01
0.1
1.0
10
Gefitinib (μM)
B
pY1068-EGFR
EGFR
pS473-Akt
Akt
pS10p27Kip1
p27Kip1
TM4SF5
α-tubulin
Gefitinib
0.01 μM
Mock
1-9
2-3
2-9
HCC827-TM4SF5
C
p27Kip1
DAPI
DAPI/p27Kip1
Vehicle
HCC827
HCC827-TM4SF5 1-9
Gefitinib 0.01 μM
HCC827
HCC827-TM4SF5 1-9

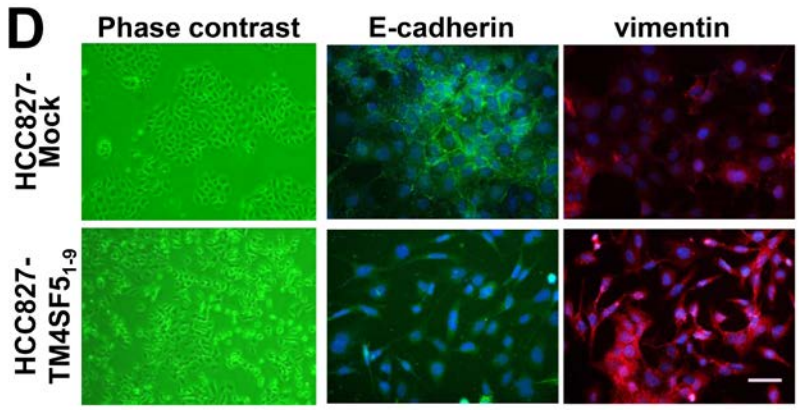
D
Phase contrast
E-cadherin
vimentin
HCC827-Mock
HCC827-TM4SF5$_{1-9}$

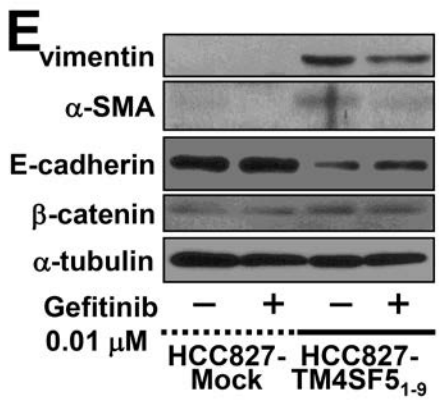
E
vimentin
α-SMA
E-cadherin
β-catenin
α-tubulin
Gefitinib − + − +
0.01 μM
HCC827-Mock
HCC827-TM4SF5$_{1-9}$

Fig. Ⅱ-6. TM4SF5 overexpression rendered gefitinib-sensitive cells to be gefitinib-resistant cells with EMT phenotypes. (A) HCC827 cells stably-transfected with mock, T790M EGFR, or TM4SF5 plasmids were analyzed by MTT assay for cell survival with DMSO or gefitinib treatment from 0.001 to 10 μM. Each value was averaged from hexaplicate in one experiment of 3 independent MTT assay (i.e., hexaplicate×3 times). (B, C, and E) Subconfluent HCC827-mock or -TM4SF5 stable clones were treated with DMSO or 0.01 μM gefitinib for 24 h and then harvested for standard Western blots for the indicated molecules (B and E), or reseeded on fibronectin (10 μg/ml) -precoated cover glasses for 2 h before DAPI staining (of nuclear DNA) and indirect immunofluorescence using anti-$p27^{Kip1}$ (green) antibody (C). Scale bars depict 20 μm. (D) The cells were imaged using a phase-contrast microscope or seeded onto the normal culture media-precoated cover glasses for 24 h and then immunostained for E-cadherin or vimentin, as explained in the Materials and methods section. Data shown represent 3 independent experiments.

6. Gefitinib resistance was reduced via suppression of TM4SF5 or $p27^{Kip1}$

TM4SF5 expression stabilizes cytosolic $p27^{Kip1}$ through enhanced stabilities of its mRNA and protein, and is correlated with the EMT process [49]. Therefore, we next examined whether suppression ofTM4SF5 or $p27^{Kip1}$ would revert gefitinib resistance of HCC827-T790M_{2-1} or HCC827-TM4SF5 cells. TM4SF5 suppression reduced phosphorylation of Akt (pS^{473}Akt) and reduced mesenchymal-like characteristics via increased E-cadherin but reduced α-SMA levels (Fig. Ⅱ-7A). Although basal $p27^{Kip1}$ was slightly increased presumably due to cytotoxicity, Ser10 phosphorylated $p27^{Kip1}$ (i.e., cytosolic $p27^{Kip1}$) decreased on TM4SF5 suppression, compared with control shRNA-transfection (Fig. Ⅱ-7A). It is thus likely that TM4SF5 suppression might block the TM4SF5-mediated effects on cytosolic $p27^{Kip1}$ stabilization and EMT and consequently gefitinib resistance. Meanwhile, when HCC827-T790M_{2-1} cells were infected with adenovirus expressing small interfering RNA (siRNA) against a control scrambled sequence or $p27^{Kip1}$. Suppression of $p27^{Kip1}$ in HCC827-T790M_{2-1} cells decreased phosphorylation of EGFR and Akt and enhanced the expression of E-cadherin and β-catenin under both basal and gefitinib-treated conditions, indicating that mesenchymal characteristics of HCC827-T790M_{2-1} cells were changed to epithelial characteristics after $p27^{Kip1}$ suppression (Fig. Ⅱ-7B). Although HCC827-T790M_{2-1}

cells were still more gefitinib resistant compared with the HCC827-T790M$_{2-1}$ cells with a suppressed TM4SF5 or p27^{Kip1} level, the cells showed a certain inhibition of EGFR by gefitinib (Fig. Ⅱ-7A and B), presumably because the exogenous T790M EGFR expression level of HCC827-T790M$_{2-1}$ cells might not be dominant over the endogenous EGFR level. Alternatively, it may be likely that HCC827-T790M$_{2-1}$ cells did not accompany the primary EGFR mutation such as the L858R mutation, so that L858R-T790M-EGFR-mediated affinity to ATP would not be available to cause an efficient blocking of ATP-competitive kinase inhibitor, gefitinib [39]. Being correlated, the p27^{Kip1}-suppressed cells reduced phosphorylation of Akt under basal conditions and further decreased activation of Akt after gefitinib treatment compared with non-suppressed cells, indicating that p27^{Kip1} suppression enhanced susceptibility to gefitinib treatment (Fig. Ⅱ-7B). Such a reversion from gefitinib-resistant to -sensitive cells via suppression of p27^{Kip1} also occurred in HCC827 cells overexpressing TM4SF5 (HCC827-TM4SF5$_{2-3}$), which decreased α-SMA, phosphorylation of EGFR and Akt but increased β-catenin after p27^{Kip1} suppression (Fig. Ⅱ-7C).

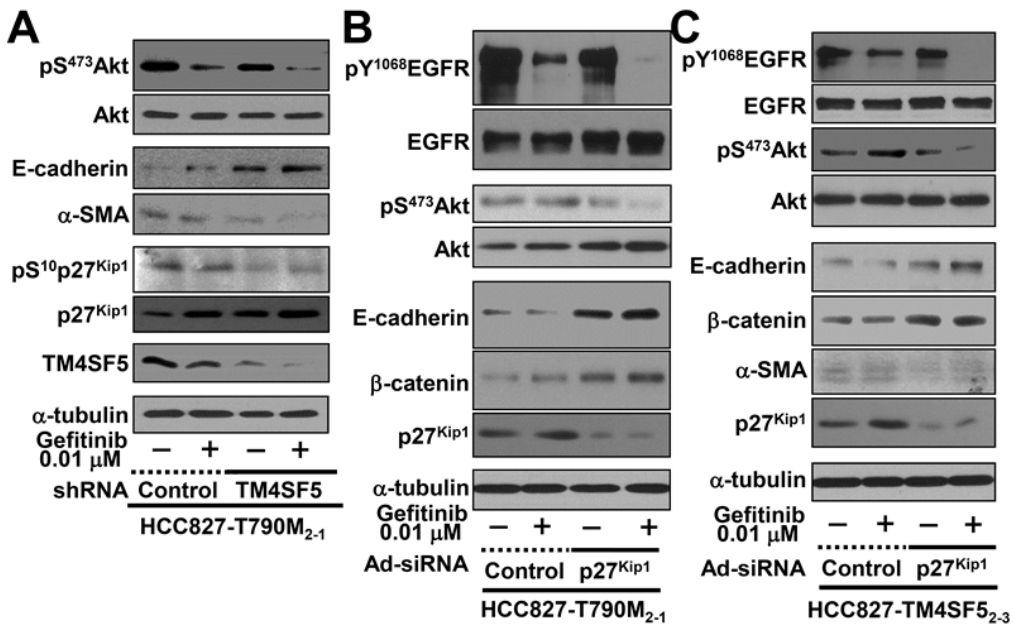
A
pS473Akt
Akt
E-cadherin
α-SMA
pS10p27Kip1
p27Kip1
TM4SF5
α-tubulin
Gefitinib 0.01 μM
– + – +
shRNA Control TM4SF5
HCC827-T790M2-1
B
pY1068EGFR
EGFR
pS473Akt
Akt
E-cadherin
β-catenin
p27Kip1
α-tubulin
Gefitinib 0.01 μM
– + – +
Ad-siRNA Control p27Kip1
HCC827-T790M2-1
C
pY1068EGFR
EGFR
pS473Akt
Akt
E-cadherin
β-catenin
α-SMA
p27Kip1
α-tubulin
Gefitinib 0.01 μM
– + – +
Ad-siRNA Control p27Kip1
HCC827-TM4SF52-3

Fig. Ⅱ-7. Gefitinib resistance was reduced via suppression of TM4SF5 or $p27^{Kip1}$. HCC827 cells stably transfected with T790M EGFR (A and B) or with TM4SF5 (C) were transiently transfected with shRNA against control sequence or TM4SF5 (A) or infected with adenovirus expressing siRNA against control sequence or $p27^{Kip1}$ overnight (B and C) and then treated with DMSO or 0.01 μM gefitinib for 24 h. Whole cell lysates were prepared, normalized and processed to standard Western blots for the indicated molecules. Data shown represent 3 isolated experiments

4. Discussion

In the present study, we observed that gefitinib resistance in cancer cells could result from expression of TM4SF5, leading to EMT, at least through cytosolic $p27^{Kip1}$ stabilization. So far evidence exists that gefitinib resistance in cancer cells is attributed to acquired mutations in EGFR (e.g., T790M) during TKI therapy that cause steric hindrance to gefitinib and enhance the affinity of mutated EGFR for ATP, thus lowering the affinity for gefitinib [38] to blunt the hypersensitivity of activating EGFR mutations [39]. T790M mutation-mediated gefitinib resistance accounts for 50% of TKI resistance in NSCLC patients carrying an EGFR mutations[39]. The resistance has also been attributed to the contribution of other membrane receptors or their downstream effectors. Gefitinib resistance of A549 cells is caused by PI3K activation and IGF1R pathway [46], which are suggested to be alternative pathways for proliferation that bypass the EGFR signaling pathway [39]. Additionally, PI3K/Akt activity and c-MET amplification, which accounts for 20% of TKI-resistant tumors [39], also result in gefitinib resistance of NSCLC [45]. However, c-MET is well-known to cause cell scattering and EMT as a receptor for hepatocyte growth factor [61]. Furthermore, loss of molecules at cell–cell contacts has recently been reported to be a possible determinant of sensitivity of NSCLC cells and xenografts against erlotinib, another EGFR kinase inhibitor [40]. Interestingly, as shown in the present study, TM4SF5, as a membrane protein that

induces EMT [49, 51], causes gefitinib resistance, and gefitinib-resistant cells with the T790M EGFR mutation (i.e., NCI-H1975 cells) showed enhanced expression of α-SMA and TM4SF5 as well. Stable transfection of T790M EGFR into HCC827 cells led to gefitinib resistance, enhanced TM4SF5 expression, and was correlated with EMT because the stable transfectants demonstrated enhanced expression of mesenchymal markers (i.e., vimentin and α-SMA) but reduced epithelial marker (i.e., E-cadherin). Stabilization of $p27^{Kip1}$ in the cytosol has been shown in diverse tumor tissues [62], and accounts for inactivation of RhoA GTPase via direct interaction, resulting in regulation of actin dynamics and cell migration [63, 64]. TM4SF5 expression causes cytosolic $p27^{Kip1}$ stabilization, and EMT with loss of E-cadherin expression, while suppression of TM4SF5 or $p27^{Kip1}$ recovers E-cadherin expression at cell–cell contacts [49]. Additionally, suppression of $p27^{Kip1}$ results in a delay of TM4SF5-accelerated G1- to S-phase entry [50]. Interestingly, cytosolic $p27^{Kip1}$ might also be involved in gefitinib resistance of NSCLC that is mediated by TM4SF5 or EGFR T790M expression, because suppression of $p27^{Kip1}$ in gefitinib-resistant cells rendered these cells to be gefitinib sensitive. Therefore, cytosolic $p27^{Kip1}$ appears to be tumorigenic by being involved in TM4SF5-mediated EMT, although nuclear $p27^{Kip1}$ can be anti-tumorigenic as a cyclin-dependent kinase inhibitor [65]. In addition to being related to EMT, TM4SF5 as a tetraspanin traversing the membrane four times may presumably locate to the

tetraspanin-enriched microdomain (TERM) of the cell plasma membrane, playing roles in organizing the integrity of membrane receptors including integrins and growth factor receptors through massive protein–protein interactions [53, 66, 67]. Integrin α5 binds to TM4SF5 and is more efficiently retained on the surface of hepatocytes that express TM4SF5, compared with the surface of cells lacking TM4SF5 [54]. Similarly, CD63 and CD82 are more likely to be found on the surface of cells that overexpress L6-Ag [68], which is another member of the transmembrane 4 L six family [52]. Thus, it cannot be ruled out that IGF1R, a player in TKI resistance [46], may also be susceptible to TM4SF5- or tetraspanin-mediated organization of receptor networks on the cell surface. TM4SF5-mediated regulation of membrane receptor networks on the cell surface may also lead to the gefitinib resistance. In the present study, we observed that gefitinib-sensitive cells showed a higher basal EGFR activity, compared with gefitinib-resistant cells. However, the EGFR activity of gefitinib-sensitive cells was dramatically reduced after gefitinib treatment, whereas the EGFR activity of resistant cells was more persistent (similar to the basal level) even after gefitinib treatment. Therefore, such persistent EGFR activity of resistant cells after gefitinib treatment might result from effective retention of EGFR on the cell surface via a physical linkage between TM4SF5 and EGFR. Indeed, in the present study, we have observed that gefitinib-resistant cells showed a co-immunoprecipitation between the both receptors.

Therefore, TM4SF5-mediated effects, including EMT and membrane retention of EGFR via protein interactions, may be involved in gefitinib resistance of cancer cells.

In epithelial cells, TM4SF5 is shown to interact with integrins α2 or α5 during migration or angiogenesis, respectively [54, 55]. In Cos7 fibroblasts, TM4SF5 regulates actin remodeling and focal adhesion dynamics through an interaction with integrin α2, which is negatively controlled by serum treatment [69]. It is thus likely that cross-talks between TM4SF5 and other membrane receptors such as integrins or growth factor receptor are involved in the regulation of diverse cellular functions, including cell–cell adhesions. It is suggested that different TERM constituents may lead to diverse membrane properties such as signaling, cytoskeletal connection or curvatures for different cellular functions [70]. In addition to TM4SF5 [48, 49], another tetraspanin, CD151 is also shown to induce EMT via a signaling through integrin α6β1 and PI3K [71]. Growth factor receptors or receptor tyrosine kinases, such as c-MET is also well-connected with EMT [72]. Furthermore, attenuation of EGFR signaling activity is obviously correlated with mesenchymal cell features [73]. Therefore, depending on roles of tetraspanins through massive protein–protein interactions at TERMs, tetraspanins may be

involved in regulation of growth factor receptor activity and concomitantly of cell–cell adhesions.

Continuous EGFR-TKI therapy causes drug resistance by acquired EGFR T790M mutation [39]. In the current study, we found that introduction of EGFR T790M into gefitinib-sensitive NSCLC cells also resulted in gefitinib resistance and TM4SF5 overexpression. Furthermore, overexpression of TM4SF5 in gefitinib-sensitive cancer cells resulted in gefitinib resistance, although it occurred at a resistance level less than that of the EGFR T790M mutation, probably indicating that more than TM4SF5 might be involved in gefitinib resistance. Such TM4SF5 overexpression-mediated resistance to gefitinib appeared not to involve the secondary acquired EGFR mutation at T790 or other residues, because resistant cells via TM4SF5 overexpression did not show any acquired EGFR mutation within exons 18, 19, 20, and 21 (Table 1). Therefore, TM4SF5 may transduce an alternative signaling pathway that bypass the EGFR signaling pathway, accounting for another major portion of gefitinib resistance in lung cancer irrelevant to acquired EGFR mutation of T790M. Interestingly, the gefitinib resistant cells alternatively due to c-MET amplification (MKN45 cells) or K-Ras activation (NCI-H358 cells) also showed higher expression levels of TM4SF5, compared to gefitinib-sensitive HCC827 cells. It may thus be likely because TM4SF5 can possibly be involved both in EMT mediated and in EGFR-bypassing signaling-

mediated resistance against gefitinib. Being consistent, TM4SF5 overexpression accelerates cell cycle progression from G1 phase to S phase [50], suggesting that TM4SF5 may efficiently stimulate a cell growth-stimulatory signaling even in the condition where EGFR signaling may be less functional.

	EGFR					
	exon	mutation	Nucleotide Change	Amino Acids Change	Forward	Reverse
HCC827-TM4SF5$_{1-9}$	e18	no Mutation	-	-	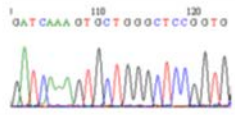	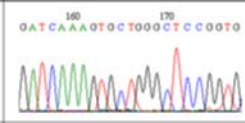
	e19	homozygote mutation	c.2236_2250del	p.Glu746_Ala750del	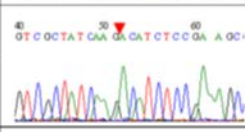	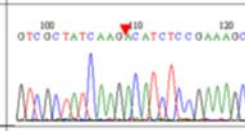
	e20	no mutation (homozygote SNP)	SNP(c.2361 G>A)	p.Gln787Gln	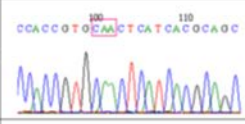	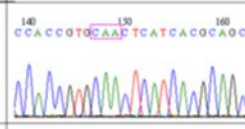
	e21	no mutation	-	-	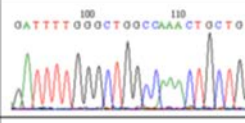	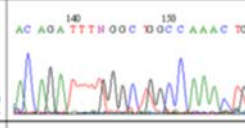
HCC827-TM4SF5$_{2-3}$	e18	no mutation	-	-	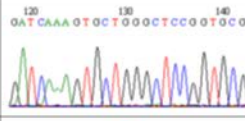	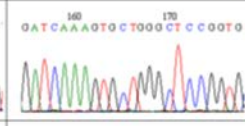
	e19	homozygote mutation	c.2236_2250del	p.Glu746_Ala750del	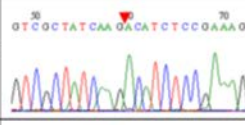	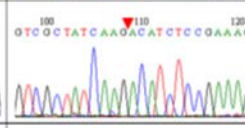
	e20	no mutation (homozygote SNP)	SNP(c.2361 G>A)	p.Gln787Gln	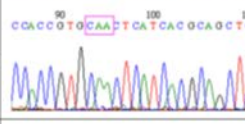	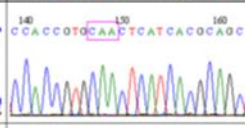
	e21	no mutation	-	-	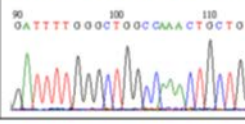	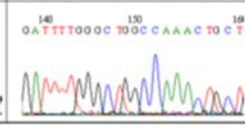

Table 1. TM4SF5-overexpressing HCC827-TM4SF5 clone cells do not accompany any mutations in *EGFR*. The HCC827-TM4SF5 clone cells were analyzed for any mutations in *EGFR* at exon 18, 19, 20, and 21. Cell pellets prepared from trypsinization were used for genomic DNA preparation and *EGFR* sequencing, as described previously [56]. Note that no mutations in *EGFR* were obtained by overexpression of TM4SF5.

5. Conclusions

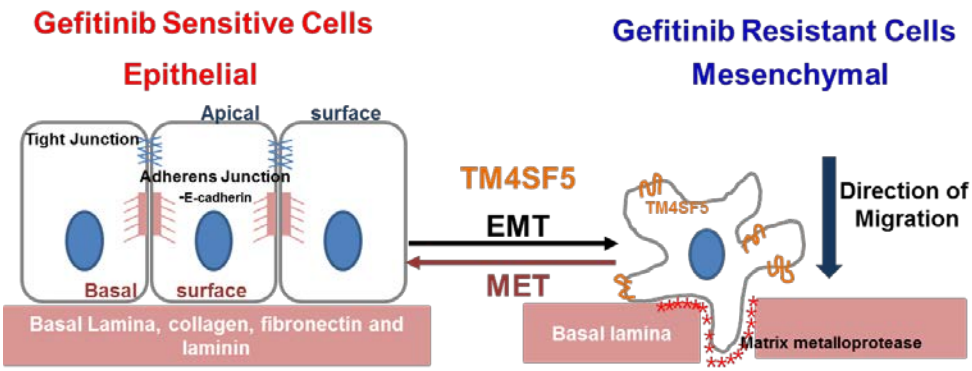

Fig. Ⅱ-8. TM4SF5-mediated EMT induced gefitinib resistance of NSCLC cells.

In this chapter, we showed that acquired EGFR T790M mutation- and/or TM4SF5-mediated EMT induced gefitinib resistance of HCC827 cells which are sensitive to gefitinib. TM4SF5-mediated EMT and regulation of activity or integrity of membrane receptors including EGFR, IGF1R, and/or c-MET on the cell surface, may likely be important for gefitinib resistance of cancer cells. It may thus be interesting to examine whether gefitinib-resistant lung cancer patients overexpress TM4SF5, compared with gefitinib-sensitive patients, to get idea whether anti-TM4SF5 reagent may be a therapeutic reagent against gefitinib-resistant lung cancer patients.

Ⅲ. Chapter 2

Regulation of migration and invasion of mesenchymal like- MDA-MB-231 cell in 3D collagen gels

1. Introduction

During metastasis, migration and invasion of cancer cell are dynamically regulated by coordinated signaling pathways that respond to the extracellular matrix (ECM) or soluble factors of the tumor microenvironment [74]. Invasion involves degradation of the ECM via formation of invasive morphological features including invadopodia and podosomes, which sense the ECM around the edges of a cell and involve adhesion-dependent signaling activities [75, 76]. Invadopodia are invasive protrusions with proteolytic activity including MT1-MMP uniquely found in tumor cells [77]. Invadopodia can regulate by cortactin during precursor formation (stage 1) which forms a complex involving cortactin, Arp2/3 and N-WASp binding domains. Cortactin is then tyrosine phosphorylated, which activates cofilin's severing activity to generate free barbed ends and the Arp2/3 complex can use these cofilin generated efficient actin polymerization (stage 2). Cortactin is then dephosphorylated, which stabilizes the invadopodium precursor for maturation (stage 3). Finally, matured invadopodium efficiently degrades ECM (stage 4) [78]. The formation of invasive features involves dynamic actin remodeling. c-Src-mediated cortactin phosphorylation causes activation of Arp2/3, consequently leading to actin branching and polymerization at lamellipodia and invadopodia [78, 79].

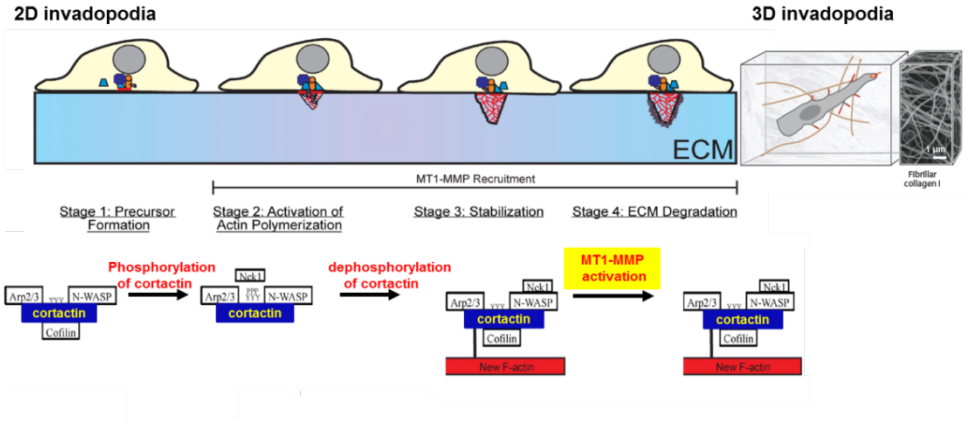

Fig. Ⅲ-1. Cortactin controls the stages of invadopodium assembly and maturation [78].

Therefore, cell migration, invasion, and the formation of invasive morphological features could be targets to prevent cancer metastasis. However, investigating the mechanisms behind certain cell behaviors is critical for developing more effective targeted-therapies. While informative, studies investigating the effects of extracellular cues on cell functions in two dimensional (2D) conditions may not relate to the *in vivo* or *in situ* behaviors of cancer cells, because cancer lesions are exposed to a 3D microenvironment [21, 80]. Cell behaviors, including migration and invasion, are often investigated in a 2D environment. Although the significance of the tumor microenvironment in promoting tumorigenesis and metastasis has been suggested in many *in vitro* and *in vivo* studies [81], studies evaluating cells in a 2D environment are limited to mimic *in vivo* tumor lesions, whereas embedding cells in a 3D environment allows for the cells to receive and

respond to environmental cues like *in vivo* situation. The tumor microenvironment includes ECM proteins, neighboring cells, and soluble factors consisting of growth factors, cytokines, and chemokines, which influence cancer cell function and behavior, and have been targeted for clinical treatment [82]. Various environmental stressors including ECM stiffness, extracellular acidity, and intratumoral hypoxia, can affect cancer cells and neighboring stromal fibroblasts and inflammatory cells eventually leading to metabolic alterations, the stimulation of mitogenic and survival signaling pathways [83] . Studies evaluating cells in a 2D environment are limited in their ability to mimic *in vivo* tumor lesions, whereas embedding cells in a 3D environment allows for the cells to receive and respond to environmental cues like *in vivo* situation. Although an *in vitro* 3D environment cannot completely mimic the *in vivo* tumor site, studying the mechanistic behaviors of cancer cells in a 3D environment is beneficial for clinical and pharmaceutical purposes. In this study, we evaluated whether and how the invasive behaviors of MDA-MB-231 breast cancer cells embedded in a 3D collagen I gel could be regulated. Exposing the MDA-MB-231 cells to various environmental parameters during culture in the 3D collagen gels decreased JNKs signaling activity (i.e., decreased Ser63 phosphorylation of c-Jun, pS63c-Jun), activated TGFβ1/Smads signaling, enhanced Snail1 expression levels, and reduced cortactin expression levels. Inactivation of the JNKs signaling pathway led to the Smad2/Smad4-activation-mediated expression of Snail1, which in turn suppressed cortactin. As a result,

invadopodia formation was less efficient within the 3D collagen I gels, further with cortactin and/or membrane type I matrix metalloproteinase (MT1-MMP) localization at perinuclear regions, leading to less migration and invasion. Therefore, the signaling network consisting of JNKs, Smads, Snail1, and cortactin was revealed to modulate migration and invasion of the MDA-MB-231 cells embedded in 3D collagen I gel.

2. Material and Methods

1. Cells, plasmids, and siRNAs

MDA-MB-231, MDA-MB-436, MDA-MB-468, T47D, and MCF7 breast adenocarcinoma cells were obtained from the American Type Culture Collection and grown in complete RPMI-1640 (JBI., Daegu, Korea) supplemented with 10% FBS (fetal bovine serum, GIBCO, Invitrogen) and antibiotics (GIBCO, Invitrogen). Cells were grown in a humidified incubator with 5% CO_2 at 37°C. DNA plasmids; pcDNA3-DN-JNK1, pcDNA3-Flag-Snail1 WT, pmCherry-MT1-MMP, or pEGFP-cortactin WT were transfected before being embedded in 3D collagen type I gel (PureCol., Advanced BioMatrix, San Diego, CA). Some cells were co-transfected with fluorescein conjugated SignalSilence® control siRNA and SignalSilence® SAPK/JNK siRNA (Cell Signal Technology) or On-Target plus Smartpool siRNA duplexes each were designed to target human snail1 (NM_005985 Dharmacon, Lafayette, CO). As a negative control, cells were transfected with nonspecific siRNA pool (Dharmacon). All cDNA vectors or siRNA transfections were done with Lipofectamine™ 2000 (Invitrogen) according to the manufacturer′s instructions.

2. Polydimethylsiloxane device fabrication

A polydimethylsiloxane (PDMS, Sylgard 184, Dow Corning) prepolymer was made using a 10:1 (w/w) mixture of PDMS base and curing agent that was cast against the master and thermally cured to obtain a negative replica-molded piece. After separation from the master, 4-or 8-well chamber was punched out of the molded PDMS with an 8 mm biopsy punch. The PDMS devices and glass coverslips were cleaned with residue-free tape and N_2 gas air gun, and then treated with oxygen plasma for 45 sec to form covalent bonding between them. To restore hydrophobicity to the PDMS after plasma treatment, the devices were kept in 60°C dry oven for at least 24 h and sterilized by UV irradiation before uses.

3. Antibodies and reagents

Antibodies and reagents were obtained from the following sources; Sigma-Aldrich, 10x RPMI, α-tubulin; BD Biosciences, anti-cortactin mAb (4F11), -human HIF-1α and BD Matrigel™ Basement Membrane Matrix; Cell Signal Technology, anti-snail mAb (L70G2), anti-smad2/3, anti-phospho-smad2, anti-phospho-smad3, anti-pS^{63}c-Jun, c-Jun, and phospho-MAPKAPK-2(Thr222) antibody; Millipore, anti-MT1-MMP mAb (MAB3328), anti-cortactin (p80/85) antibody (4F11), Alexa Fluor® 488; Santa Cruz Biotechnology, Inc., anti-JNK rabbit pAb; Invitrogen, diaminophenylindole (DAPI), and rhodamine phalloidin; Jackson ImmunoResearch Laboratories, HRP-conjugated secondary antibodies; LC-LABs,

SP600125, U0126, SB203580; Advanced BioMatrix, PureCol type I bovine collagen solution (3.2 mg/ml); PeproTech, TGFβ1; R&D systems, anti-TGFβ (1,2,3) antibody (MAB1835)

4. Cell culture in three-dimensional type I collagen gels

3D collagen type I gels for cell culture were prepared using PureCol type I bovine collagen (Advanced BioMatrix, Poway, CA) in 24-well culture plate. Collagen I mixtures (2.5 mg/ml) were made by adding the appropriate volumes of 10x reconstitution buffer (260 mM sodium bicarbonate and 200 mM HEPES), 10x RPMI (Sigma Aldrich) to the purchased collagen 1 solution, with slowly and gently pipetting up and down. To adjust the pH of the collagen I solution mixture, we used the ice-cold solution of 2 N NaOH and measured the pH of the neutralized collagen with pH paper strip. The pH must be in the range of 7.2 to 7.4. The neutralized solution of collagen I was incubated on ice for 3 to 5 min to allow the pH of the solution to be equilibrated, and then centrifuged at 10,000 g for 3 min to get rid of air bubbles at 4°C. The bottom layer of 2.5 mg/ml collagen I was made in each well with 30 μl and allowed to gel by incubation for 30 min at 37°C. Top layer that cell suspension containing 300,000 cells was mixed with the 150 μl neutralized collagen I mixture was loaded onto the bottom layer, and allowed to gel by incubation for 30 min at 37°C. In cases, three-dimensional Matrigel (BD

Biosciences) or a mixture of Matrigel™ and type 1 Collagen (t a ratio of 5 mg/ml to 1.25 mg/ml) was also prepared by the same procedure as above. Media with 10% FBS was then overlaid on top of the gel with or without SP600125 (50 μM) for 24 to 72 h. The medium was replaced every other day. In case, pH-controlled media (using filter 1N HCl) with 10% FBS was replenished every day for 2 days after the embedding, or hypoxic condition at 5% 5% O_2 was applied for 4 h after the embedding, in parallel to the normal condition.

5. Immunoblottings

Whole cell lysates from 2D cultures were prepared, as described previously [84]. To obtain the whole cell lysates from 3D collagen cell cultures, cells embedded into 3D collagen I and cultured for 3 days were transferred into ice-cool 1.5 ml tubes from 24-well culture plate using truncated-pipette tips and spun down for 1 min at 2,500 g to remove residual medium and collagen at 4°C. Cell pellets within collagen masses were washed with ice-cold PBS and then solubilized in a modified RIPA (50 mM Tris-HCl, 150 mM NaCl, 1% NP-40, and 0.25% sodium deoxycholate) with a protease inhibitor cocktail (GenDepot, USA) homogenizing with truncated pipette tips once every 20 min for 60 min on ice. The extracts were centrifuged at 15,000 g for 30 min at 4°C and then the lysate was collected from the supernatant. The obtained whole extracts were diluted with 4x SDS

polyacrylamide gel electrophoresis (SDS-PAGE) sample buffer and boiled at 100℃ for 10 min. Because of the presence of the collagen I, protein concentrations could not be used to normalize the protein amount in the lysates. The lysates at an equal sample volume were initially loaded for α-tubulin levels by standard Western blotting. Based on the intensities of α-tubulin bands in the experimental conditions, the samples were normalized for equal protein loading in standard Western blots.

6. RT-PCR and quantitative real time PCR (qPCR)

Total RNA was extracted from cells in 3D collagen I gels using TRIzol (Invitrogen) according to the manufacturer′s protocol. One μg of total RNA was reverse transcribed using amfiRivert Platinum cDNA Synthesis master mix (GenDepot, USA), and qPCR was performed using DreamTaq Green PCR Mater Mix (Thermo Scientific) and 7900HT Fast real time system (Applied Biosystems). Primers for *Snail1, Cortactin, JNK1, Smad2/3, Twist, Snail2/Slug and GAPDH* mRNA were designed using Primer3 software. Primer sequences were as follow: *CDH1(E-cadherin)*, forward 5′-TGCCCAGAA AAT GAAAAAGG-3′ and reverse 5′-GTGTATGTGGCAATGCGTTC-3′ ; *CTTN(cortactin)*, forward 5′-CCTGGAA ATTCCTCATTGGA-3′ and reverse 5′-CACAAAATCAGGGTCGGTCT-3′; *JNK1*,

forward 5′-TTGGAACAC CATGTCCTGAA-3′ and reverse 5′-ATGTACGG GTGTTGGAGAGC-3′; *Snail1*, forward 5′-GGTTCTTCTG CGCTACTGCT-3′ and reverse 5′-TAGGGCTGCTGGAAGGTAAA-3′; *Smad2*, forward 5′-CGAAATGC CACGGTAGAAAT-3′ and reverse 5′-CCAGAAGAGCAGCAAATTCC-3′; *Smad3*, forward 5′-CCCCAGAGCAATATTCCAGA-3′ and reverse 5′-GGCTCGCAG TAGGTAACTGG-3′; *Twist*, forward 5′- GGAGTCCGCAGTCTTACGAG-3′ and reverse 5′-TCTGGAGGACCTGGT AGAGG-3′; *Snail2/slug*, forward 5′-GGGGA GAAGCCTTTTTCTTG-3′ and reverse 5′-TCCTCATGTTTGTGCA GGAG-3, *GAPDH*, forward 5′-GAGTCAACGGATTTGGTCGT-3′ and reverse 5′-GACAAGCTTCCCGTTCTC AG-3′.

7. 3D immunofluorescence analysis

Cells were cultured within Polydimethylsiloxane prepolymer (PDMS) glass coverslip and fixed directly with 4% formaldehyde for 30 min at room temperature (RT), and subsequently treated with 100 mM glycine to quench residual aldehyde groups. After PBS washing, cells were permeabilized for 30 min with 0.5% Triton X-100 at room temperature (RT) and blocked for 2 h with PBS in 3% BSA. Some cells were stained with either fluorescein-labeled phalloidin (Molecular

Probes, 1:250) or Alexa Fluor® 488-labeled anti-cortactin (Millipore, 1: 200) at 4°C overnight. Cells were then washed with washing buffer (PBS in 130 mM NaCl, 13 mM Na_2HPO_4, 3.5 mM NaH_2PO_4, pH 7.4). Nuclei were counterstained with diaminophenylindole (DAPI; Molecular Probes). Confocal images were captured using a confocal microscope with a Nikon Plan-Apochromat 60x/1.4 N.A. oil objective (Nikon eclipse Ti; NiKon, Japan) and analyzed using the NIK software or IMARIS imaging software (Bitplane AG, Zurich, Swiss).

8. Chromatin immunoprecipitation (ChIP) analysis

The MDA-MB-231 cells were embedded in 3D collagen I and cultured in the absence (control) or presence of SP600125 (50 μM) for 3 days. Cell culture media were sucked out and cells in 3D collagen I were fixed with 3.7% formaldehyde for 30 min at RT and washed with 100 mM glycine addition and PBS. The fixed cells were transferred 1.5 ml centrifuge tube on ice and washed with ice-cold PBS including protease inhibitor cocktails and spun down at 5,000 ×*g* for 1 min at 4°C. The supernatants were removed and the cells were lyzed with SDS buffer (1% SDS, 10 mM EDTA, 50 mM Tris, pH 8.1 and 1 mg/ml each of aprotinin, leupeptin, and pepstatin A) on ice. Samples were sonicated on ice (5 sec each time at intervals of 10 sec for 1 min; Ultrasonic sonicator) to homogenize cells in the collagen gel, and spun down at 15,000 ×*g* for 3 min at 4°C to remove

collagen I rest prior to collection of the supernatants. Aliquoted supernatants (400 μl) were sonicated on ice to fragment DNA to 200 ~ 1,000 base pair length and centrifuged at 15,000 ×*g* for 20 min at 4°C. The sonicated samples were diluted 10-fold in ChIP buffer (0.01% SDS, 1.1% Triton X-100, 1.2 mM EDTA, 16.7 mM Tris, pH 8.1, 167 mM NaCl, and 1 mg/ml each of aprotinin, leupeptin, and pepstatin A). The diluted chromatin solutions (400 μl) were incubated with 10 μl antibody of either anti-pS^{63}c-Jun, anti-Smad2, anti-Smad3 (Cell Signaling Tech.), or anti-Snail1 antibody (Santa Cruz Biotech. Inc.) at 4°C with rotation overnight. Before immunoprecipitation, 400 μl of chromatin solution was saved (input chromatin). The immune complexes were collected by adding 50 μl of salmon sperm DNA/protein A and G-beads and rotating for 4 h at 4°C. The beads were recovered by brief centrifugation, washed with low salt complex wash buffer (0.1% SDS, 1% Triton X-100, 2 mM EDTA, 20 mM Tris-HCl, pH 8.1, 150 mM NaCl), high salt complex wash buffer (0.1% SDS, 1% Triton X-100, 2 mM EDTA, 20 mM Tris-HCl, pH 8.1, 500 mM NaCl), LiCl immune complex buffer (0.25% LiCl, 1% NP-40, 1% sodium deoxycholate, 1 mM EDTA, 1mM EDTA, 10 mM Tris-HCl, pH 8.1), and TE (20 mM Tris, 1 mM EDTA), pH 8.0, buffer with a brief centrifugation between each wash to recover the beads. The immune complexes were eluted from the beads by the addition of 500 μl 1% SDS in 0.1 M $NaHCO_3$ to

the bead pellet, voltexing and rotating at 4°C for 10 min. To reverse the cross-linking process, 200 mM NaCl was added to the eluates before incubation at 65°C overnight. Incubation at 55°C for 1 h was done within 10 mM EDTA, 40 mM Tris-HCl, pH 6.5, and 2 ml of 10 mg/ml proteinase K. DNA was recovered by phenol/chloroform extraction and ethanol precipitation. Promoter sequences were detected in immunoprecipitated and input DNA by PCR using specific primers; primer for *snail1* gene; forward1, 5′-TCCAAACTCCTACGAGGC-3′ and reverse1, 5-GAAGAAGTGGCAACTGCT-3, forward2, 5′-AGCAGTTGCCACTTCTTC-3′ and reverse2, 5′-GCAAAGGGAAGTGTGCTT-3′, forward3, 5′- GGAGACG AGCCTCCGATT-3′ and reverse3, 5′-CAGTAGCGCAGAAGAACCACT-3′, primer for negative control regions, forward 5′-CGTAAACACTGGATAAG G-3′ and reverse 5′-GGAAACGCACATCACTGG-3′, primer for the *cortactin (CTTN)* gene; forward 5′-TCTGCAGACTCGCCACAG-3′ and reverse 5′-CAGG CACCAGGCTCTACTTC-3′ primer for negative control regions, forward 5′-AGTGTTATGATTACA GGC-3′ and reverse 5′-ATAGAGCACAGCGAAGAC-3′,

primers for the *snail1*; forward 5′-AGCA CACTTCCCTTTGCATT-3′ and reverse 5′-CACCCGTTCCTTCCCTTATC-3′

9. Time-lapse imaging

Time-lapse cell images in 3D type 1 collagen gel were captured with IX81-ZDC (Olympus) for 24 h. The cells embedded in 3D collagen I gels were cultured in the absence (control) or presence of 50 μM SP600125 in PDMS glass coverslips. In some cases, cells expressing GFP or mCherry protein imaged with a Nikon eclipse Ti microscope (Nikon) with a Nikon Plan-Apochromat 60X/1.4 N.A. oil objective. All microscopes were equipped with a Chamlide Incubator systems (LCI live cell instrument, Korea), and an environmental chamber mounted on the microscope maintained constantly at 37°C, 5% CO_2 and 95% humidity.

10. Immunohistochemistry

The corresponding whole-mount slides were used for validation of immunoblotting data by immunostaining for snail1, pS63-c-Jun (cell signaling) and cortactin (BD, bioscience). Sections (4 μm) of paraffin-embedded tissue were deparaffinized and rehydrated. After treatment with 3% hydrogen peroxide for 10 min to block endogenous peroxidases, the sections were boiled in 10 mM citrate buffer (pH 6.0)

in a microwave oven for 20 min. The sections were subsequently incubated at 4°C overnight with the aforementioned primary antibodies. After thorough rinsing in phosphate-buffered saline, the sections were processed using the DAKO LSAB streptavidin-biotin labeling kit, stained with amino-ethyl carbazole, and counterstained with Mayer′s hematoxylin.

11. Statistical Methods

Student′s *t*-tests were performed for comparisons of mean values to determine significance. p values < 0.05 were considered significant.

3. Results

1. Diverse tumor microenvironmental factors revealed a correlationship among JNKs inactivation, Snail1 induction, and cortactin suppression.

To mechanistically investigate migratory and invasive behaviors of tumor cells embedded in a 3D environment, we cultured MDA-MB-231 breast cancer cells in 3D collagen gel with 10% serum under different environmental parameters to promote continuous tumor cell growth showed reduced Ser63 phosphorylation levels of c-Jun (i.e., pS63c-Jun), although proliferating cell nuclear antigen (PCNA) was not changed to indicate no significant cytotoxicity during the culture (Fig. Ⅲ-2A). Concomitantly, Snail1 expression increased but cortactin expression decreased, although Snail2/Slug and c-Jun levels were unchanged (Fig. Ⅲ-1A). The increased Snail1 and decreased pS63c-Jun and cortactin levels depended on cell densities, since continuous culture at a high cell density showed more dramatic changes, compared with less cells (Fig. Ⅲ-2B). We then found that extracellular acidity caused the same effect (Fig. Ⅲ-2C). Acute hypoxia with an HIF1α induction showed also the same effect (Fig. Ⅲ-2D). Furthermore, breast tumor tissues showed Snail1 immunostaining in a random distribution around the distal and proximal edges of a large invasive tumor nest (Fig. Ⅲ-2E, top), compared with pS63c-Jun and cortactin expression at the invasive tumor edges (Fig. Ⅲ-2E, bottom). These interestingly suggest an exclusive relationship between Snail1 and

cortactin for invasion JNK inhibition caused Snail1 induction and cortactin suppression, leading to reduced migration and invasion in 3D collagen gels.

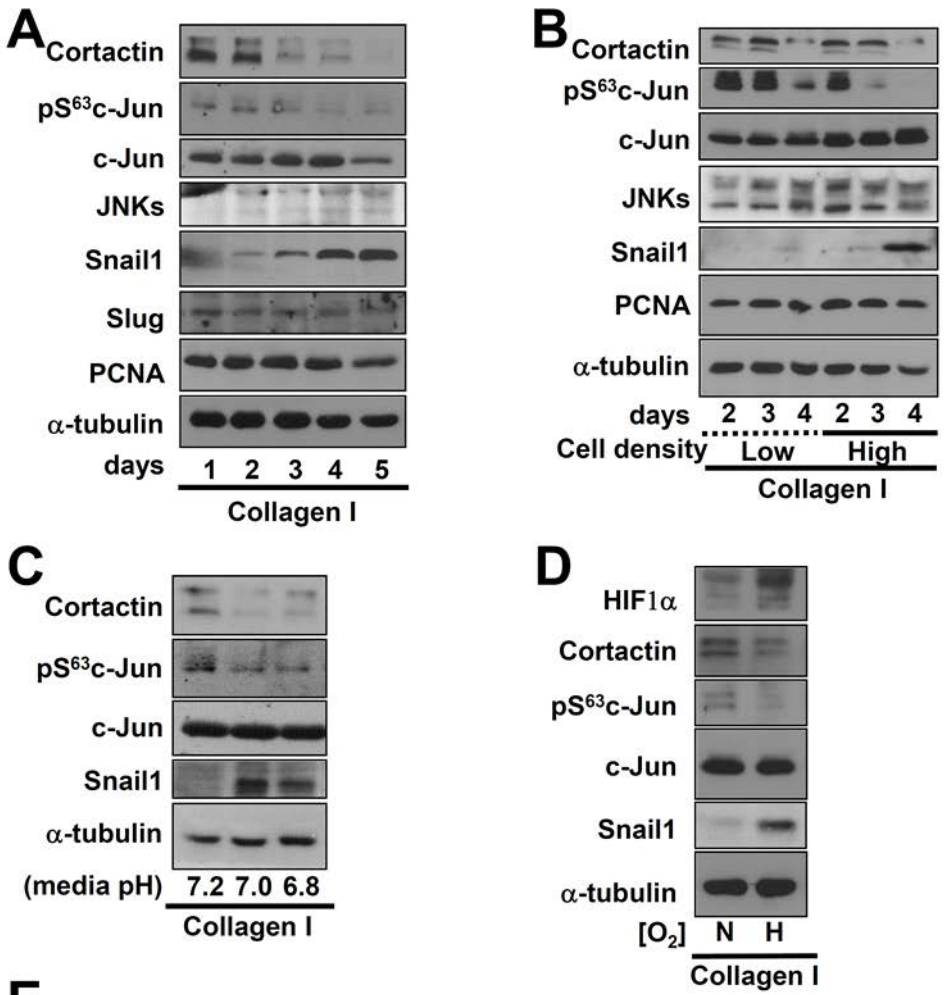
A
Cortactin
pS63c-Jun
c-Jun
JNKs
Snail1
Slug
PCNA
α-tubulin
days 1 2 3 4 5
Collagen I
B
Cortactin
pS63c-Jun
c-Jun
JNKs
Snail1
PCNA
α-tubulin
days 2 3 4 2 3 4
Cell density Low High
Collagen I
C
Cortactin
pS63c-Jun
c-Jun
Snail1
α-tubulin
(media pH) 7.2 7.0 6.8
Collagen I
D
HIF1α
Cortactin
pS63c-Jun
c-Jun
Snail1
α-tubulin
[O2] N H
Collagen I
E
Snail1 100 x
Snail1 400 x
pS63c-Jun 200 x
Cortactin 200 x

Fig. Ⅲ-2. Diverse tumor microenvironmental factors caused JNK signaling inactivation, Snail1 induction, and cortactin suppression. (A to D) Whole cell lysates were prepared from MDA-MB-231 cells embedded in 3D collagen gels with the normal serum-containing culture media refreshment every day for upto 5 days (A) and upto 4 days of culture at lower or higher densities (B), in different-pH medium that was replenished every day (C), in hypoxic condition for 4 h (D). N depicts normoxia and H depicts hypoxia. Cell lysates were processed for standard immunoblotting to analyze the indicated molecules. Data represent three independent experiments. (E) Breast cancer tissues were immunostained for Snail1, pS63c-Jun, and cortactin in human breast cancer tissues (magnifications of 100×, 200×, or 400×).

2. Inhibition of JNK signaling caused Snail1 induction and cortactin suppression, leading to reduced migration and invasion in 3D collagen gels

We next examined the morphology and behavior of MDA-MB-231 cells embedded in 3D collagen gels. Pharmacological JNKs inhibition by SP600125 treatment caused an elongation in cellular morphology (Fig. Ⅲ-3A), with a higher length/width ratio (Fig. Ⅲ-3B). However, MDA-MB-231 cells embedded in 3D Matrigel or a mixture of Matrigel and collagen (at a 4:1 w/w ratio) did not show the elongation, indicating an ECM-specific morphological effect (Fig. Ⅲ-4A). RT-PCR and immunoblotting after JNK inhibition showed that Snail1 and Twist mRNAs expression increased, but cortactin mRNA decreased, although Snail2/Slug mRNA level was not changed (Fig. Ⅲ-3C). More importantly, the Snail1 mRNA levels were not correlated with E-cadherin (CDH1) level, indicating that the Snail1 might not be linked to E-Cadherin suppression (Fig. Ⅲ-3C). These gene expression changes occurred in the cells embedded only in collagen gel but not Matrigel or the mixture of Matrigel and collagen I. Phosphorylated-ERKs and -p38 were not involved in the effects on alterations in gene expression, because there were no similar changes upon JNK inhibition (Fig. Ⅲ-3D). SP600125 treatment did not alter actin nucleator Arp2 and mDia expression levels, either (Fig. Ⅲ-4D). Thus, the morphological elongation by JNK inhibition might be correlated with the alterations in expression levels of Snail1 and Cortactin. Live cell imaging

was used to monitor morphological changes and/or motility upon treatment with or without SP600125. Cells by JNKs inhibition exhibited relatively-steady locations and morphological protrusions during time-lapse imaging, whereas control cells showed dynamic growth of invasive protrusions (Fig. Ⅲ-3E) leading to more consistent migration in 3D collagen gels (Fig. Ⅲ-3F). Therefore, it is possible that JNK inhibition-mediated effects may control migratory and invasive properties of MDA-MB-231 cells in 3D collagen gel.

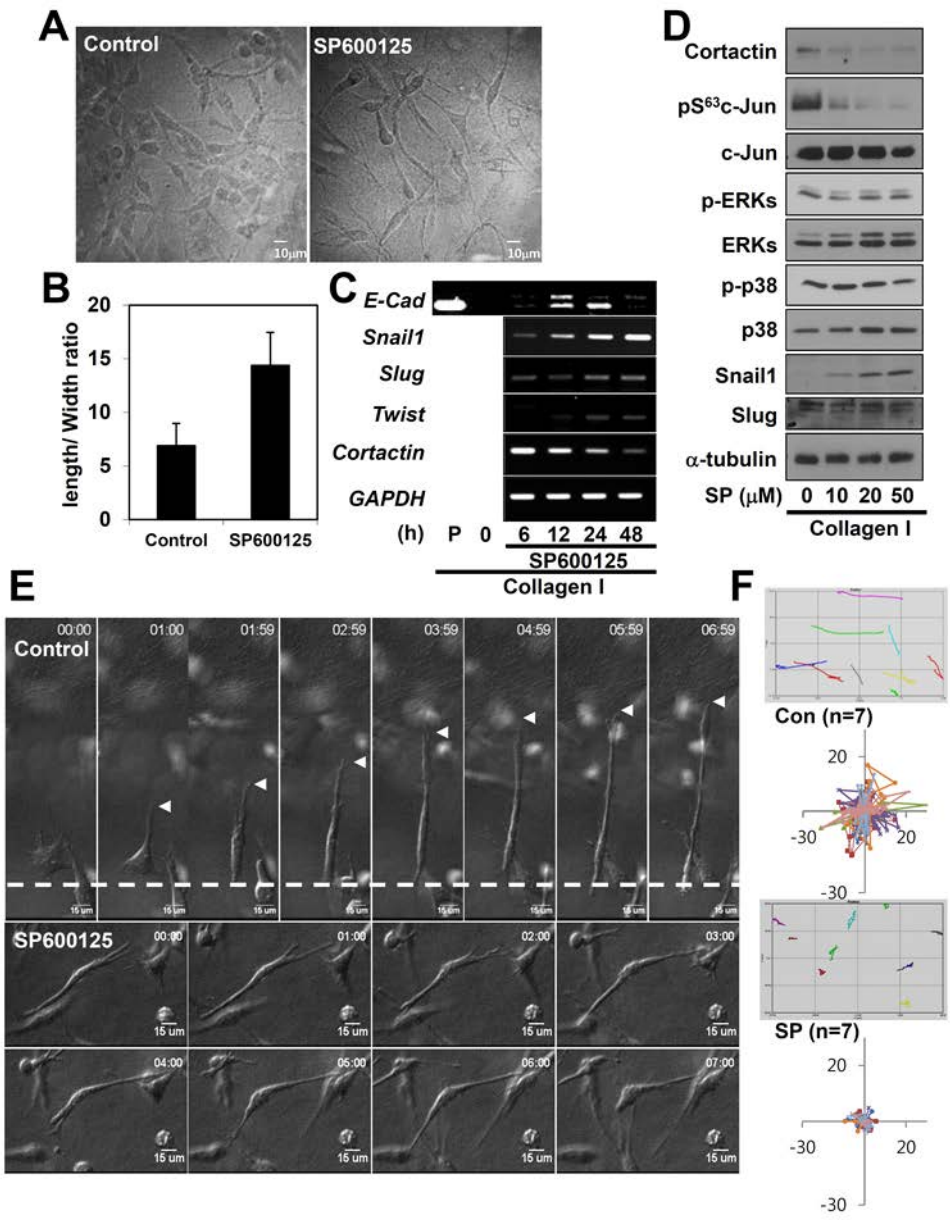
A
Control
SP600125
10μm
B
length/ Width ratio
20
15
10
5
0
Control
SP600125
C
E-Cad
Snail1
Slug
Twist
Cortactin
GAPDH
(h) P 0 6 12 24 48
SP600125
Collagen I
D
Cortactin
pS63c-Jun
c-Jun
p-ERKs
ERKs
p-p38
p38
Snail1
Slug
α-tubulin
SP (μM) 0 10 20 50
Collagen I
E
Control
00:00
01:00
01:59
02:59
03:59
04:59
05:59
06:59
SP600125
00:00
01:00
02:00
03:00
04:00
05:00
06:00
07:00
15 um
F
Con (n=7)
20
-30
20
-30
SP (n=7)
20
-30
20
-30

Fig. Ⅲ-3. Inhibition of JNK signaling caused Snail1 induction and cortactin suppression, leading to less dynamic MDA-MB-231 cell migration and invasion within 3D collagen gels. (A and B) Images of elongated morphology of MDA-MB-231 cells in 3D collagen gels after pharmacological inhibition of JNK signaling for 3 days were saved (A) and quantified to get length/width ratio using imaging software (B). (C) RT-PCR analysis from the cells embedded in 3D collagen gels and treated with 50 μM SP600125 for different times. P depicts a positive control. (D) Immunoblots were performed using whole lysates of cells embedded in 3D collagen gels and treated with SP600125 (SP) at different concentrations for 24 h. (E and F) Time-lapse microscopic images of the cells embedded in 3D collagen gels and treated with vehicle (DMSO, Control) or 50 μM SP600125. Arrow head in the control condition indicates dynamically and invasively growing tips (E). Tracking analysis of each control cell showed dynamic migration for longer distances (Con, n = 7), but SP600125 treated cells exhibited decreased motilities (SP, n = 7). The data represent three independent experiments.

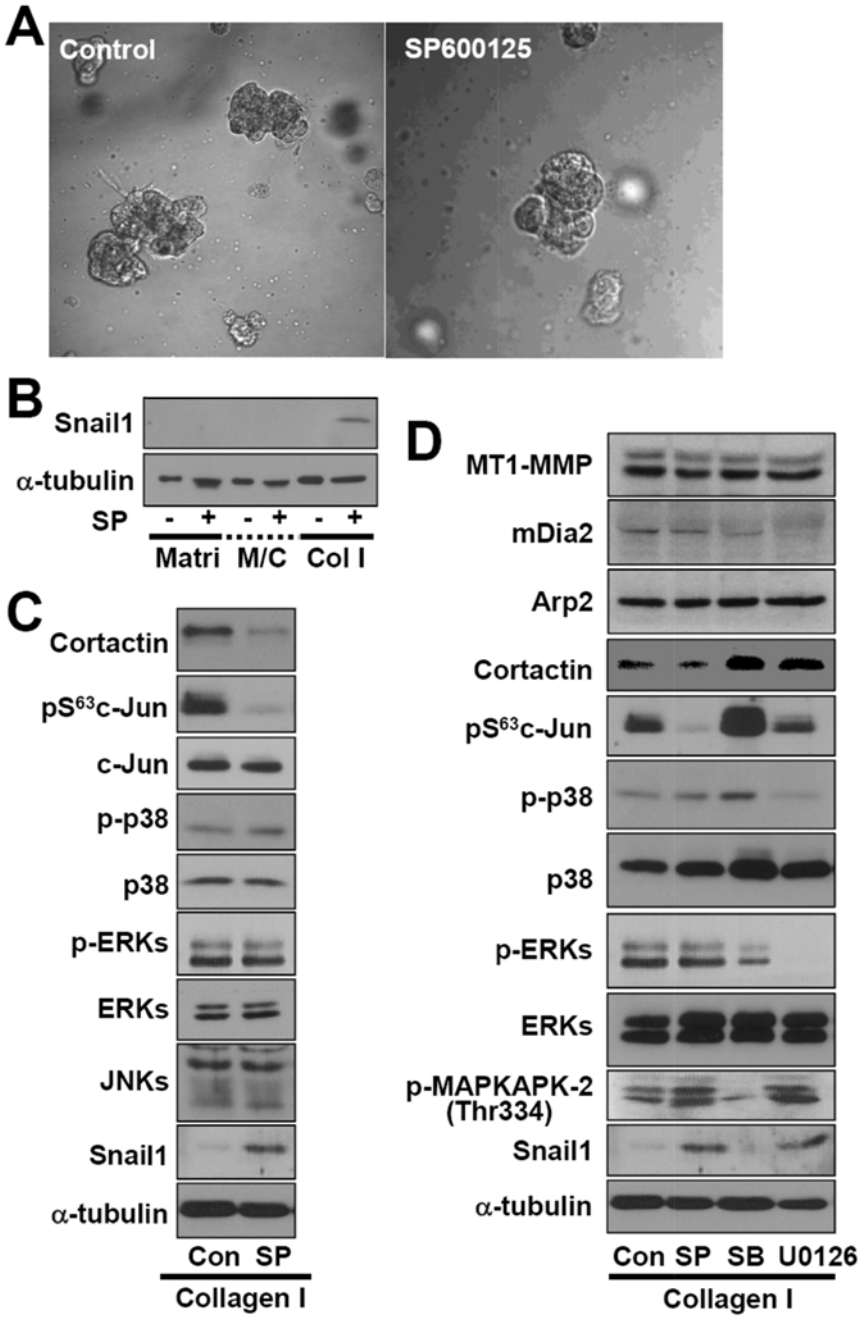
A
Control
SP600125
B
Snail1
α-tubulin
SP
- + - + - +
Matri M/C Col I
C
Cortactin
pS63c-Jun
c-Jun
p-p38
p38
p-ERKs
ERKs
JNKs
Snail1
α-tubulin
Con SP
Collagen I
D
MT1-MMP
mDia2
Arp2
Cortactin
pS63c-Jun
p-p38
p38
p-ERKs
ERKs
p-MAPKAPK-2 (Thr334)
Snail1
α-tubulin
Con SP SB U0126
Collagen I

Fig. Ⅲ-4. JNK signaling inhibition, but not ERKs or p38 signaling inhibition, in cells embedded in 3D collagen I (but not Matrigel-containing) gels caused increases in Snail1 expression and decreased cortactin expression. (A) MDA-MB-231 cells embedded in Matrigel did not show morphological changes upon SP600125 treatment. (B) SP600125 treatment to MDA-MB-231 cells embedded in 3D collagen I gel and cultured for 3 days , but not in Matrigel or a mixture of Matrigel and collagen I gel (at a ratio of 5 mg/ml to 1.25 mg/ml), resulted in an increased Snail1 expression. (C) JNK signaling inhibition (i.e., decreased pS63c-Jun) by SP600125 treatment to MDA-MB-231 cells embedded in 3D collagen I gel resulted in increased Snail1 and decreased cortactin expression without affecting ERKs and p38 activities. (D) JNK signaling inhibition, but not ERKs and p38 signaling inhibition, resulted in increased Snail1 expression and decreased cortactin expression without effects on mDia and Arp2 expression that are involved in actin branching and polymerization

3. JNK inhibition caused less efficient formation of actin and cortactin-enriched invadopodia.

When we costained cells with cortactin and F-actin, which are known to localize at the invadopodia [85], software-based z-stacked 3D images following staining with Alexa488®-tagged anti-cortactin (green) and phalloidin (red) clearly showed more yellowish overlapped spots (i.e., invadopodia) in control, vehicle-treated cells. This is demonstrated by the green and the red overlapping peaks in the histogram representing the intensity profile throughout the xz cut-stack (white dotted line, Fig. Ⅲ-5). However, SP600125-tretaed cells did not show such overlaps, leading to less green and red overlapped peaks in the histogram (Fig. Ⅲ-5B). We also observed dynamic turnover in GFP-cortactin localization along the frequently altered boundaries of control cells, whereas its localization in SP600125-treated cells was steady and not at the cellular boundary. Human breast cancer cell lines cultured on 3D-laminin-rich ECM gels are grouped into four different morphological classifications: round, mass, grape-like, and stellate [86]. When diverse breast cancer cell lines were tested for the JNK inhibition-mediated effects in the 3D collagen I environment, mass (T-47D and MCF-7) or grape-like (MDA-MB-468) cells did not show morphological elongation, whereas stellate cells (MDA-MB-436 and MBA-MB-231 cells) showed morphological elongation with a loss of cortactin- and actin-colocalized spots (yellow spots) upon JNK inhibition (Fig. Ⅲ-

5C). Further, like MDA-MB-231 cells, MDA-MB-436 cells decreased pS63c-Jun, increased Snail1 expression, and decreased cortactin expression upon JNK inhibition (Fig. Ⅲ-5D). These observations support that certain breast cancer cells (i.e., stellate-grouped cells) could become less invasive by the signaling link between pS63c-Jun, Snail1, and cortactin.

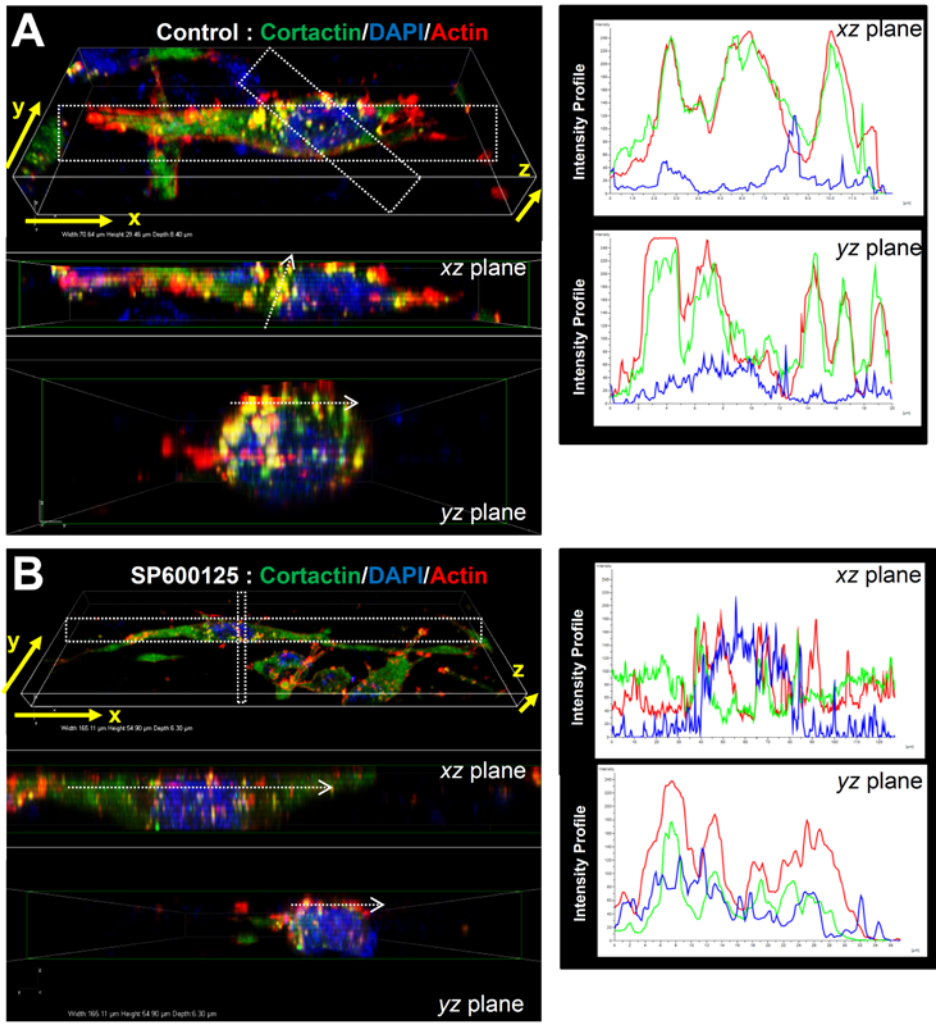
A
Control : Cortactin/DAPI/Actin
y
x
z
xz plane
yz plane
Intensity Profile
xz plane
Intensity Profile
yz plane
B
SP600125 : Cortactin/DAPI/Actin
y
x
z
xz plane
yz plane
Intensity Profile
xz plane
Intensity Profile
yz plane

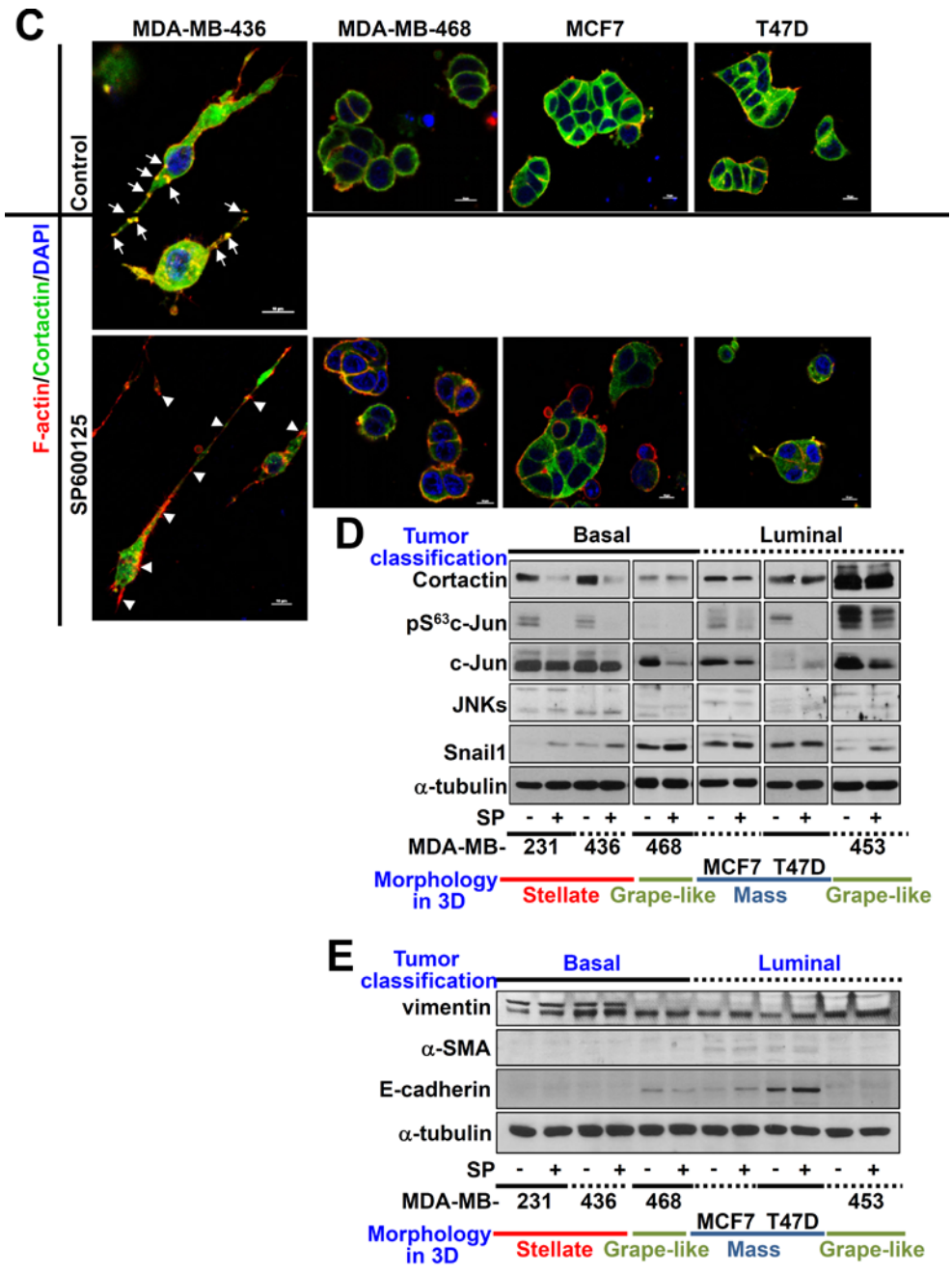
C
MDA-MB-436
MDA-MB-468
MCF7
T47D
Control
SP600125
F-actin/Cortactin/DAPI
D
Tumor classification
Basal
Luminal
Cortactin
pS63c-Jun
c-Jun
JNKs
Snail1
α-tubulin
SP
MDA-MB-
231
436
468
MCF7
T47D
453
Morphology in 3D
Stellate
Grape-like
Mass
Grape-like
E
Tumor classification
Basal
Luminal
vimentin
α-SMA
E-cadherin
α-tubulin
SP
MDA-MB-
231
436
468
MCF7
T47D
453
Morphology in 3D
Stellate
Grape-like
Mass
Grape-like

Fig. Ⅲ-5. JNK inhibition-mediated effects among different breast cancer cell lines. (A and B) Snap images [A and B] and 3D-stacked fluorescent images of 3D rendition (with x, y, and z axes) are shown for confocal fluorescent images of MBA-MB-231 cells treated with DMSO (vehicle, Control, A) or SP600125 (B). Each xz or yz plane of a confocal slice is shown separately and fluorescent intensities throughout the white-arrow sections in each plane are represented as histograms in the right side. The xz or yz planes (white-dotted boxes and white arrows) were the stacks for fluorescence intensity profiles through the layers and their fluorescence histograms throughout the white-arrowed section were shown to clearly demonstrate the overlap among green and red, but not blue, fluorescence. Cortactin is green, nucleus is blue, and F-actin is red. (C to E) Different breast cancer cells embedded in 3D collagen were analyzed for F-actin (red), cortactin (green), and nucleus (DAPI) using confocal microscopy at confocal slices (C), or immunoblotting for the indicated molecules (D and E). The data represent three different experiments.

4. Snai1l expression decreased invadopodia formations and caused the inverse relationship between Snail1 and cortactin expression

When Snail1 was overexpressed, cortactin was reduced, but pS63c-Jun was not changed (Fig. Ⅲ-6A), suggesting c-Jun upstream of Snail1. Overexpression of Snail1 (marked by cotransfected mCherry plasmid) decreased cortactin-enriched spots, compared with mCherry alone-transfected control or exogenic Snail1-negative (i.e., only greenish) cells showing more frequent cortactin-positive spots (Fig. Ⅲ-6B, C). More cortactin was located around cellular boundaries of the control cells, whereas Snail1-overexpressing cells showed more perinuclear cortactin localizations. Following transfection with siSnail1, CTTN mRNA increased and JNK1 mRNA were not changed (Fig. Ⅲ-6D). The JNK inhibition-mediated decrease in cortactin expression was abolished by knockdown of Snail1 (Fig. Ⅲ-6E).

.

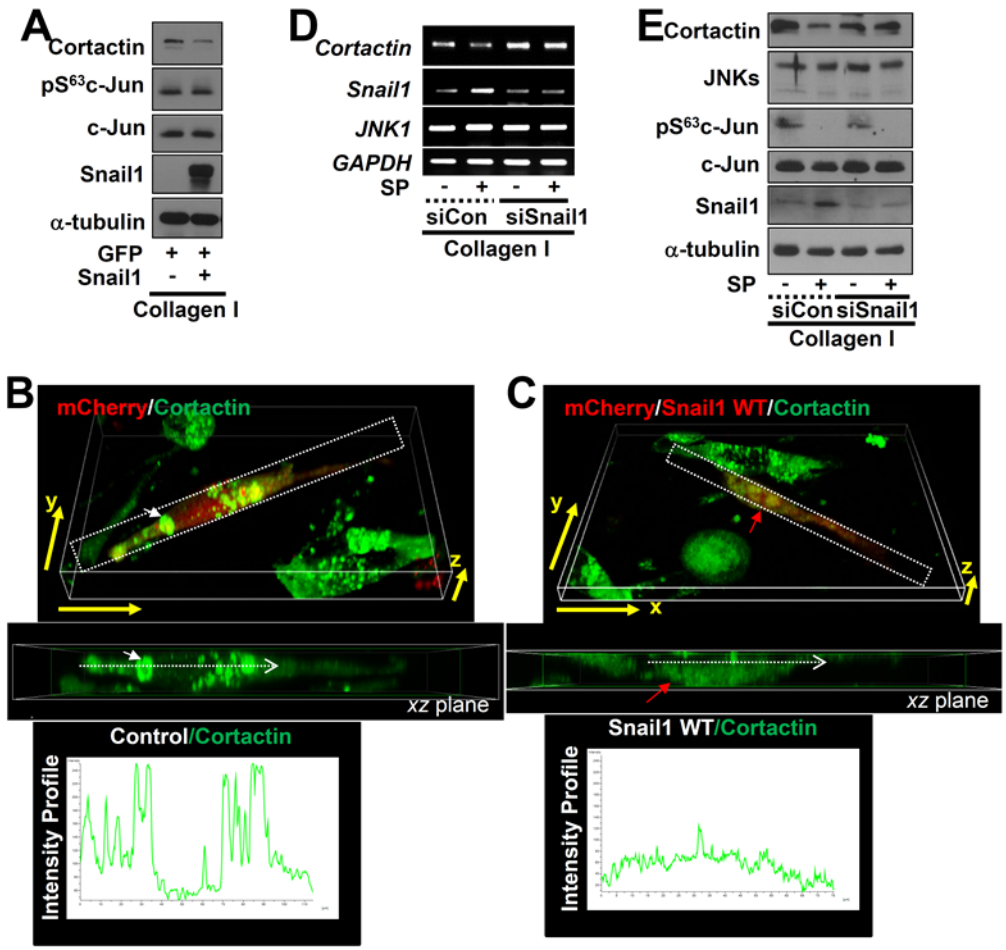
A
Cortactin
pS63c-Jun
c-Jun
Snail1
α-tubulin
GFP + +
Snail1 - +
Collagen I
D
Cortactin
Snail1
JNK1
GAPDH
SP - + - +
siCon siSnail1
Collagen I
E
Cortactin
JNKs
pS63c-Jun
c-Jun
Snail1
α-tubulin
SP - + - +
siCon siSnail1
Collagen I
B
mCherry/Cortactin
y
z
xz plane
Control/Cortactin
Intensity Profile
C
mCherry/Snail1 WT/Cortactin
y
x
z
xz plane
Snail1 WT/Cortactin
Intensity Profile

Fig. Ⅲ-6. JNK inhibition-mediated snail1 expression caused also an inverse relationship between Snail1 and cortactin and decreased actin and cortactin-enriched invadopodia formation. (A to C) Immunoblots (A) or 3D-stacked images of 3D rendition (B and C) were processed from MDA-MB-231cells transiently transfected with empty plasmid (-) or plasmid encoding Snail1 WT together with plasmid encoding GFP or mCherry to mark the transfectants (red, B and C). Note that mCherry/Snail1 WT-cotransfected cells (bottom, red arrow) showed less cortactin-enriched spots, compared with cells transfected with mCherry plasmid alone. The xz planes (white-dotted boxes) of confocal slices represent cut-layers for green fluorescence intensity profiles, and fluorescence histograms along the white-arrow sections are shown to illustrate the green fluorescence peaks. (D and E) RT-PCR (D), immunoblots (E) of cells embedded in 3D collagen gels treated with vehicle (-) or SP600125 (SP) after transient transfection with siRNAs against control sequence (siCon) or Snail1 (siSnail1). The data represent three different experiments

5. The relationship among pS63c-Jun, Snail1, and cortactin occurred at transcriptional level.

We next tested whether these molecular changes occurred at the transcriptional level by chromatin immunoprecipitation (ChIP) assay. There found AP1 binding sites in the human Snail1 gene promoter region and E-box binding sites in the human cortactin (CTTN) gene promoter region (Fig. Ⅲ-7A). Chromatin extracts, prepared cells in 3D collagen gel in the presence of SP600125 treatment with enhanced Snail1 and reduced pS63c-Jun and cortactin levels (Fig. Ⅲ-7B), were immunoprecipitated with either anti-pS63c-Jun or anti-Snail1 antibody (Fig. Ⅲ-7C, D). PCR product representing region p1 of the Snail1 promoter (Snail1-p1), but not a control region (i.e., a non-AP1-binding site, Snail1-n), was only detected from pS63c-Jun immunoprecipitated chromatin (Fig. Ⅲ-7C), indicating a binding of pS63c-Jun to the Snail1 promoter region. However, there may be other factors involved in Snail1 transcription because reduced pS63c-Jun correlated with enhanced Snail1 mRNA levels (see below). Meanwhile, chromatin precipitated with anti-Snail1 antibody showed more PCR product representing region p of the CTTN promoter (cortactin-p), but not from a control region in the promoter (cortactin-n), in SP600125-treated cells (Fig. Ⅲ-7D). Snail1, a transcriptional suppressor [59], could thus bind a promoter region of the CTTN gene and suppress cortactin expression. RT-PCR revealed that Snail1 mRNAs were more stable in

control cells (treated with actinomycin D alone) than cells treated with actinomycin D and SP600125 together (Fig. Ⅲ-7E). Quantitative real time PCR (qPCR) analysis showed that CTTN mRNA had a half-life longer than 48 h in control cells, but a half-life of approximately 24 h in cells treated with both actinomycin D and SP600125 (Fig. Ⅲ-7F). The half-lives of Snail1 and cortactin proteins were < 6 h for Snail1 and ≅ 12 h for cortactin, being independent of SP600125 treatment (Fig. Ⅲ-7G). pS63-c-Jun binding to a Snail1 gene promoter region occurred without SP600125 treatment. Thus, increased Snail1 transcript upon JNK inhibition indicated that another factor(s) could be involved in Snail1 transcription.

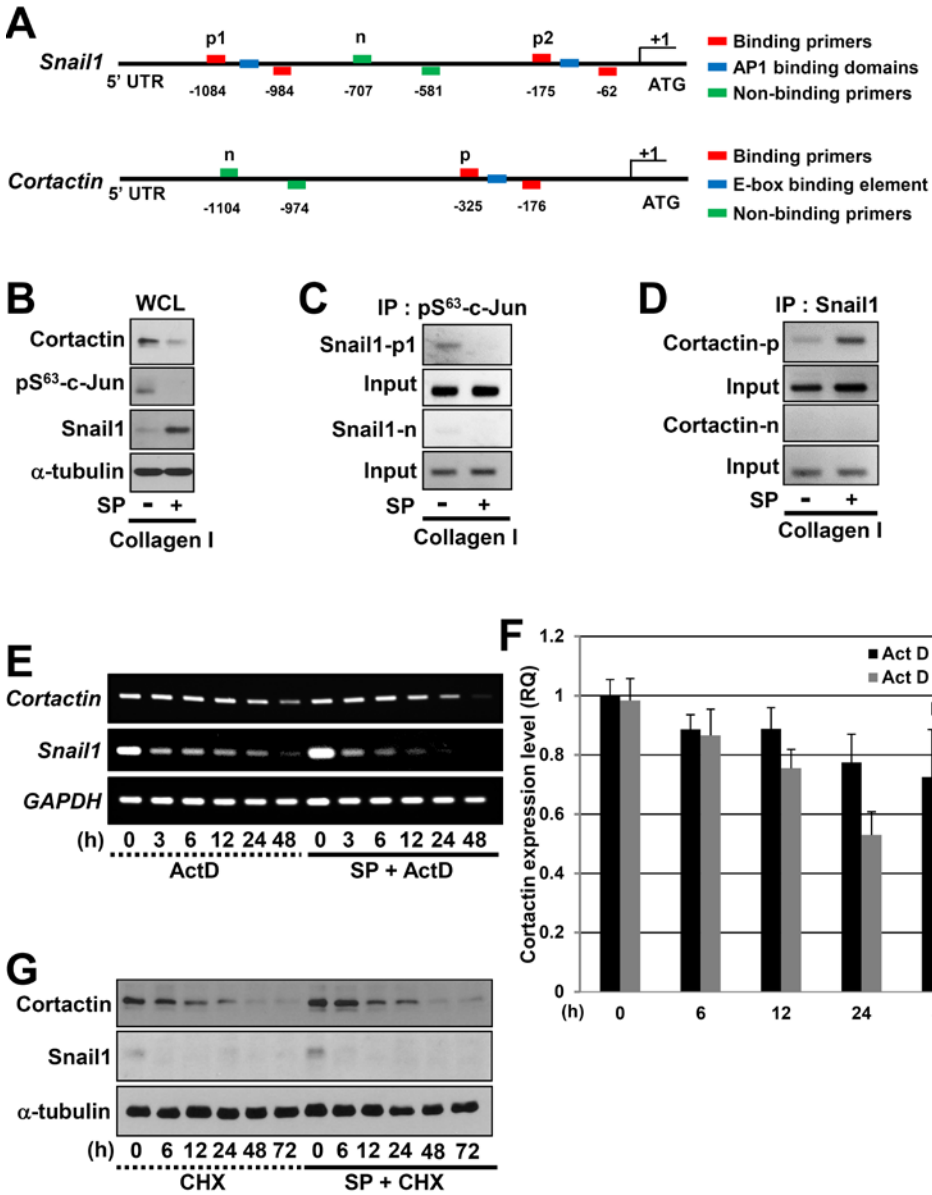
A
Snail1
5' UTR
p1
n
p2
+1
-1084
-984
-707
-581
-175
-62
ATG
Binding primers
AP1 binding domains
Non-binding primers
Cortactin
5' UTR
n
p
+1
-1104
-974
-325
-176
ATG
Binding primers
E-box binding element
Non-binding primers
B
WCL
Cortactin
pS63-c-Jun
Snail1
α-tubulin
SP - +
Collagen I
C
IP : pS63-c-Jun
Snail1-p1
Input
Snail1-n
Input
SP - +
Collagen I
D
IP : Snail1
Cortactin-p
Input
Cortactin-n
Input
SP - +
Collagen I
E
Cortactin
Snail1
GAPDH
(h) 0 3 6 12 24 48 0 3 6 12 24 48
ActD
SP + ActD
F
Act D
Act D + SP
Cortactin expression level (RQ)
1.2
1
0.8
0.6
0.4
0.2
0
(h) 0 6 12 24 48
G
Cortactin
Snail1
α-tubulin
(h) 0 6 12 24 48 72 0 6 12 24 48 72
CHX
SP + CHX

Fig. Ⅲ-7. The relationship between pS63c-Jun, Snail1, and cortactin occurred at the transcriptional level. (A) Schematic presentations of AP1-binding domains in the promoter region of the Snail1 gene (top) or E-box binding element in the promoter regions of the CTTN gene (bottom). (B to D) ChIP assay using chromatin immunoprecipitates using anti-pS63c-Jun antibody (C) or anti-Snail1 antibody (D) prepared from whole cell lysates (WCL, B) of cells treated with vehicle (-) or SP600125 (SP, +) in 3D collagen gels. (E and F) RT-PCR analysis for Snail1 or cortactin (E) or quantitative RT-PCR for cortactin (F) from the cells treated with DMSO or SP600125 with or without actinomycin D (ActD). (G) Immunoblotting for Snail1 or cortactin from the cells treated with DMSO or SP600125 with or without cycloheximide (CHX). The data represent three independent experiments.

6. Snail1 induction by JNKs inhibition enhanced by TGFβ1/Smad signaling.

Snail1 mRNA increased but CTTN mRNA decreased in cells cultured for 3 days in 3D collagen gel, whereas Smad2 and Smad4 mRNA was not altered (Fig. Ⅲ-8A), indicating that cells embedded in 3D collagen gel may secrete TGFβ1 leading to autocrine effects. However, immunoblottings showed increased TGFβ1, Smad2, and Smad3 protein levels and Smad2 phosphorylation (Fig. Ⅲ-8B). JNK inhibition or extracellular acidity also enhanced TGFβ1 and Smad2 expression (Fig. Ⅲ-8C, D). Cells were then analyzed for Snail1 and cortactin expression after transfection with shRNA against GFP or each Smad. The JNK inhibition-mediated changes in Snail1 and cortactin expression were blocked by Smad2 or Smad4 knockdown, whereas Smad3 knockdown did not block the changes (Fig. Ⅲ-8E). SP600125-treated cells showed Smad-binding element in the Snail1 gene promoter region (Snail1-p3), as demonstrated by RT-PCR amplification of chromatin precipitated using anti-Smad2 or -Smad4 (but not -Smad3) antibodies (Fig. Ⅲ-8F), suggesting that TGFβ1/Smad activity in MDA-MB-231 cells embedded into 3D collagen gel might induce Snail1 transcription, following JNK inhibition.

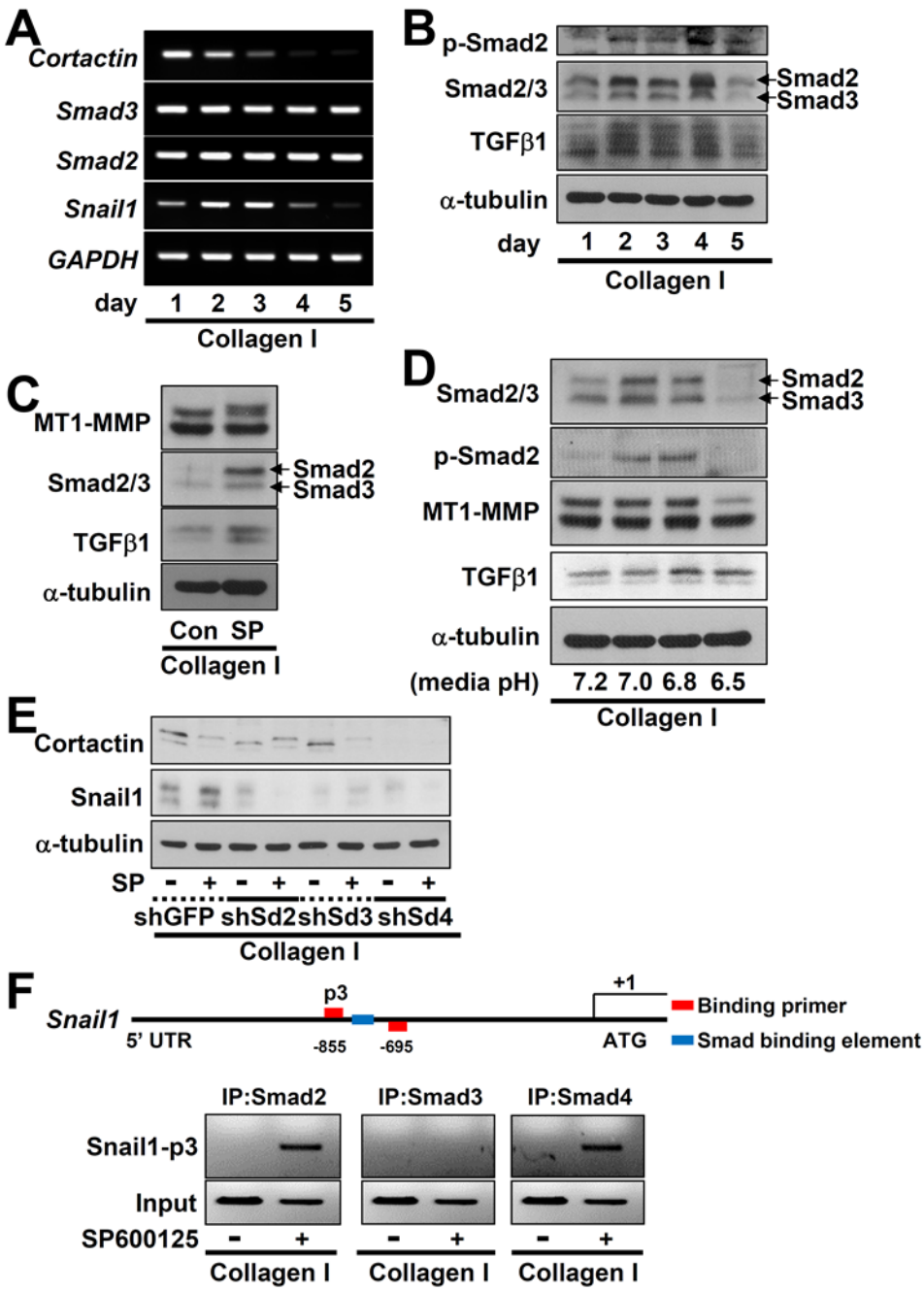
A
Cortactin
Smad3
Smad2
Snail1
GAPDH
day 1 2 3 4 5
Collagen I
B
p-Smad2
Smad2/3
Smad2
Smad3
TGFβ1
α-tubulin
day 1 2 3 4 5
Collagen I
C
MT1-MMP
Smad2/3
Smad2
Smad3
TGFβ1
α-tubulin
Con SP
Collagen I
D
Smad2/3
Smad2
Smad3
p-Smad2
MT1-MMP
TGFβ1
α-tubulin
(media pH) 7.2 7.0 6.8 6.5
Collagen I
E
Cortactin
Snail1
α-tubulin
SP - + - + - + - +
shGFP shSd2 shSd3 shSd4
Collagen I
F
Snail1
5' UTR
p3
-855
-695
+1
ATG
Binding primer
Smad binding element
IP:Smad2
IP:Smad3
IP:Smad4
Snail1-p3
Input
SP600125 - + - + - +
Collagen I
Collagen I
Collagen I

Fig. Ⅲ-8. Enhanced TGFβ1/Smad signaling in 3D collagen gel was responsible for increased Snail1 transcription upon JNK signaling inhibition. (A to D) RT-PCR (A) or immunoblotting analysis (B to D) for the indicated molecules in MDA-MB-231 cells cultured in 3D collagen upto 5 days (A and B) or for 24 h (C and D), treated with vehicle (DMSO, Con) or SP600125 (SP) (C), or with culture media replenished every day at different pH (D). (E) Immunoblots using lysates from the cells treated with DMSO (-) or SP600125 (+) after transient transfection of shGFP or shRNA against each Smad protein (shSd). (F) Schematic presentations of the Smad-binding element in the promoter regions of the Snail1 gene (top) and ChIP assay using chromatin immunoprecipitates using anti-Smad antibodies (bottom) prepared from whole lysates of cells treated with vehicle (-) or SP600125 (+) in 3D collagen gels. The data represent three independent experiments.

7. Specific JNK1 inactivation or suppression reduced pS63c-Jun and cortactin and enhanced Snail1 expression.

To avoid nonspecific effects by SP600125, cells were transfected with GFP plasmids (to mark transfectants during imaging) together with or without dominant-negative (DN) JNK1. DN-JNK1 expression reduced pS63c-Jun, enhanced Snail1, decreased cortactin expression (Fig. Ⅲ-9A), and less actin-enriched spots (shown as peaks in the histogram, Fig. Ⅲ-9B). When JNK1 was suppressed by siRNA introduction, the relationship among JNK1, Snail1, and cortactin levels were similar to those found in MDA-MB-231 cells continuously cultured in 3D collagen gels with SP600125 treatment (Fig. Ⅲ-9C, D). Further, siJNK1-transfected cells [marked with cotransfected GFP-tagged control siRNA as a green spot marked with a white arrow showed reduced actin-enriched spots, compared with untransfected neighboring cells (i.e., siJNK1-negative cell without green spots, Fig. Ⅲ-9E).

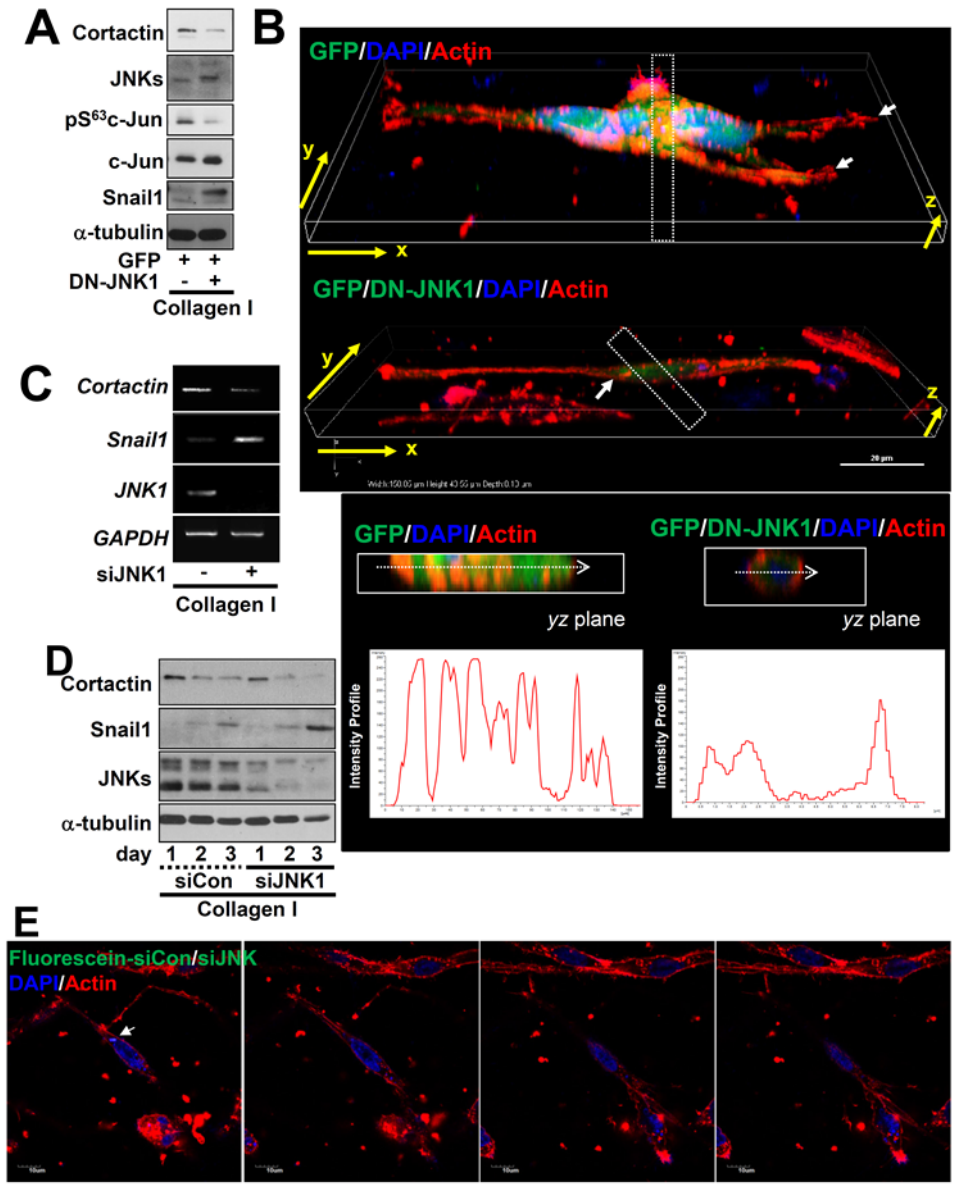
A
Cortactin
JNKs
pS63c-Jun
c-Jun
Snail1
α-tubulin
GFP + +
DN-JNK1 - +
Collagen I
B
GFP/DAPI/Actin
y
x
z
GFP/DN-JNK1/DAPI/Actin
y
x
z
C
Cortactin
Snail1
JNK1
GAPDH
siJNK1 - +
Collagen I
GFP/DAPI/Actin
yz plane
Intensity Profile
GFP/DN-JNK1/DAPI/Actin
yz plane
Intensity Profile
D
Cortactin
Snail1
JNKs
α-tubulin
day 1 2 3 1 2 3
siCon siJNK1
Collagen I
E
Fluorescein-siCon/siJNK
DAPI/Actin

Fig. Ⅲ-9. JNK1 suppression caused an inverse relationship among Snail1 and cortactin expression and resulted in decreased invadopodia formation. (A and B) Immunoblots (A) or 3D-stacked images of 3D rendition (B) were processed from cells transiently transfected with empty plasmid (-) or plasmid encoding DN-JNK1 together with pEGFP (GFP) plasmid to mark the transfectants (green, B). The yz planes (white-dotted boxes) of confocal slices represent cut-layers for fluorescence intensity profiles, and fluorescence histograms corresponding to a section throughout the layers (white-dotted arrow) are shown to illustrate the red fluorescence peaks. (C and D) RT-PCR (C) or immunoblots (D) of cells embedded in 3D collagen gels after transient transfection with siRNAs against GFP (siGFP) or JNK1 (siJNK1). (E) Confocal fluorescent images (slices) of cells cotransfected with siJNK1 and GFP-tagged siControl [to mark siJNK1-transfectants, green spot (arrow)]. GFP-siControl plus siJNK1 is green, F-actin is red, and nucleus is blue. The data represent three independent experiments.

8. JNK1 inactivation caused localization of MT1-MMP at perinuclear regions but not membrane boundaries.

When actin and collagen fibers were stained or visualized, control cells showed clear ECM-degraded areas (yellow arrow heads), whereas SP600125-tretaed cells showed no clear ECM-degraded areas (Fig. Ⅲ-10A). We then imaged the invadopodia using a different marker, matrix metalloproteinase MT1-MMP [85]. When cells transfected with mCherry tagged MT1-MMP were embedded into 3D collagen gel before double-staining for MT1- MMP (red) and actin (green), MT1-MMP was overlapped with actin-enriched spots, as demonstrated by frequent overlapping throughout the xz or yz cut-stacks (Fig. Ⅲ-10B). MDA-MB-231 cells embedded in 3D collagen gels did not exhibit changes in MT1-MMP expression, unlike cortactin (Fig. Ⅲ-7C, D). When mCherry-tagged MT1-MMP was transfected into cells, the vehicle-treated control cells showed dynamic turnover of MT1-MMP-positive spots along peripheral and/or central regions of the cells, frequent alterations in morphological boundaries, and led to enhanced cellular locomotion (Fig. Ⅲ-10C, Supplementary movie 3), However, SP600125-treated cells showed a steady morphology and more stable invadopodia with greater intensities for MT1-MMP (Fig. Ⅲ-10D). Cells cotransfected with mCherry-MT1-MMP and GFP-cortactin showed dynamic translocation of spots doubly-positive for cortactin and MT1-MMP (i.e., yellowish spots) along the cellular boundaries

(arrow heads, Fig. Ⅲ-10E), whereas the cortactin and MT1-MMP double-positive spots in SP600125-treated cells were more localized around the nucleus than cell boundaries (Fig. Ⅲ-10F).

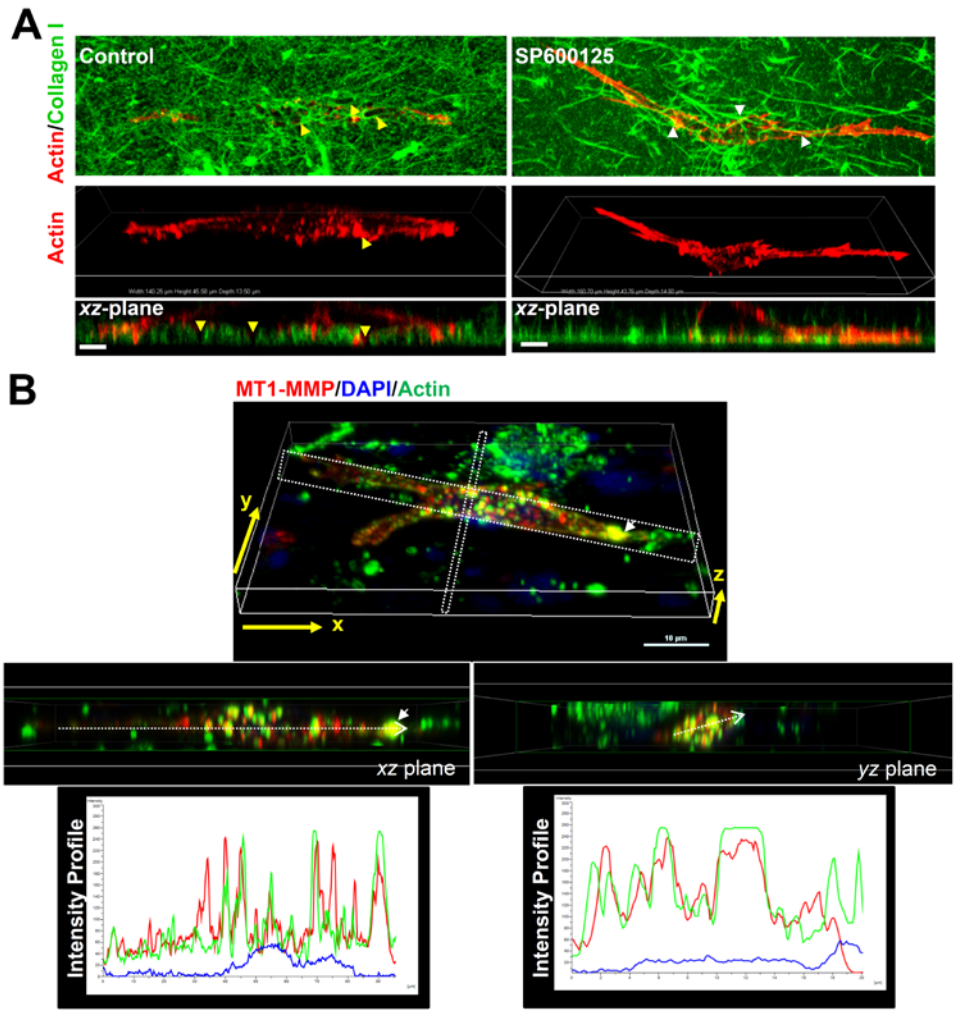
A
Actin/Collagen I
Control
SP600125
Actin
xz-plane
xz-plane
B
MT1-MMP/DAPI/Actin
y
x
z
xz plane
yz plane
Intensity Profile
Intensity Profile

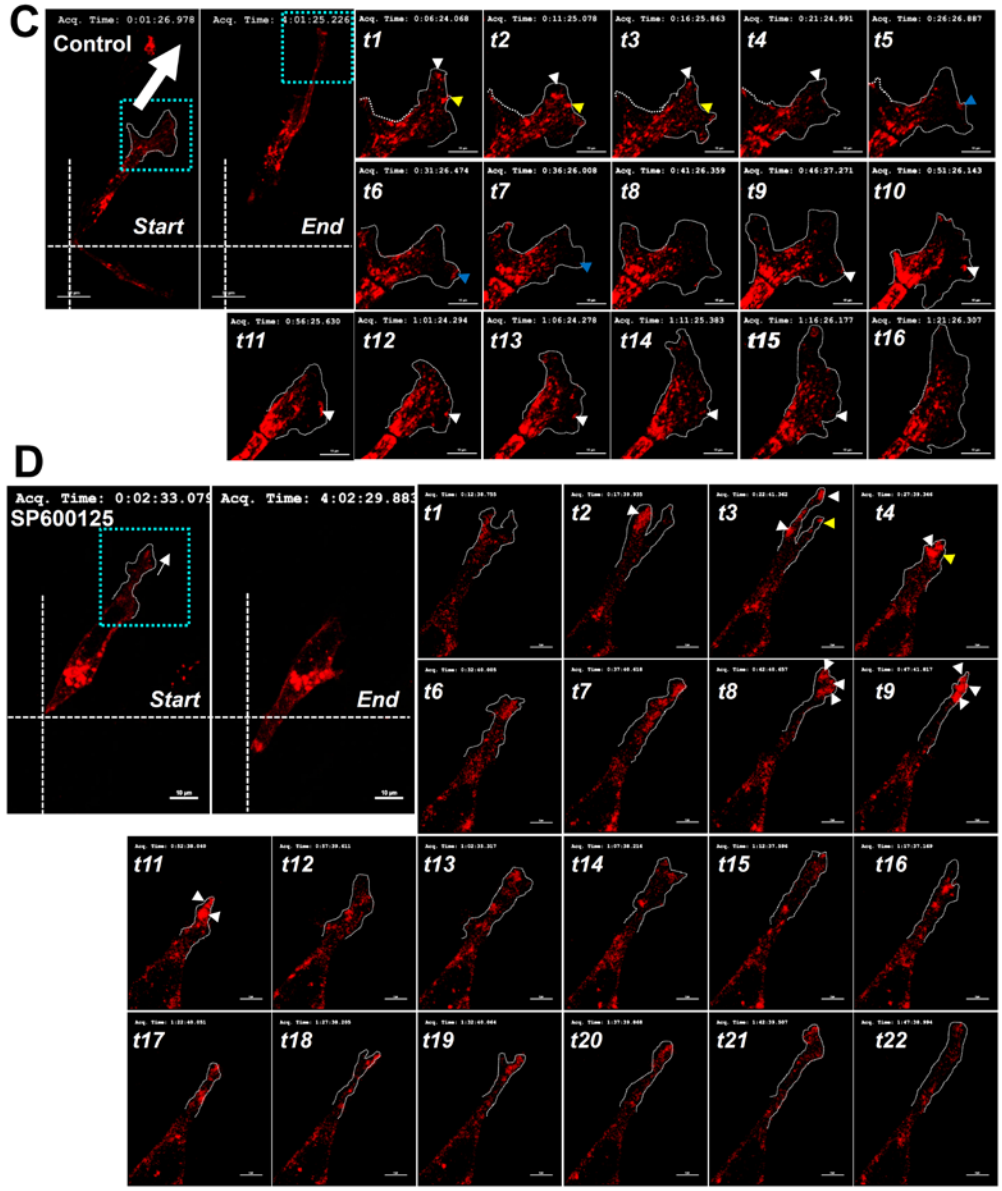
C
Control
Start
End
t1
t2
t3
t4
t5
t6
t7
t8
t9
t10
t11
t12
t13
t14
t15
t16
D
SP600125
Start
End
t1
t2
t3
t4
t6
t7
t8
t9
t11
t12
t13
t14
t15
t16
t17
t18
t19
t20
t21
t22

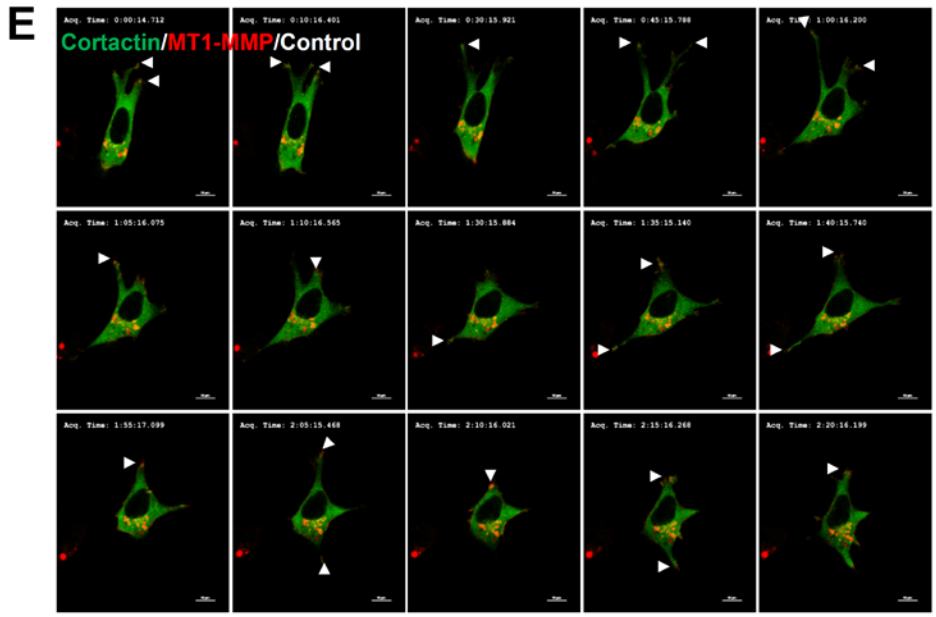
E
Cortactin/MT1-MMP/Control
Acq. Time: 0:00:14.712
Acq. Time: 0:10:16.401
Acq. Time: 0:30:15.921
Acq. Time: 0:45:15.788
Acq. Time: 1:00:16.200
Acq. Time: 1:05:16.075
Acq. Time: 1:10:16.565
Acq. Time: 1:30:15.884
Acq. Time: 1:35:15.140
Acq. Time: 1:40:15.740
Acq. Time: 1:55:17.099
Acq. Time: 2:05:15.468
Acq. Time: 2:10:16.021
Acq. Time: 2:15:16.268
Acq. Time: 2:20:16.199

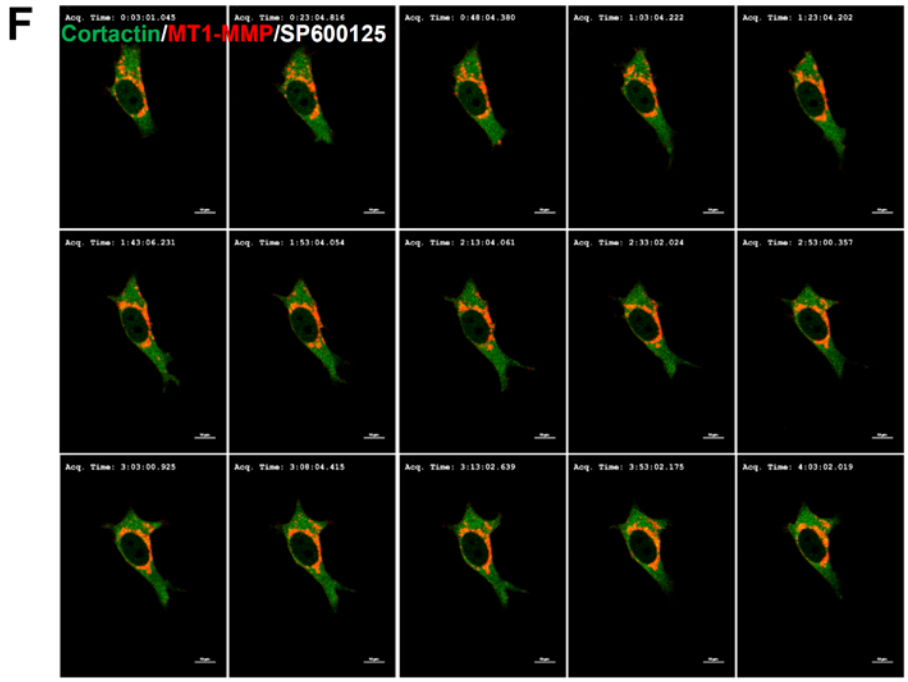
F
Cortactin/MT1-MMP/SP600125
Acq. Time: 0:03:01.045
Acq. Time: 0:23:04.816
Acq. Time: 0:48:04.380
Acq. Time: 1:03:04.222
Acq. Time: 1:23:04.202
Acq. Time: 1:43:06.231
Acq. Time: 1:53:04.054
Acq. Time: 2:13:04.061
Acq. Time: 2:33:02.024
Acq. Time: 2:53:00.357
Acq. Time: 3:03:00.925
Acq. Time: 3:08:04.415
Acq. Time: 3:13:02.639
Acq. Time: 3:53:02.175
Acq. Time: 4:03:02.019

Fig. Ⅲ-10. Cortactin and MT1-MMP were enriched at the membrane boundaries of cells embedded in 3D collagen in a manner that was dependent on JNK signaling. (A) Cells in 3D collagen were stained for actin (red) and visualized at confocal slices for FITC-collagen I fibers (green) to see dark ECM-degraded regions (arrowheads) in the presence of DMSO or SP600125 treatment. Yellow arrowheads indicated the dark area after collagen I degradation (as shown in xz-plane at a confocal slice), whereas white arrowheads in 600125-treated cells showed overlappings of actin and collagen I without degradation of collagen I (not to be dark in xz-plane). (B to D) Cells were transiently transfected with plasmid encoding mCherry-tagged MT1-MMP for 2 days and embedded into 3D collagen gels before immunostaining for MT1-MMP (red) and actin (green) (B) or before live imaging for upto 4 h in the presence of DMSO (Control, C) or SP600125 (D) treatment using confocal fluorescent microscopy with controlled temperature and CO2. (B) The xz or yz planes (white dotted boxes) of confocal slices represent cut-layers for fluorescence intensity profiles, and their fluorescence histograms along white-arrow sections are shown to illustrate the overlap between green and red fluorescence, but not blue fluorescence (DAPI). (C and D) Sky-blue dotted boxes mark the regions for the snap images and white-dotted lines indicate cellular boundaries to show alterations in cell morphology. Note that MT1-MMP positive spots in control cells show dynamic turnover along the membrane boundary (B), whereas the spots in SP600125-treated cells are stable and lack frequent turnovers

(C) as shown in some cases via colorful arrowheads. These snap images were from Supplementary Movies 3 (Control) and 4 (SP600125-treated). The data represent three isolated experiments. (E and F) The MDA-MB-231 cells were transfected with plasmid encoding mCherry-tagged MT1-MMP and GFP tagged cortactin, embedded into 3D collagen gels and treated with vehicle (DMSO, Control, E) or SP600125 (F) prior to imaging for MT1-MMP (red) and cortactin (green). Arrow heads indicate regions along the membrane boundary where both cortactin and MT1-MMP localized together (B). Note that costained spots (yellow) are enriched in perinuclear regions of the cells treated with SP600125 (C), compared with localization on membrane boundaries in the control (B). The data represent three isolated experiments.

4. Discussion

This study revealed that the environmental parameters around tumor cells including cell density, extracellular acidity, and hypoxia could cause JNK signaling inactivation (i.e., decreased c-Jun phosphorylation), TGFβ1/Smad signaling activation, Snail1 induction, and cortactin suppression. This signaling network led to stabilized localization of cortactin and MT1-MMP (both proteins are invadopodia markers) at perinuclear regions rather than at cell membrane boundaries, resulting in the reduced formation of actin and cortactin-enriched invadopodia along the edges of cells embedded in 3D collagen gels. We have compared the invasive features of MDA-MB-231 breast cancer cells embedded in either 3D collagen gels, 3D Matrigel, or a mixture of Matrigel and collagen I (at a 4:1 w/w ratio). Cells embedded in 3D Matrigel or the mixture of Matrigel and collagen I did not exhibit the JNK, Snail1, cortactin linkage demonstrated in cells in 3D collagen gels. A specific communication between MDA-MB-231 cells and surrounding ECM types appeared to regulate invasive behaviors. Among the diverse morphologically-different breast cancer cells [87], only stellate cells (MDA-MB-231 and MDA-MB-436) showed JNK activity-dependent morphological elongation and signaling network change, leading to a decreased invadopodia formation, indicating that invasiveness in certain types of breast cancer may be regulated by the JNK, Smads, Snail1, and cortactin network.

However, Mass grouped cells (T-47D and MCF-7) that have been established from IDC tumors [87], did not show the JNK-dependent effects on snail1 induction and cortactin suppression. Consistent with increased Snail1 stains approaching the central necrotic area of ductal carcinoma in situ (DCIS) [88], here Snail1 was randomly expressed in clinical breast tumor tissues rather than being localized around the invasive edges. The JNK, Smads, Snail1, and cortactin signaling network may thus be related to noninvasive DCIS. Snail1 induces EMT by suppressing E-cadherin [15, 89], being associated with the metastatic potential of infiltrating ductal carcinoma (IDC) [90, 91]. However, in DCIS, Snail1 is also localized in the nucleus, being correlated with higher tumor grade and proliferation rather than with migration [88], and expressed at similar levels in both the tumor and the normal zone of DCIS tissues [92]. Therefore, Snail1 expression may have differential effects on metastasis depending on the local invasiveness. In this study, Snail1 induced by JNKs inhibition was not correlated with E-cadherin (CDH1) mRNA suppression. Instead, Snail1 bound the promoter of Cortactin (CTTN) and negatively regulated its expression. Snail1 may thus have different downstream targets leading to less metastatic potential in DCIS (an early noninvasive breast cancer), rather than leading to E-cadherin suppression and enhanced migration and invasion in IDC. Indeed, hypoxia-mediated Snail1 expression in breast cancer cells did not enhance migration, following a partial hypoxia-induced EMT phenotype [88]. In control MDA-MB-231 cells in 3D collagen gels, pS63c-Jun

bound to the promoter of the Snail1 gene, indicating that active c-Jun may regulate basal Snail1 transcription. However, in the conditions where pS^{63}c-Jun decreased via the influence of extracellular environments, Snail1 mRNA and protein levels increased, indicating that proteins others than c-Jun could be involved in Snail1 transcription. Inhibiting JNK activity in E12.5 lung explants causes TGFβ1-activated Smad2 phosphorylation and gene expression changes for branching morphogenesis [93]. C-Jun associates with the oncoprotein, Ski, to suppress Smad2 transcriptional activity [94]. It may thus be that JNK inhibition is coordinated with TGFβ1-activated Smad2/4 binding to the Snail1 gene promoter region. Although it is reported that TGFβ1 regulates cross-talk between Smad and JNK signaling during EMT of rat peritoneal mesothelial cells [95], there are other reports that c- Jun activity is inversely correlated with TGFβ1 and Smad signaling activity [96, 97] , in agreement with this study. Therefore, this study reveals that MDA-MB-231 cells embedded in 3D collagen gels and exposed to various microenvironmental parameters inactivate the JNK/c-Jun signaling pathway, which was in turn coordinated with the TGFβ1/Smad2/4 activation to promote Snail1 transcription. This effect was observed only in cells embedded in 3D collagen gels, but not in cells cultured in 2D environments, 3D Matrigel, or 3D mixture of collagen I and Matrigel, indicating a specific communication existing between the

3D microenvironment and the cells. We demonstrated here that Snail1 could suppress cortactin expression. Cortactin is an actin binding protein at actin-enriched invasive morphological features, such as invadopodia [98]. Snail1 could bind to the CTTN promoter and suppressed cortactin mRNA and protein levels only when JNK was inactivated in the cells embedded in 3D collagen gel. In addition, cortactin and MT1-MMP invadopodia markers were dynamically localized along the cellular boundaries in control cells, but enriched at perinuclear regions upon JNK inhibition or Snail1 overexpression. Thus, JNK inhibition mediated effects (cortactin suppression and perinuclear localization of cortactin and MT1- MMP) decreased invadopodia formation and invasion in 3D collagen gels. As suggested in previous studies where Snail1 does not elicit a complete EMT [88] and that invasion is not dependent on an EMT phenotype [99], Snail1-decreased cell invasion in this study may be relevant to DCIS; noninvasive DCIS may be maintained by Snail1-mediated suppression and/or abnormal localization of cortactin and/or MT1-MMP, following the JNK/c-Jun pathway inactivation via tumor cell communication with the microenvironment.

5. Conclusions

Although an *in vitro* 3D environment cannot completely mimic the *in vivo* tumor site, embedding tumor cells in a 3D extracellular matrix (ECM) allows for the study of cancer cell behaviors and the screening of anti-metastatic reagents with a more *in vivo*-like context. Here I explored the behaviors of MDA-MB-231 breast cancer cells embedded in 3D collagen I. Diverse tumor environmental conditions (including cell density, extracellular acidity, or hypoxia as mimics for a continuous tumor growth) reduced JNKs, enhanced TGFβ1/Smad signaling activity, induced Snail1, and reduced cortactin expression. The reduced JNKs activity blocked efficient formation of invadopodia labeled with actin, cortactin, or MT1-MMP. JNKs inactivation activated Smad2 and Smad4, which were required for snail1 expression. Snail1 then repressed cortactin expression, causing reduced invadopodia formation and prominent localization of MT1-MMP at perinuclear regions. MDA-MB-231 cells thus exhibited less efficient invasion in 3D collagen I upon JNKs inhibition. These observations support a signaling network among JNKs, Smads, Snail1, and cortactin to regulate the invasion of MDA-MB-231 cells embedded in 3D collagen I, and this system may likely be a platform for screening of anti-metastatic reagents.

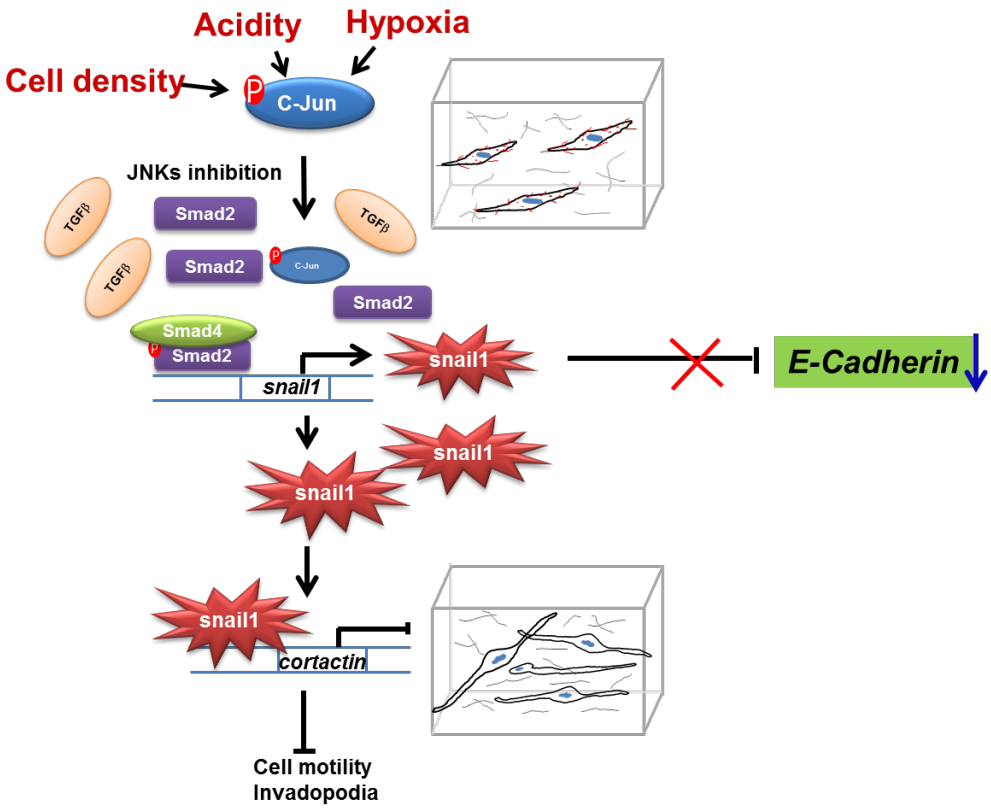

Fig. Ⅲ-11. Migration and invasion of MDA-MB-231 cells in 3D collagen gels were regulated by c-Jun/TGF-b1/Snail1/Cortactin linkage.

Ⅳ. Conclusions

EMT is a process by which epithelial cells lose their cell polarity and cell-cell or cell-matrix adhesion, and subsequently accompanies morphological changes of cell and gains migratory and invasive properties to become mesenchymal cells. In this study, I investigated how EMT causes gefitinib resistance and how mesenchymal properties of cancer cells following EMT process could regulate invasion of TM4SF5-positive and E-cadherin negative cells through 3D collagen I gel systems. As the results shown in the chapter 1, EMT-mediated gefitinib resistance occurred increase in expression of TM4SF5 and TM4SF5-mediated gefitinib resistance was involved in EMT. Additionally, in some results showed that EMT-mediated TM4SF5 and regulation of activity or integrity of EGFR may likely be important for gefitinib resistance of cancer cells. TM4SF5 induced EMT for enhanced cell migration and invasion. In the chapter 2, I investigated using the highly-invasive and TM4SF5-positive MDA-MB-231 breast cancer cells, their invasive properties such as invadopodia formation and ECM degradation in 3D collagen I gels with normal serum-containing media were monitored for the underlying mechanisms. The results showed that MDA-MB-231 cells by JNKs inhibition caused an elongation in cellular morphology and invasion of MDA-MB-231 cells in 3D collagen gels were regulated by c-Jun/ TGF-β1/ Snail1/ Cortactin linkage. Altogether, this study reveals that mesenchymal properties acquired by EMT process, which can be induced by membrane proteins such as TM4SF5 can cause drug resistance and enhanced metastatic potentials of cancer cells, suggesting that EMT process can be targeted for anti-metastatic reagents.

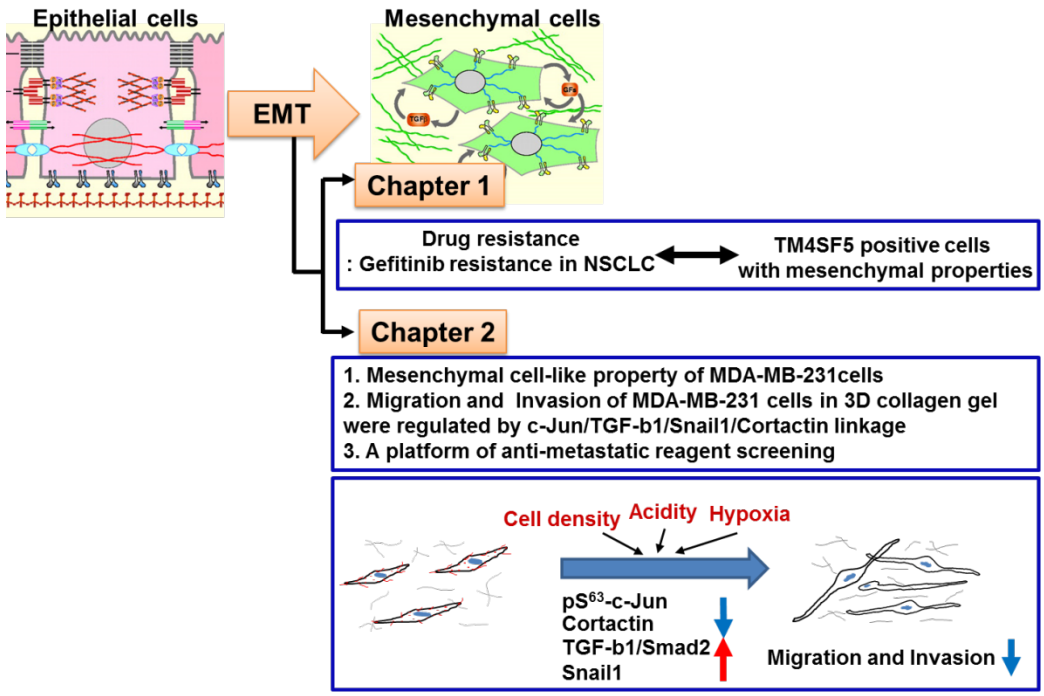

Fig. Ⅳ-1. EMT is correlated with TM4SF5-mediated gefitinib resistance in NSCLC cells and invasion of mesenchymal-like cells following EMT process is regulated by c-Jun/TGF-b1/Snail1/Cortactin linkage in 3D collagen gels

Ⅴ. References

1. Kim, H., et al., *JNK signaling activity regulates cell-cell adhesions via TM4SF5-mediated p27(Kip1) phosphorylation.* Cancer Lett, 2012. **314**(2): p. 198-205.
2. Gumbiner, B.M., *Cell adhesion: the molecular basis of tissue architecture and morphogenesis.* Cell, 1996. **84**(3): p. 345-57.
3. Miyoshi, J. and Y. Takai, *Structural and functional associations of apical junctions with cytoskeleton.* Biochim Biophys Acta, 2008. **1778**(3): p. 670-91.
4. Niessen, C.M., *Tight junctions/adherens junctions: basic structure and function.* J Invest Dermatol, 2007. **127**(11): p. 2525-32.
5. Hartsock, A. and W.J. Nelson, *Adherens and tight junctions: structure, function and connections to the actin cytoskeleton.* Biochim Biophys Acta, 2008. **1778**(3): p. 660-9.
6. Lukashev, M.E. and Z. Werb, *ECM signalling: orchestrating cell behaviour and misbehaviour.* Trends Cell Biol, 1998. **8**(11): p. 437-41.
7. Thiery, J.P., *Epithelial-mesenchymal transitions in tumour progression.* Nat Rev Cancer, 2002. **2**(6): p. 442-54.
8. Christiansen, J.J. and A.K. Rajasekaran, *Reassessing epithelial to mesenchymal transition as a prerequisite for carcinoma invasion and metastasis.* Cancer Res, 2006. **66**(17): p. 8319-26.
9. Grunert, S., M. Jechlinger, and H. Beug, *Diverse cellular and molecular mechanisms contribute to epithelial plasticity and metastasis.* Nat Rev Mol Cell Biol, 2003. **4**(8): p. 657-65.
10. Kalluri, R. and R.A. Weinberg, *The basics of epithelial-mesenchymal transition.* J Clin Invest, 2009. **119**(6): p. 1420-8.
11. Spaderna, S., et al., *The transcriptional repressor ZEB1 promotes metastasis and loss of cell polarity in cancer.* Cancer Res, 2008. **68**(2): p. 537-44.

12. Yang, J., et al., *Twist, a master regulator of morphogenesis, plays an essential role in tumor metastasis.* Cell, 2004. **117**(7): p. 927-39.
13. Moh, M.C. and S. Shen, *The roles of cell adhesion molecules in tumor suppression and cell migration: a new paradox.* Cell Adh Migr, 2009. **3**(4): p. 334-6.
14. Hirohashi, S. and Y. Kanai, *Cell adhesion system and human cancer morphogenesis.* Cancer Sci, 2003. **94**(7): p. 575-81.
15. Thiery, J.P., et al., *Epithelial-mesenchymal transitions in development and disease.* Cell, 2009. **139**(5): p. 871-90.
16. Tredan, O., et al., *Drug resistance and the solid tumor microenvironment.* J Natl Cancer Inst, 2007. **99**(19): p. 1441-54.
17. Lu, P., V.M. Weaver, and Z. Werb, *The extracellular matrix: a dynamic niche in cancer progression.* J Cell Biol, 2012. **196**(4): p. 395-406.
18. Vaupel, P., F. Kallinowski, and P. Okunieff, *Blood flow, oxygen and nutrient supply, and metabolic microenvironment of human tumors: a review.* Cancer Res, 1989. **49**(23): p. 6449-65.
19. Sung, S.Y., et al., *Tumor microenvironment promotes cancer progression, metastasis, and therapeutic resistance.* Curr Probl Cancer, 2007. **31**(2): p. 36-100.
20. Place, A.E., S. Jin Huh, and K. Polyak, *The microenvironment in breast cancer progression: biology and implications for treatment.* Breast Cancer Res, 2011. **13**(6): p. 227.
21. Yamada, K.M. and E. Cukierman, *Modeling tissue morphogenesis and cancer in 3D.* Cell, 2007. **130**(4): p. 601-10.
22. Chitcholtan, K., et al., *Differences in growth properties of endometrial cancer in three dimensional (3D) culture and 2D cell monolayer.* Exp Cell Res, 2013. **319**(1): p. 75-87.
23. Vidi, P.A., M.J. Bissell, and S.A. Lelievre, *Three-dimensional culture of human breast epithelial cells: the how and the why.* Methods Mol Biol, 2013. **945**: p. 193-219.

24. Bissell, M.J. and M.A. Labarge, *Context, tissue plasticity, and cancer: are tumor stem cells also regulated by the microenvironment?* Cancer Cell, 2005. **7**(1): p. 17-23.
25. Cukierman, E., R. Pankov, and K.M. Yamada, *Cell interactions with three-dimensional matrices.* Curr Opin Cell Biol, 2002. **14**(5): p. 633-9.
26. Discher, D.E., P. Janmey, and Y.L. Wang, *Tissue cells feel and respond to the stiffness of their substrate.* Science, 2005. **310**(5751): p. 1139-43.
27. Friedl, P., *Prespecification and plasticity: shifting mechanisms of cell migration.* Curr Opin Cell Biol, 2004. **16**(1): p. 14-23.
28. Wirtz, D., K. Konstantopoulos, and P.C. Searson, *The physics of cancer: the role of physical interactions and mechanical forces in metastasis.* Nat Rev Cancer, 2011. **11**(7): p. 512-22.
29. David, L., et al., *Hyaluronan hydrogel: an appropriate three-dimensional model for evaluation of anticancer drug sensitivity.* Acta Biomater, 2008. **4**(2): p. 256-63.
30. Horning, J.L., et al., *3-D tumor model for in vitro evaluation of anticancer drugs.* Mol Pharm, 2008. **5**(5): p. 849-62.
31. Nurwidya, F., et al., *Lung cancer stem cells: tumor biology and clinical implications.* Asia Pac J Clin Oncol, 2012. **8**(3): p. 217-22.
32. Sharma, S.V., et al., *Epidermal growth factor receptor mutations in lung cancer.* Nat Rev Cancer, 2007. **7**(3): p. 169-81.
33. Pao, W. and J. Chmielecki, *Rational, biologically based treatment of EGFR-mutant non-small-cell lung cancer.* Nat Rev Cancer, 2010. **10**(11): p. 760-74.
34. Ercan, D., et al., *Amplification of EGFR T790M causes resistance to an irreversible EGFR inhibitor.* Oncogene, 2010. **29**(16): p. 2346-56.
35. Lynch, T.J., et al., *Activating mutations in the epidermal growth factor receptor underlying responsiveness of non-small-cell lung cancer to gefitinib.* N Engl J Med, 2004. **350**(21): p. 2129-39.
36. Paez, J. and A. Allona, *[A case of adult Wilms tumor].* Arch Esp Urol, 1947. **4**(4): p. 324-32.

37. Chong, C.R. and P.A. Janne, *The quest to overcome resistance to EGFR-targeted therapies in cancer.* Nat Med, 2013. **19**(11): p. 1389-400.
38. Suda, K., et al., *EGFR T790M mutation: a double role in lung cancer cell survival?* J Thorac Oncol, 2009. **4**(1): p. 1-4.
39. Nguyen, K.S., S. Kobayashi, and D.B. Costa, *Acquired resistance to epidermal growth factor receptor tyrosine kinase inhibitors in non-small-cell lung cancers dependent on the epidermal growth factor receptor pathway.* Clin Lung Cancer, 2009. **10**(4): p. 281-9.
40. Thomson, S., et al., *Epithelial to mesenchymal transition is a determinant of sensitivity of non-small-cell lung carcinoma cell lines and xenografts to epidermal growth factor receptor inhibition.* Cancer Res, 2005. **65**(20): p. 9455-62.
41. Uramoto, H., et al., *Epithelial-mesenchymal transition in EGFR-TKI acquired resistant lung adenocarcinoma.* Anticancer Res, 2010. **30**(7): p. 2513-7.
42. Guo, A., et al., *Signaling networks assembled by oncogenic EGFR and c-Met.* Proc Natl Acad Sci U S A, 2008. **105**(2): p. 692-7.
43. Kim, H.P., et al., *Combined lapatinib and cetuximab enhance cytotoxicity against gefitinib-resistant lung cancer cells.* Mol Cancer Ther, 2008. **7**(3): p. 607-15.
44. Bean, J., et al., *MET amplification occurs with or without T790M mutations in EGFR mutant lung tumors with acquired resistance to gefitinib or erlotinib.* Proc Natl Acad Sci U S A, 2007. **104**(52): p. 20932-7.
45. Engelman, J.A., et al., *MET amplification leads to gefitinib resistance in lung cancer by activating ERBB3 signaling.* Science, 2007. **316**(5827): p. 1039-43.
46. Guix, M., et al., *Acquired resistance to EGFR tyrosine kinase inhibitors in cancer cells is mediated by loss of IGF-binding proteins.* J Clin Invest, 2008. **118**(7): p. 2609-19.

47. Rho, J.K., et al., *Epithelial to mesenchymal transition derived from repeated exposure to gefitinib determines the sensitivity to EGFR inhibitors in A549, a non-small cell lung cancer cell line.* Lung Cancer, 2009. **63**(2): p. 219-26.
48. Muschel, R.J. and A. Gal, *Tetraspanin in oncogenic epithelial-mesenchymal transition.* J Clin Invest, 2008. **118**(4): p. 1347-50.
49. Lee, S.A., et al., *Tetraspanin TM4SF5 mediates loss of contact inhibition through epithelial-mesenchymal transition in human hepatocarcinoma.* J Clin Invest, 2008. **118**(4): p. 1354-66.
50. Kim, H., et al., *TM4SF5 accelerates G1/S phase progression via cytosolic p27Kip1 expression and RhoA activity.* Biochim Biophys Acta, 2010. **1803**(8): p. 975-82.
51. Muller-Pillasch, F., et al., *Identification of a new tumour-associated antigen TM4SF5 and its expression in human cancer.* Gene, 1998. **208**(1): p. 25-30.
52. Wright, M.D., J. Ni, and G.B. Rudy, *The L6 membrane proteins--a new four-transmembrane superfamily.* Protein Sci, 2000. **9**(8): p. 1594-600.
53. Berditchevski, F., *Complexes of tetraspanins with integrins: more than meets the eye.* J Cell Sci, 2001. **114**(Pt 23): p. 4143-51.
54. Choi, S., et al., *Cooperation between integrin alpha5 and tetraspan TM4SF5 regulates VEGF-mediated angiogenic activity.* Blood, 2009. **113**(8): p. 1845-55.
55. Lee, S.A., et al., *The extracellular loop 2 of TM4SF5 inhibits integrin alpha2 on hepatocytes under collagen type I environment.* Carcinogenesis, 2009. **30**(11): p. 1872-9.
56. Han, S.W., et al., *Predictive and prognostic impact of epidermal growth factor receptor mutation in non-small-cell lung cancer patients treated with gefitinib.* J Clin Oncol, 2005. **23**(11): p. 2493-501.
57. Lee, S.A., et al., *Transmembrane 4 L six family member 5 (TM4SF5) enhances migration and invasion of hepatocytes for effective metastasis.* J Cell Biochem, 2010. **111**(1): p. 59-66.

58. Kang, M., et al., *Cross-talk between TGFbeta1 and EGFR signalling pathways induces TM4SF5 expression and epithelial-mesenchymal transition.* Biochem J, 2012. **443**(3): p. 691-700.
59. Stipp, C.S., T.V. Kolesnikova, and M.E. Hemler, *Functional domains in tetraspanin proteins.* Trends Biochem Sci, 2003. **28**(2): p. 106-12.
60. Kobayashi, S., et al., *EGFR mutation and resistance of non-small-cell lung cancer to gefitinib.* N Engl J Med, 2005. **352**(8): p. 786-92.
61. Naldini, L., et al., *Scatter factor and hepatocyte growth factor are indistinguishable ligands for the MET receptor.* EMBO J, 1991. **10**(10): p. 2867-78.
62. Chu, I.M., L. Hengst, and J.M. Slingerland, *The Cdk inhibitor p27 in human cancer: prognostic potential and relevance to anticancer therapy.* Nat Rev Cancer, 2008. **8**(4): p. 253-67.
63. Besson, A., et al., *p27Kip1 modulates cell migration through the regulation of RhoA activation.* Genes Dev, 2004. **18**(8): p. 862-76.
64. Besson, A., S.F. Dowdy, and J.M. Roberts, *CDK inhibitors: cell cycle regulators and beyond.* Dev Cell, 2008. **14**(2): p. 159-69.
65. Coqueret, O., *New roles for p21 and p27 cell-cycle inhibitors: a function for each cell compartment?* Trends Cell Biol, 2003. **13**(2): p. 65-70.
66. Yang, X., et al., *Palmitoylation supports assembly and function of integrin-tetraspanin complexes.* J Cell Biol, 2004. **167**(6): p. 1231-40.
67. Yanez-Mo, M., et al., *Tetraspanin-enriched microdomains: a functional unit in cell plasma membranes.* Trends Cell Biol, 2009. **19**(9): p. 434-46.
68. Sellarajah, S., et al., *Synthesis and testing of peptides for anti-prion activity.* Eur J Med Chem, 2008. **43**(11): p. 2418-27.
69. Lee, S.Y., et al., *Focal adhesion and actin organization by a cross-talk of TM4SF5 with integrin alpha2 are regulated by serum treatment.* Exp Cell Res, 2006. **312**(16): p. 2983-99.
70. Richardson, M.M., L.K. Jennings, and X.A. Zhang, *Tetraspanins and tumor progression.* Clin Exp Metastasis, 2011. **28**(3): p. 261-70.

71. Ke, A.W., et al., *CD151 amplifies signaling by integrin alpha6beta1 to PI3K and induces the epithelial-mesenchymal transition in HCC cells.* Gastroenterology, 2011. **140**(5): p. 1629-41 e15.
72. Desiderio, M.A., *Hepatocyte growth factor in invasive growth of carcinomas.* Cell Mol Life Sci, 2007. **64**(11): p. 1341-54.
73. Thomson, S., et al., *A systems view of epithelial-mesenchymal transition signaling states.* Clin Exp Metastasis, 2011. **28**(2): p. 137-55.
74. Friedl, P. and K. Wolf, *Proteolytic interstitial cell migration: a five-step process.* Cancer Metastasis Rev, 2009. **28**(1-2): p. 129-35.
75. Destaing, O., et al., *Invadosome regulation by adhesion signaling.* Curr Opin Cell Biol, 2011. **23**(5): p. 597-606.
76. Linder, S., *The matrix corroded: podosomes and invadopodia in extracellular matrix degradation.* Trends Cell Biol, 2007. **17**(3): p. 107-17.
77. van Horssen, R., et al., *Cancer cell metabolism regulates extracellular matrix degradation by invadopodia.* Eur J Cell Biol, 2013. **92**(3): p. 113-21.
78. Oser, M., et al., *Cortactin regulates cofilin and N-WASp activities to control the stages of invadopodium assembly and maturation.* J Cell Biol, 2009. **186**(4): p. 571-87.
79. Albiges-Rizo, C., et al., *Actin machinery and mechanosensitivity in invadopodia, podosomes and focal adhesions.* J Cell Sci, 2009. **122**(Pt 17): p. 3037-49.
80. Friedl, P., et al., *New dimensions in cell migration.* Nat Rev Mol Cell Biol, 2012. **13**(11): p. 743-7.
81. Hanahan, D. and L.M. Coussens, *Accessories to the crime: functions of cells recruited to the tumor microenvironment.* Cancer Cell, 2012. **21**(3): p. 309-22.
82. Box, C., et al., *Tumour-microenvironmental interactions: paths to progression and targets for treatment.* Semin Cancer Biol, 2010. **20**(3): p. 128-38.

83. Taddei, M.L., et al., *Microenvironment and tumor cell plasticity: An easy way out.* Cancer Lett, 2013.
84. Lee, M.S., et al., *Gefitinib resistance of cancer cells correlated with TM4SF5-mediated epithelial-mesenchymal transition.* Biochim Biophys Acta, 2012. **1823**(2): p. 514-23.
85. Klemke, R.L., *Trespassing cancer cells: 'fingerprinting' invasive protrusions reveals metastatic culprits.* Curr Opin Cell Biol, 2012. **24**(5): p. 662-9.
86. Kenny, P.A., et al., *The morphologies of breast cancer cell lines in three-dimensional assays correlate with their profiles of gene expression.* Mol Oncol, 2007. **1**(1): p. 84-96.
87. Kenny, P.A., *Three-dimensional extracellular matrix culture models of EGFR signalling and drug response.* Biochem Soc Trans, 2007. **35**(Pt 4): p. 665-8.
88. Lundgren, K., B. Nordenskjold, and G. Landberg, *Hypoxia, Snail and incomplete epithelial-mesenchymal transition in breast cancer.* Br J Cancer, 2009. **101**(10): p. 1769-81.
89. Cano, A., et al., *The transcription factor snail controls epithelial-mesenchymal transitions by repressing E-cadherin expression.* Nat Cell Biol, 2000. **2**(2): p. 76-83.
90. Blanco, M.J., et al., *Correlation of Snail expression with histological grade and lymph node status in breast carcinomas.* Oncogene, 2002. **21**(20): p. 3241-6.
91. Sou, P.W., et al., *Snail transcription factors in keratinocytes: Enough to make your skin crawl.* Int J Biochem Cell Biol, 2010. **42**(12): p. 1940-4.
92. Kim, B.G., et al., *Laminin-332-rich tumor microenvironment for tumor invasion in the interface zone of breast cancer.* Am J Pathol, 2011. **178**(1): p. 373-81.
93. Wu, S., et al., *Inhibition of JNK enhances TGF-beta1-activated Smad2 signaling in mouse embryonic lung.* Pediatr Res, 2009. **65**(4): p. 381-6.

94. Pessah, M., et al., *c-Jun associates with the oncoprotein Ski and suppresses Smad2 transcriptional activity.* J Biol Chem, 2002. **277**(32): p. 29094-100.
95. Liu, Q., et al., *A crosstalk between the Smad and JNK signaling in the TGF-beta-induced epithelial-mesenchymal transition in rat peritoneal mesothelial cells.* PLoS One, 2012. **7**(2): p. e32009.
96. Dennler, S., et al., *c-Jun inhibits transforming growth factor beta-mediated transcription by repressing Smad3 transcriptional activity.* J Biol Chem, 2000. **275**(37): p. 28858-65.
97. Ventura, J.J., et al., *JNK regulates autocrine expression of TGF-beta1.* Mol Cell, 2004. **15**(2): p. 269-78.
98. Buday, L. and J. Downward, *Roles of cortactin in tumor pathogenesis.* Biochim Biophys Acta, 2007. **1775**(2): p. 263-73.
99. Kovacs, A., J. Dhillon, and R.A. Walker, *Expression of P-cadherin, but not E-cadherin or N-cadherin, relates to pathological and functional differentiation of breast carcinomas.* Mol Pathol, 2003. **56**(6): p. 318-22.

국문 초록

암세포 부착 기능에 의한 항암제 내성 유발 기전 및 3 차원적 전이 제어에 관한 연구

李 美 淑

EGF 수용체 돌연변이가 원인이 되어 발생한 일부 폐암 환자는 TKI(tyrosine kinase inhibitor)인 gefitinib 과 같은 항암제를 복용하며 암을 치료한다. 그러나 지속적인 gefitinib 치료는 EGF 수용체에 또 다른 돌연변이를 유발하거나, c-MET 의 증폭 혹은 EMT (epithelial mesenchymal transition)등의 신호 전달경로가 활성화되면서 획득 저항성(acquired resistance)을 얻게 되어 더 이상 항암제로 작용하지 못하게 된다. 본 연구는 EGF 수용체의 돌연변이로 인해 발생한 비소세포 폐암 (non-small cell lung cancer, NSCLC)에서 항암제의 획득 저항성이 세포 막단백질인 TM4SF5 (Transmembrane 4 L6 family member 5)와 상관관계가 있는지, 또 TM4SF5 에 의해 발생하는

EMT 가 이러한 저항성에 어떻게 영향을 미칠 수 있는지를 살펴보았다. 그 결과 gefitinib 저항성이 있는 폐암 세포는 TM4SF5 의 발현이 높게 유지되며, TM4SF5 의 하위 신호로 알려진 세포질의 $p27^{Kip1}$ 을 안정화 시킴으로써 간엽계(mesenchymal) 세포의 표현형을 나타내는 것을 확인하였다. 더불어 gefitinib 에 민감한 세포에서도 EGF 수용체에 획득 돌연변이인 T790M 돌연변이가 추가적으로 생기게 되면 저항성 있는 세포로 전환되면서 TM4SF5 와 cytosolic $p27^{Kip1}$ 인산화가 높게 유지되며 세포연접에 중요한 E-cadherin 발현이 감소되어 세포가 gefitinib 에 저항성을 나타내어 survival 신호를 활성화 시키게 되는 것을 확인하였다. 부가적으로 gefitinib 에 민감함 세포에 TM4SF5 를 과량발현 시키게 되면 gefitinib 의 감수성이 떨어졌으며, gefitinib 저항성이 있는 세포에서 TM4SF5 또는 $p27^{Kip1}$ 을 억제시키면 다시 gefitinib 에대한 민감성을 회복하게 된다는 사실도 확인하였다. 본 연구 결과는 비소세포 폐암에서 항암제의 획득 저항성이 TM4SF5 의 발현을 증가시키며, 이렇게 증가된 TM4SF5 에 의한 EMT 가 gefitinib 의 저항성에도 영향을 주고 있음을 증명하고 있다. 선행 연구를 통해 우리는 TM4SF5 에 의해 유도된 EMT 가 항암제의 저항성 뿐만 아니라 암전이에도 중요하게 영향을 미친다는 것을 알고 있다. 약물에 대해 저항성을 갖게 되는 암세포는 주변 미세환경 인자와의 소통을 통해 전이를 위한 이동 및 침윤의 기능을 갖게 된다. 암세포의 약물 저항성과 전이능력은 세포 미세환경 인자에 의해 영향 받을 수 있을 것이다. 기존의 항암제 개발은

암세포를 이차원적 환경에서 단층 배양하여 항암제의 효능을 검증하고 drug efficacy 를 측정하여 암세포의 침윤과 전이를 연구하여 왔으나 항암제 개발의 성공 확률을 높이기 위해 삼차원 세포배양 방법을 도입하여 암세포의 침윤 과정을 모니터링 함으로써 암세포의 이동과 침윤 억제를 위한 물질 개발에 보다 현실적으로 기여 할 수 있을 것으로 기대하였다. 이러한 가정하에 강한 전이능을 가진 MDA-MB-231 세포와 그 외의 유방암 세포를 삼차원 콜라젠 젤 안에 embedding 한 후 세포의 behaviors 를 연구했다. 우선 암세포의 밀도, 주변의 산성도와 산소 포화도 등 다양한 세포 미세환경 인자들이 조절될 때 삼차원 콜라젠 젤 안에서 세포의 증식과 다양한 신호 인자들이 어떻게 변하는지 살펴보았다. 그 결과 삼차원 콜라젠 젤 안에서의 세포배양은 다양한 세포 미세환경에 영향을 받아 c-Jun 의 활성을 감소시키고 Cortactin 의 발현을 감소시켰으며, 전사 인자인 Snail1 의 양을 증가시킨다는 사실을 확인하였다. 이를 바탕으로 본 연구는 다양한 실험적 방법으로 콜라젠 젤 안에서 증가된 Snail1 이 Cortactin 의 발현을 감소시켜 결과적으로 암세포의 침윤에 중요한 invadopodia 의 형성이 억제 되는 것을 확인하였다. 뿐만 아니라 Cortactin 의 감소는 암세포 침윤 시 세포막에 위치하여 기질을 분해해 주는 MT1-MMP 의 localization 에도 영향을 준다는 것을 확인하였다. 본 연구는 삼차원 세포배양을 이용하여 초기 유방암인 유관상피내암(Ductal Carcinoma In Situ, DCIS)에서 침윤성 유방암(Invasive Ductal Carcinoma, IDC)으로 전이되는 과정을 유사하게

보여주는 in vitro 실험 시스템으로 이용될 수 있을 것이며, 암세포의 전이 억제제 개발에도 활용될 수 있을 것이다.

주요어 : NSCLC (Non-small cell lung carcinoma), EMT(Epithelial-mesenchymal transition), Gefitinib, 항암제 내성, EGF 수용체, TM4SF5 (transmembrane 4 L six family member 5), $p27^{Kip1}$, 3 차원 세포배양, Cortactin, Invadopodia, Snail1, MT1-MMP

학 번 : 2010-30467